QUANTIFICATION OF ARSENIC MOBILISATION AND ATTENUATION BY COUPLED FLOW AND MULTI-COMPONENT REACTIVE TRANSPORT MODELLING

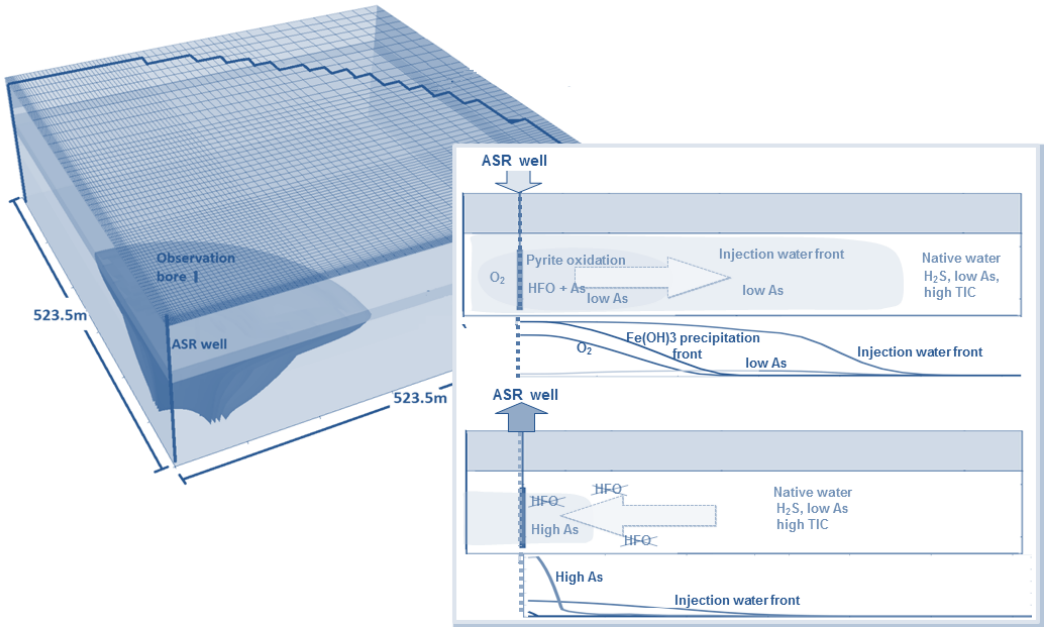

SUBMITTED BY

ILKA WALLIS

AS A REQUIREMENT IN FULL FOR THE DEGREE OF DOCTOR OF PHILOSOPHY IN THE SCHOOL OF THE ENVIRONMENT, AT FLINDERS UNIVERSITY, SOUTH AUSTRALIA

2012

Flinders UNIVERSITY

TABLE OF CONTENTS

LIST OF FIGURES

LIST OF TABLES

SUMMARY

Knowledge about the human toxicity of arsenic (As), combined with widespread naturally and anthropogenically-induced elevated As concentration in groundwaters in many parts of the world (e.g. Argentina, Bangladesh, India and Vietnam), have sparked an increasing interest in the factors controlling the distribution of As and the mechanisms that influence the fate of As in groundwater systems.

Several common naturally-occurring geochemical processes can play an important role in controlling the distribution of As. However, in natural systems, it is often difficult to discern which chemical or biochemical processes take the lead in controlling the fate of arsenic, or whether its fate might be predominantly controlled by physical transport processes. In such cases integrated flow and reactive transport modelling can provide an important and consistent quantitative framework for advancing our understanding of the complex and often non-intuitive field-scale behaviour of arsenic.

This thesis describes the development and evaluation of detailed process-based simulation capabilities for two selected managed aquifer recharge (MAR) operations in Langerak, the Netherlands and Bradenton, Florida. At both field sites, injection of potable, oxygenated water into anoxic aquifers for storage and later withdrawal resulted in the mobilisation of arsenic. Both sites were well-characterised and benefited from the controlled hydraulic flow conditions that were induced by the MAR operations and from the availability of comprehensive data describing the geochemical evolution of the aquifer.

The simulators used for the studies were the USGS flow model MODFLOW in conjunction with the reactive multi-component transport model PHT3D (Prommer et al. 2003). PHT3D couples the three-dimensional transport simulator MT3DMS (Zheng and Wang, 1999) with the geochemical model PHREEQC-2 (Parkhurst and Appelo, 1999).

The model-based data interpretation provided conceptual insight into the predominating reaction patterns, their spatial variability and their dependence on the flow regime under a variety of MAR operating conditions. The integrated flow and reactive transport modelling illustrated that arsenic was initially released/mobilised following pyrite oxidation triggered by the injection of oxygenated water into the anoxic aquifers. Dissolved concentrations were controlled by complexation to neo-formed hydrous ferric oxides during injection. Modelling suggested this to be an effective arsenic attenuation mechanism, albeit a temporary one. During recovery arsenic was remobilized as a result of both dissolution of hydrous ferric oxides and displacement from sorption sites by competing anions.

The numerical framework allowed detailed assessments of arsenic partitioning among mineral phases, surface complexes and aqueous phases during injection, storage and recovery and the evaluation of the temporal and areal extent of arsenic mobility and capture within the aquifer.

During the model development and applications it became clear that computational efficiency and accuracy consideration can play an important role for the simulation of arsenic fate at field scale. This motivated additional and more systematic investigations on the efficiency and accuracy of the numerical modelling approaches for multi-dimensional field-scale reactive transport.

Taken collectively, this thesis creates a depth of knowledge on the science and simulation capabilities of field-scale As behaviour. The work demonstrates, that a clear understanding of the fundamental geochemical processes affecting the mobility of arsenic and their interaction with physical transport can only be achieved, if flow, transport and reactive processes are considered simultaneously. A contribution to understanding the complete cycling of arsenic in complex field-scale groundwater systems as a coupled process of hydraulic and geo(bio)chemical controls is made.

The practical aspect of the work is the provision of a tool to assess the suitability of different MAR sites and techniques in relation to As mobility, to optimize operational conditions as well as to evaluate proposed engineering solutions that could mitigate the As problem at affected MAR sites.

DECLARATION OF ORIGINALITY

I certify that this thesis does not incorporate, without acknowledgment, any material previously submitted for a degree or diploma in any other university; and that to the best of my knowledge and belief it does not contain any material previously published or written by another person except where due reference is made in the text.

Ilka Wallis

ACKNOWLEDGEMENTS

I like to thank colleagues and friends for their contributions to this PhD. First and foremost, I am deeply indebted to my supervisors: I owe much to Prof. Craig Simmons (Flinders University, SA) for his enthusiastic and expert guidance. I greatly value the numerous conversations I had with Dr. Vincent Post (Flinders University, SA), which clarified my thinking on various scientific matters and for the support he provided in general. I feel deeply indebted to Prof. Henning Prommer (CSIRO Land and Water) for being so generous with his time, for scientific discussions, reviewing and improving manuscripts and for knowing and understanding what it means to have kids! Without his tireless support I would not have been able to simultaneously explore the intricacies of reactive transport modeling and explore the science of raising twins. His friendship and professional collaboration means a great deal to me.

I would like to express my gratitude to a number of people who have shared their ideas, gave their time and comments. These include Andy Love, Carlos Descourvieres, Janek Greskowiak, Simone Seibert, Evelien Martens, David Kinniburgh, Pieter Stuyfzand and Thomas Pichler.

Financial support for the PhD project was provided by former Land and Water Australia, CSIRO Land and Water and the Centre for Groundwater Studies and is gratefully acknowledged.

Most thanks should go, however, to my family: Marianne and Klaus Neumann for providing spiritual support, my sister Astrid for selflessly offering to take care of my twins on prolonged stays in Europe for conferences and work, Hannah and Jan for hours of babysitting and Frank for tolerating all the above. Above all, I am deeply indebted to Alex, my husband. Time has been more than a highly priced commodity during the last few years and I thank him for his patience and support. Last but not least I would like to thank my twin boys Tristan and Torge for being there and making it all worthwhile.

Ilka Wallis, Adelaide 12.01.2012

Chapter 1. INTRODUCTION

1.1 THE RESEARCH PROBLEM

Naturally and anthropogenically induced elevated As concentrations in groundwaters are reported from a wide range of hydrogeological and geochemical settings in many parts of the world (e.g. Argentina, Bangladesh, India and Vietnam). Arsenic is both a toxin and a carcinogen and is recognised as one of the most serious inorganic threats to drinking water on a global scale (Smedley and Kinniburgh 2002). Pathways of arsenic into and within groundwater systems are still not fully understood. However, several common naturally-occurring geochemical processes are confirmed to play an important role in controlling the distribution of As at the near-neutral pH range that is typical for many groundwaters. The oxidation of As-bearing sulphides (e.g. pyrite) under aerobic conditions (Jones and Pichler 2007) and the reductive dissolution of Fe-oxides under reducing groundwater conditions were shown to be important release mechanism for As (Smedley and Kinniburgh 2002, Burnol 2007, Dixit and Hering 2003) and played a key role in many studies that investigated naturally high As groundwaters. Major processes mitigating the mobilisation of arsenic are adsorption, i.e., surface complexation and (co)-precipitation. Minerals such as ferrihydrite, Al-oxides or Mn-oxides are known to be effective scavengers for As under oxic conditions, while precipitation of As-bearing sulphides may reduce dissolved concentrations under reducing conditions (Stollenwerk 2003, Saunders et al. 2008, Wolthers et al. 2008). Other processes such as competitive displacement of sorbed As by increasing carbonate and phosphate concentrations (Smedley and Kinniburgh 2002, Welch et al. 2000, Stollenwerk 2007), adsorption of As on carbonates and clay minerals (Goldberg 2002, Charlet et al. 2007) or biochemical processes (Oremland and Stolz 2003, Islam et al. 2004, He et al. 2009) may also be important components of As cycling in groundwaters and sediments.

In natural systems, it is often difficult to discern which of these chemical or biochemical processes take the lead in controlling the fate of arsenic, or if its fate might even be controlled predominantly by physical transport processes. The underlying causes of elevated arsenic concentrations will vary from site to site and are affected by the composition of the aquifer matrix, the composition of the ambient groundwater and recharge water and the hydrogeological conditions of the site. Since these interactions are generally highly nonlinear and non-intuitive, integrated coupled flow and reactive transport simulations can greatly assist in the analysis of field data and can provide a useful framework for advancing our understanding of field-scale arsenic behaviour in hydrogeologically and geochemically complex aquifer systems. Conceptual models can be

formulated and their applicability tested, with the results eventually providing constraints for the interpretation of measured geochemical data.

Transport behaviour of As under controlled laboratory conditions was previously successfully quantified by numerical modelling (e.g. Dzombak and Morel 1990; Appelo et al. 2002, Jang and Dempsey 2008, Saunders 2008, Jeppu et al., 2010). Recent modeling efforts have built on these studies and quantified As behavior under the simplifying assumption of 1D flow conditions; e.g. Appelo and de Vet (2003), Moldovan and Hendry (2005), Postma, et al. (2007) and Stollenwerk et al. (2007). An early example at using a comprehensive three-dimensional transport model (PHAST, Parkhurst et al. 2010) to simulate arsenic behavior on a regional scale was provided by Parkhurst et al . (1996, 1999). The evolution of naturally high arsenic concentrations present in the Central Oklahoma aquifer was simulated over geological times. A 2D reactive transport model study on arsenic attenuation under field conditions was reported by Jung et al. in 2009. However, a wider range of studies which demonstrate the ability of laboratory-derived conceptual models to capture the processes that influence and control As distribution at the field scale is still lacking.

The research presented in this thesis investigates conceptual and numerical models to provide an integrated, process-based quantification of mechanisms that control As mobility at two hydrogeologically and geochemically heterogeneous “field-laboratory” sites. These well-characterised sites, both at which managed aquifer recharge (MAR) operations were closely studied, benefit from strictly controlled hydraulic flow conditions that are induced through the MAR operations and from the availability of detailed temporal and spatial data describing the geochemical evolution at the study sites. This provided effective constraints for the development of plausible conceptual and numerical models and offered the opportunity to investigate field-scale As behaviour under otherwise rarely found, well-controlled and characterised conditions. This is a significant advantage over most other sites, where high As groundwaters were studied, and where factors such as unknown source history, uncertain flow rates and a general scarcity of hydrogeological and hydrogeochemical data together with the associated parameter uncertainties may limit the robustness of any proposed conceptual and/or numerical model.

The two managed aquifer recharge operations analysed in this PhD study were (i) a deepwell injection experiment in the Netherlands and (ii) an aquifer storage and recovery operation in Florida. At both sites, injection of potable, oxygenated water into anoxic aquifers for storage and later withdrawal has resulted in the mobilisation of arsenic.

Chapter 2 describes the first of the two cases, where flow and reactive transport modelling was undertaken to provide a consistent interpretation of the observed spatial and temporal hydrochemical changes that were documented during an aquifer storage transfer and recovery (ASTR) experiment in a siliclastic pyritic aquifer at Langerak, the Netherlands. Following injection of aerated water into the anoxic target aquifer, arsenic mobilisation was detected close to the injection well, but elevated concentrations diminished to background levels with increasing travel distance. Pyrite oxidation and the formation of amorphous iron-oxides (HFO) in the progressively expanding oxic conditions of the aquifer were shown to be the key chemical processes for water quality changes, which in turn controlled the observed fate of arsenic during the experiment. In the model that best reproduced field observations the fate of arsenic could be explained by (i) release/mobilisation via co-dissolution of arsenopyrite, stoichiometrically linked to pyrite oxidation (ii) kinetically controlled oxidation of dissolved As(III) to As(V) and (iii) adsorption via surface complexation of As on neo-precipitated amorphous iron oxides. The adsorption of As on HFOs was simulated using the generalized two-layer surface complexation model (SCM) of Dzombak and Morel (1990) for sorption on ferrihydrite, extended by reactions for Fe^{2+} and HCO_3^- to allow competitive sorption between arsenic and other ions. The model assumes that sorption sites on the solid HFO surface can be described by average surface site characteristics with no specific correlation to the actual solid surface structure. The model was chosen over the more recently developed charge distribution multi-site complexation model CD-MUSIC (Hiemstra and van Riemsdijk, 1996), which distinguishes between different surface site types based on the crystal structure of the mineral. At field scale, where there is no experimental evidence to determine the exact nature and surface structure of the surface complexes, the use of the chemically more simplistic Dzombak and Morel model with a smaller number of adjustable parameters was regarded preferable over highly parameterised SCMs.

The second study (Chapter 3) allowed for significant expansion of the work described in Chapter 2 with an emphasis on the understanding of the remobilisation of arsenic which was observed during the recovery phases of an aquifer storage and recovery (ASR) trial. ASR operations involve the cyclic injection of a water source into a target aquifer and its later withdrawal from the aquifer through the same well. In this study conservative and reactive transport modelling was used to analyse the multi-cycle hydrochemical and hydrogeological data from a site in south-west Florida, where As mobilisation was detected in response to the cyclic injection of oxygenated potable water into anaerobic sections of a pyrite-containing limestone target aquifer. The coupled simulation of the highly transient

flow field and geochemical conditions was used to evaluate and quantify the processes controlling the redox dynamics and the related fate of arsenic within the aquifer that surrounds the ASR well under a variety of operating conditions. The numerical modelling illustrated that pyrite oxidation and the precipitation/dissolution of amorphous iron-oxides together with competitive displacement of As from sorption sites on HFO by competing anions were the key chemical processes that controlled the mobility of arsenic.

The third study (Chapter 4) was motivated by the significant computational costs that were associated with the multi-dimensional field scale MAR model applications discussed in Chapters 2 and 3. The work described in Chapter 4 therefore focused on exploring suitable numerical modelling techniques to allow for computationally more efficient simulation of reactive transport problems around point sources/sinks. Several options of simulating radial-symmetric conservative and reactive solute transport were investigated and their applicability, accuracy and computational cost was evaluated.

1.2 OBJECTIVES

In this work coupled flow and reactive transport modelling of two well-characterised managed aquifer recharge field sites was utilized to advance our understanding of arsenics' complex and often non-intuitive field-scale behaviour. The studies were underpinned by work into numerical modelling techniques, which allow for computationally more efficient simulation of reactive transport problems around point sources/sinks. The specific objectives were as follows:

- to develop conceptual models of arsenic release and attenuation at two well characterised MAR field sites,
- to develop a numerical modelling framework that provides a process-based description of the coupled flow, solute transport and reaction mechanisms controlling the fate of arsenic during MAR
- Testing the developed quantification framework for two comprehensive field data sets collected from a deepwell injection experiment in the Netherlands and an aquifer storage and recovery operation in Florida to investigate its applicability to simulate As behaviour in natural systems, where flow, transport and reactive processes need to be considered simultaneously.

- Test computationally efficient modelling approaches for simulating multi-dimensional field scale reactive transport, applicable to MAR operations.

1.3 SUMMARY OF THE RESEARCH CONTRIBUTION

Previous numerical studies that have investigated arsenic fate and transport have mostly focused on the identification of hydrogeochemical processes affecting its mobility under controlled laboratory conditions or in simplified 1-D field situations, while detailed quantitative assessment frameworks of As behaviour in more complex groundwater systems were generally not established. The work presented in this thesis aimed to fill this gap. The well-controlled and characterised conditions at two managed aquifer recharge (MAR) sites offered the unique opportunity to up-scale and advance our understanding and simulation capabilities of field-scale As behaviour of groundwater systems, where geological, hydrogeological, and geo(bio)chemical aspects have to be considered simultaneously.

Reactive transport modelling allowed integrated consideration of the dynamics between physical (e.g. flow, mixing) and reactive processes at different spatial and temporal scales. As a consequence a deepened understanding of the subsurface processes governing the fate of As has emerged and the research makes a contribution to understanding the complete cycling of arsenic in complex field-scale groundwater systems as a coupled process of hydraulic and geo(bio)chemical controls. It also extends our process-based quantification capabilities of water quality changes in complex groundwater systems.

The numerical data interpretation presented in this thesis provides guidance for sampling design and analysis for other MAR operations, where As mobilisation is suspected. Possible oxidants (e.g. O_2, NO_3, SO_4), ions competing with As for sorption sites (e.g. PO_4, DOC, HCO_3), arsenic speciation (As^{3+}, As^{5+}) and analytes which characterise the redox conditions of the aquifer (e.g. Fe, Mn) are shown to be essential for a quantitative understanding of arsenic behaviour and should be part of any future routine analysis. A lack thereof induces considerable uncertainty in the determination of the key chemical process influencing arsenic mobilisation.

A practical aspect of the developed quantification framework is its use as a tool for the assessment of the suitability of different MAR sites and different MAR techniques in regards to As mobility. It also provides a basis to assess and optimize operational conditions

and their impact on As mobility as well as to evaluate proposed engineering solutions that could mitigate the As problem at affected MAR sites.

1.4 STRUCTURE OF THIS THESIS

This thesis comprises this introduction, three separate pieces of research work and supplementary information included as appendices. The general introduction (Chapter 1) gives a brief overview of the fundamental processes that occur in groundwater systems in relation to arsenic mobilisation and attenuation and our current ability to quantify these using numerical modelling and details the objectives of this thesis. The main research work is described in Chapters 2, 3 and 4. Written as manuscripts for publication in peer-reviewed journals, each of these chapters can be read independently as a stand-alone piece of research, including introduction, methodology, results and discussion and conclusions. The three manuscripts included in this thesis are:

(1) WALLIS, I., PROMMER, H., SIMMONS, C., POST, V. AND STUYFZAND, P. (2010): EVALUATION OF CONCEPTUAL AND NUMERICAL MODELS FOR ARSENIC MOBILIZATION AND ATTENUATION DURING MANAGED AQUIFER RECHARGE. *ENVIRONMENTAL SCIENCE & TECHNOLOGY*, VOL. 44 (13) P. 5035-5041 [CHAPTER 2]

(2) WALLIS, I., PROMMER, H., PICHLER, T., POST, V., NORTON, S.B., ANNABLE, M. AND SIMMONS, C. (2011): A PROCESS-BASED REACTIVE TRANSPORT MODEL TO QUANTIFY ARSENIC MOBILITY DURING AQUIFER STORAGE AND RECOVERY OF POTABLE WATER. *ENVIRONMENTAL SCIENCE & TECHNOLOGY*, 45(16):6924-31 [CHAPTER 3]

(3) WALLIS, I., PROMMER, H., POST, V., VANDENBOHDE, A., AND SIMMONS, C. (2012): SIMULATING MODFLOW-BASED REACTIVE TRANSPORT UNDER RADIAL-SYMMETRIC FLOW CONDITIONS. *GROUND WATER*, (IN PRESS). [CHAPTER 4]

Supplementary information for Chapters 2 and 3 are included as an appendix at the end of the document. In Chapters 2-4 some repetition of introductory information can be found. This was necessary for the autonomy of the papers. Additionally, conference papers, which were the direct result of this work are also included as appendices. The following appendices are included:

Appendix A: Additional figures and tables and supporting findings for Chapter 2

Appendix B: Additional figures and tables and supporting findings for Chapter 3

Appendix C: Example model input data for the Geometry, Langevin and Louwyck methods

C1: Geometry method

C2: Langevin method

C3: Louwyck method

Appendix D: Published conference proceedings resulting from the research work

D1: Numerical evaluation of arsenic mobilisation during deepwell injection of aerobic groundwater into a pyritic aquifer, *Goldschmidt 2009*

D2: Evaluation of Conceptual and Numerical Model for Arsenic Mobilisation During Managed Aquifer Recharge, *2010 Ground Water Summit*

D3: Reactive transport modelling to quantify arsenic mobilization and capture during aquifer storage and recovery of potable water, *Goldschmidt 2011*

D4: Modelling of Arsenic fate during ASR of potable water, *ModelCare 2011*

Chapter 2. EVALUATION OF CONCEPTUAL AND NUMERICAL MODELS FOR ARSENIC MOBILIZATION AND ATTENUATION DURING MANAGED AQUIFER RECHARGE

ABSTRACT

Managed Aquifer Recharge (MAR) is promoted as an attractive technique to meet growing water demands. An impediment to MAR applications, where oxygenated water is recharged into anoxic aquifers, is the potential mobilization of trace metals (e.g. arsenic). While conceptual models for arsenic transport under such circumstances exist, they are generally not rigorously evaluated through numerical modeling, especially at field-scale. In this work, geochemical data from an injection experiment in The Netherlands, where the introduction of oxygenated water into an anoxic aquifer mobilized arsenic, was used to develop and evaluate conceptual and numerical models of arsenic release and attenuation under field-scale conditions. Initially, a groundwater flow and nonreactive transport model was developed. Subsequent reactive transport simulations focused on the description of the temporal and spatial evolution of the redox zonation. The calibrated model was then used to study and quantify the transport of arsenic. In the model that best reproduced field observations, the fate of arsenic was simulated by (i) release via co-dissolution of arsenopyrite, stoichiometrically linked to pyrite oxidation (ii) kinetically controlled oxidation of dissolved As(III) to As(V) and (iii) As adsorption via surface complexation on neo-precipitated iron oxides.

2.1 INTRODUCTION

Managed Aquifer Recharge (MAR) is widely promoted as an attractive technique to meet growing water demands. It involves adding a water source such as recycled water to confined or semi-confined aquifers for later withdrawal in times of demand. Often these aquifers contain considerable amounts of pyrite, which dissolves under the influence of oxidised recharge waters. Adverse impacts of pyrite oxidation on the evolution of the water quality include the possible mobilization of trace metals and metalloids including arsenic (As). Well-documented examples of As mobilization exist for MAR schemes operating in west-central and southwest Florida, the Netherlands, Denmark and Australia (Jones and Pichler 2007, Mirecki 2004, Stuyfzand and Timmer 1999, Vanderzalm et al. 2007).

Elevated concentrations of naturally occurring arsenic in groundwater are, however, reported from a much wider range of hydrogeological and geochemical settings (e.g. Kinniburgh et al. 2003, Smedley and Kinniburgh 2002). The causes are in many cases still being debated and pathways of arsenic into groundwater are not fully understood. Several hypotheses have been formulated, such as (i) release of sorbed As associated with the reductive dissolution of iron oxides, (ii) oxidative dissolution of As-pyrite and (iii) competitive displacement of sorbed As by increasing carbonate and phosphate concentrations (Smedley and Kinniburgh 2002, Welch et al. 2000 among others).

The mobility of arsenic at the near-neutral pH typical of most groundwaters is severely limited by strong sorption onto mineral surfaces such as ferrihydrite. Adsorption efficiency, however, depends strongly on the solution composition (arsenic concentration, pH and presence of competing ions) and the oxidation state of arsenic (Oremland and Stolz 2003, Plant et al. 2007). Arsenate (As(V)) is the prevalent chemical species under oxic conditions and arsenite (As(III)) the prevalent chemical species under anoxic conditions.

Both biochemical and abiotic processes influence arsenic speciation and mobility. Several microbial respiratory and non-respiratory enzymatic systems that influence the oxidation state of arsenic have been reported (Oremland and Stolz 2003). Abiotic oxidation of As(III) is mainly significant where catalysis by mineral surfaces occurs, i.e. iron oxides (De Vitre et al. 1991, Manning et al. 2002b), manganese oxides (Oscarson et al. 1981, Manning et al. 2002a, Amirbahman et al. 2006) or by dissolved, adsorbed or structural Fe(II) (Hug and Leupin 2003, Roberts et al. 2004).

Arsenic behaviour has been quantified successfully under laboratory conditions by numerical modeling (e.g. Dzombak and Morel 1990; Appelo et al. 2002). Recent modeling studies for 1D flow conditions include those of Appelo and de Vet (2003), Moldovan and Hendry (2005), Postma et al. (2007) and Stollenwerk et al. (2007). While a 2D reactive transport model study on arsenic attenuation under field conditions was reported by Jung et al. (2009), a wider range of studies which demonstrate the applicability of numerical models to hydrogeologically and geochemically heterogeneous porous media systems is still lacking. In natural systems, it is more difficult to discern which chemical or biochemical processes take the lead in controlling the fate of arsenic, or if its fate might even be controlled by physical transport processes. Therefore, coupled flow and reactive transport simulations can provide a useful framework for advancing our understanding of such complex field-scale systems. Conceptual models can be formulated and their applicability

tested, with the results eventually providing constraints for the interpretation of measured geochemical data.

In the present study, geochemical data from a deep-well injection trial in South-West Netherlands, where arsenic mobilization resulted from the introduction of oxygenated water into a deep anoxic aquifer (Stuyfzand and Timmer 1999), was used to develop and evaluate conceptual and numerical models of arsenic mobilization and attenuation under field-scale conditions.

2.2 MATERIALS AND METHODS

2.2.1 FIELD SITE

The Dutch water supply company Oasen investigated the technical feasibility for deep well injection of pretreated river Rhine water as a technique to meet growing water demands (Stuyfzand and Timmer 1999). A trial site was built in Langerak in South-West Netherlands. The target aquifer is composed of permeable fluvial sands at depths ranging between 68 m and 95 m b.g.s. underlain and overlain by clayey aquitards which confine the aquifer. The Langerak Aquifer Storage, Transfer and Recovery (ASTR) system consists of one recharge and one recovery well, at a distance of 190 m, with three monitoring wells sited along the flow direction (Figure 2.1). Injection at 35 m^3 hr^{-1} and recovery (60 m^3 hr^{-1}) proceeded without significant interruptions for close to 600 days, accompanied by a detailed monitoring program.

2.2.2 SITE HYDROGEOCHEMISTRY

The recharged aquifer is composed of alternating coarse- and fine-grained fluvial sand layers, which contain small amounts of organic carbon, calcite and pyrite (up to 200 mg S/kg). Based on aqua regia extraction of core samples, As, Co, Ni and Zn were found to be associated with pyrite, with a most probable stoichiometry of $Fe_{0.98}Co_{0.0037}Ni_{0.01}Zn_{0.01}S_2As_{0.0053}$ (Stuyfzand and Timmer 1999). The cation exchange capacity (CEC) is low with appreciable amounts of adsorbed NH_4^+, Fe^{2+} and Mn^{2+} but dominated by adsorbed Ca^{2+}.

A summary of both the ambient and recharge water chemistry is given in Table 2.1. The groundwater in the target aquifer, prior to the start of injection was anoxic as indicated by high methane, relatively high Fe^{2+} and Mn^{2+} concentrations and the absence of appreciable

concentrations of oxygen, nitrate or sulphate. Total dissolved arsenic concentrations, determined by Atomic Absorption Spectrophotometry (AAS) with graphite furnace, were below detection limit (DL = 1 µg L^{-1}). Arsenic speciation was not determined.

Treated groundwater was used as injectant. Chemical differences between ambient groundwater and injectant resulted from the applied water treatment, i.e., aeration and rapid sand filtration. After treatment, O_2, NO_3^- and SO_4^{2-} were present, while reduced species (Fe^{2+}, Mn^{2+}, NH_4^+, CH_4) were absent or occurred at very low concentrations. During the first month of the injection trial, NaCl was added to the injectant as a tracer, while $NaNO_3$ was added continuously to increase the oxidative capacity of the injectant.

The injection of oxygenated water into the deep anoxic aquifer at the Langerak site led to the oxidation of pyrite as the most important reaction influencing the water chemistry, evidenced by diminishing O_2 and NO_3^- concentrations and an increase in SO_4^{2-} and Fe^{2+}. Trace elements found in significant amounts in pyrite (As, Ni and Zn) were mobilised following pyrite oxidation. Arsenic concentrations increased to a maximum of 90 µg L^{-1} during aquifer passage with a distinct concentration peak coinciding with the arrival of the aerated recharge water front.

Table 2-1 Equilibrated and charge balanced initial background and injectant water composition [mol L^{-1}, except pH, pe and temperature (in ºC)], initial mineral and bulk organic matter (BOM) concentrations [mol L^{-1}_{bulk}] and exchanger composition [mol L^{-1}]

Component /Mineral	Equilibrated Initial Background, Mineral and Bulk Organic Matter (BOM) concentrations and initial exchanger composition			Recharge Water
	Layer 1	Layer2-4	Layer 5	Conc. range
Temp	13.90	13.36	14.2	9.8 - 14.9
pH	7.2	7.2	7.18	7.5-7.88
pe	-3.9	-3.9	-3.9	13.6 - 15
Na	3.03×10^{-3}	1.99×10^{-3}	2.80×10^{-3}	$9.00 \times 10^{-4} – 3.70 \times 10^{-3}$
Ca	1.61×10^{-3}	1.66×10^{-3}	1.61×10^{-3}	1.45×10^{-3} - 1.54×10^{-3}
K	1.08×10^{-4}	1.87×10^{-4}	1.45×10^{-4}	1.61×10^{-4} - 1.73×10^{-4}
Mg	3.60×10^{-4}	5.50×10^{-4}	4.60×10^{-4}	4.43×10^{-4} - 4.71×10^{-4}
Cl	3.77×10^{-4}	2.11×10^{-4}	2.11×10^{-4}	2.45×10^{-4} - 2.83×10^{-3}
N(5)	0	0	0	4.85×10^{-5} - 4.89×10^{-4}
N(3)	0	0	0	0
N(0)	0	0	0	0
Amm	6.30×10^{-5}	5.40×10^{-5}	5.90×10^{-5}	0 - 4.26×10^{-6}
O(0)	0	0	0	2.71×10^{-4} - 3.25×10^{-4}
S(6)	9.40×10^{-11}	8.30×10^{-11}	9.16×10^{-11}	5.16×10^{-5} - 1.01×10^{-4}
S(2)	0	0	0	0
Fe(2)	4.70×10^{-5}	4.90×10^{-5}	4.80×10^{-5}	0
Fe(3)	0	0	0	2.69×10^{-7} - 1.24×10^{-6}
Si	3.50×10^{-4}	3.50×10^{-4}	3.50×10^{-4}	3.56×10^{-4} - 3.56×10^{-4}
C(4)	8.17×10^{-3}	7.97×10^{-3}	8.48×10^{-3}	4.76×10^{-3} - 5.49×10^{-3}
C(-4)	7.10×10^{-4}	3.90×10^{-4}	4.30×10^{-4}	0
Mn(2)	5.30×10^{-6}	3.90×10^{-6}	3.50×10^{-6}	0 - 4.37×10^{-7}
Mn(3)	0	0	0	0
As(3)	1.00×10^{-8}	1.00×10^{-8}	1.00×10^{-8}	0
As(5)	0	0	0	1.00×10^{-8}
Pyrite	0.0081	0.0081	0.04	n.a.
BOM	0.548	0.22	0.146	n.a.
$Fe(OH)_3(a)$	0	0	0	n.a.
$CaCO_3$	0.106	0.106	0.106	n.a.
$MnCO_3$	3.3×10^{-6}	3.3×10^{-6}	3.3×10^{-6}	n.a.
Total CEC	0.023	0.023	0.072	n.a.

2.2.3 MODELING FRAMEWORK

Simulations were carried out with the reactive multi-component transport model PHT3D (Prommer et al. 2003), based on flow fields computed with MODFLOW. In the first step, a flow and non-reactive transport model was developed to realistically represent the flow pattern created by the deep-well injection and recovery scheme (Figure 2.1). The conceptual hydrogeological model was adopted from Stuyfzand and Timmer (1999). The resulting flow model served as a basis for the subsequent transport simulations. Addition of NaCl during the first 30 days of the injection trial at approximately 10 times the ambient chloride concentration provided an ideal tracer to establish groundwater travel times. The flow and non-reactive transport model were jointly calibrated using measured Cl as a primary constraint. The model was then extended to include reactive multi-component transport. A reaction network was developed which enabled the simulation of the major ion and redox chemistry as well as the evaluation of various conceptual models for arsenic release and sorption.

2.2.4 REACTION NETWORK

The reaction network includes equilibrium-based speciation of all major ions, cation exchange processes and redox reactions. The observed temporary simultaneous presence of Fe^{2+}, NO_3^- and O_2 in the aquifer indicated deviations from redox equilibrium. Therefore Fe(II) was excluded from redox equilibrium and the oxidation of ferrous iron was modeled as a kinetically controlled reaction, employing the rate law of Singer and Stumm (1970) for mildly acidic to neutral water (pH >3.5), modified by the inclusion of an additional rate dependency on nitrate, as discussed in Eckert and Appelo (2002).

$$-\frac{dFe}{dt} = k[OH^-]^2(733C_{O_2} + C_{NO_3^-})C_{Fe^{2+}} \quad (1)$$

where k is the rate constant, P_{O_2} the partial pressure of oxygen, and OH^- the hydroxyl ion activity. C_{O_2}, $C_{Fe^{2+}}$ and $C_{NO^{3-}}$ are the concentrations of oxygen, nitrate and ferrous iron. The oxidized iron was assumed to precipitate as ferrihydrite ($Fe(OH)_3$). Methane was also excluded from redox equilibrium to inhibit the locally occurring, but unrealistic, oxidation by sulfate under redox equilibrium conditions.

Based on the results of the sediment analysis, calcite ($CaCO_3$) and rhodochrosite ($MnCO_3$) were included in the reaction network and allowed to dissolve and/or precipitate during the injection trial. Reaction rate laws for these were developed based on Plummer et al. (1978) for calcite and the standard formulation for dissolution and precipitation of minerals otherwise:

$$R_k = k_k\left(1-\left(\frac{IAP}{K_{SP}}\right)\right) \tag{2}$$

where k_k is an empirical constant and IAP/K_{SP} is the saturation ratio. Kinetic reactions were formulated for the oxidation of organic matter by oxygen, nitrate or sulphate, simulated based on the Monod-type rate expression described by Parkhurst and Appelo (1999):

$$r_{DOC} = \left[k_{O_2}\frac{C_{O_2}}{2.94\times10^{-4}+C_{O_2}} + k_{NO_3^-}\frac{C_{NO_3^-}}{1.55\times10^{-4}+C_{NO_3^-}} + k_{SO_4^{2-}}\frac{C_{SO_4^{2-}}}{1.0\times10^{-4}+C_{SO_4^{2-}}}\right] \tag{3}$$

where r_{DOC} is the overall degradation rate of organic matter, k_{O_2}, $k_{NO^{3-}}$, $k_{SO_4^{2-}}$ are the rate constants of carbon mineralisation under aerobic, denitrifying and sulphate-reducing conditions and C_{O_2}, $C_{NO^{3-}}$, $C_{SO_4^{2-}}$ are the concentrations of oxygen, nitrate and sulphate in the groundwater. The temperature-dependency of this reaction (Prommer and Stuyfzand 2005) was not included, based on comparative simulations (not shown), which demonstrated negligible difference in simulated concentrations due to the stable groundwater temperature over time at the site. Pyrite oxidation by oxygen and nitrate was included in the reaction network, based on previously proposed and applied rate expressions (Williamson and Rimstidt 1994, Eckert and Appelo 2002, Prommer and Stuyfzand 2005).

$$r_{pyr} = \left[\left(C_{O_2}{}^{0.5} + f_2 C_{NO_3^-}{}^{0.5}\right)C_{H^+}{}^{-0.11}\left(10^{-10.19}\frac{A_{pyr}}{V}\right)\left(\frac{C}{C_0}\right)_{pyr}^{0.67}\right] \tag{4}$$

where r_{pyr} is the specific oxidation rate for pyrite, C_{O_2}, $C_{NO_3^-}$ and C_{H^+} are the oxygen, nitrate and proton groundwater concentrations, A_{pyr}/V is the ratio of mineral surface area to solution volume and (C/C_o) is a factor that accounts for changes in A_{pyr} resulting from the progressing reaction. f_2 is a constant, which was assumed to be unity, as in previous work (Eckert and Appelo 2002, Prommer and Stuyfzand 2005).

2.2.5 ARSENIC RELEASE

The dissolution of sulfide minerals, most notably As-rich pyrite, containing up to 10 wt% arsenic, and arsenopyrite, is generally regarded as a primary source for As where oxic groundwaters are brought into contact with the sediments (Welch et al. 2000, Sracek et al. 2004, Plant et al. 2007, Price and Pichler 2006). The same mechanism was considered to cause elevated arsenic concentrations during the present experiment, with arsenic detected in pyrite in significant amounts (Arthur 2002). Prior to injection, pyrite was stable while in contact with the highly reducing native groundwater and ferrihydrite was undersaturated (SI = -5.2). With the commencement of injection, the redox conditions became gradually more oxidising, triggering pyrite dissolution. Subsequently, trace metals associated with pyrite, including As, were released. Simultaneously, ferrous iron in the native groundwater and, more importantly, from pyrite dissolution was oxidized and precipitated as ferrihydrite (hydrous ferric oxides, HFO).

Initial release of arsenic is likely to occur as As(III) under the prevailing redox conditions (e.g. Nesbitt et al. 1995, Walker et al. 2006). Based on the above, arsenic release was linked to pyrite oxidation at a molar ratio of 0.0053, as established from the aqua regia extractions. Accordingly, As release was simulated through arsenopyrite dissolution that was stoichiometrically linked to the computed pyrite oxidation rate.

2.2.6 ARSENIC SORPTION

Sorption of arsenic was assumed to occur as a surface complexation reaction with neo-precipitated ferrihydrite inside the oxidized zone of the aquifer. The generalized two-layer surface complexation model of Dzombak and Morel (1990) for sorption on ferrihydrite was employed, extended by reactions for Fe^{2+} and HCO_3^- (Appelo et al. 2002). This allowed competitive sorption between arsenic and other ions for a finite number of sorption sites to be considered. The successively increasing sorption capacity provided by increasing

amounts of ferrihydrite was modeled by coupling the moles of the surface complex to the mass of ferrihydrite. The properties of ferrihydrite were defined according to the values proposed by Dzombak and Morel (1990), i.e., weak and strong site densities were 0.2 and 0.005 mol/mol of ferrihydrite, respectively and a surface area of 600m^2 g^{-1}.

2.2.7 EQUILIBRIUM CONTROLLED ARSENIC OXIDATION

In the first investigated conceptual model arsenic redox status and speciation were simulated assuming local redox equilibrium. Arsenic, released as As(III), transformed over time to As(V) under the progressively more oxidizing conditions. Based on work by Dixit and Hering (2003), Stollenwerk et al. (2007) and others it is expected, that under the neutral pH conditions and the relatively low As concentrations found at the Langerak site, As(III) has a relatively lower adsorption affinity for HFO than As(V). Thus, As would have remained in solution until arsenate, which readily adsorbs onto the steadily increasing amount of neo-formed HFOs, became immobilized.

2.2.8 ABIOTIC, KINETICALLY CONTROLLED ARSENIC OXIDATION

Deviation from equilibrium controlled arsenic speciation, however, is commonly observed and the rate of oxidation of As(III) in groundwater is considered to be slow (Smedley and Kinniburgh 2002). A large body of literature suggests arsenic speciation in natural flow systems to be influenced or controlled by abiotic oxidation processes and a model, which includes kinetically controlled arsenic oxidation was developed. The redox status of arsenic was disconnected from the overall redox equilibrium and a kinetic rate expression was defined to describe the transfer from As(III) to As(V).

Abiotic As(III) oxidation has been attributed to MnO_2 (Manning et al. 2002a, Amirbahman et al. 2006, Oscarson et al. 1981), iron oxides and Fe(II) (De Vitre et al. 1991, Manning et al. 2002b, Hug and Leupin 2003, Leupin and Hug 2005). The most likely electron acceptors for As(III) at the Langerak site are freshly precipitated Mn and Fe-oxides. Based on batch experiments that reported the interactions of arsenic with pyrolusite (Radu et al. 2008), arsenic oxidation was modelled as a second-order kinetic reaction:

$$\frac{\partial As(III)}{\partial t} = -k \times C_{As(III)} \times C_{oxidant} \qquad (5)$$

where $C_{As(III)}$ and $C_{oxidant}$ are the arsenite and oxidant concentrations and k is the second-order rate constant.

2.2.9 BIOLOGICALLY MEDIATED ARSENIC OXIDATION

Besides abiotic arsenic oxidation, several microbial respiratory and non-respiratory enzymatic systems influencing the oxidation state of arsenic have been reported (Oremland and Stolz 2003). Physiologically diverse, they include both heterotrophic and chemolithoautotrophic arsenite oxidizers, with the oxidation being either a metabolic or a detoxification mechanism. Based on Oremland and Stolz (2003), a numerical model was developed, which describes the microbial dynamics by quantifying microbial growth and decay of a single group of specific arsenite oxidizers. Growth rates were assumed to depend on the availability of As(III) (electron donor) and nitrate (electron acceptor), with the energy derived being used to fix carbon into organic cellular material and to maintain growth according to:

$$6NO_3^- + 5HCO_3^- + 19H_2AsO_3^- \rightarrow C_5H_7O_2N + 5NO_2^- + 2H_2O + 19HAsO_4^{2-} + 13H^+ \qquad (6)$$

The mass balance of the arsenic oxidizing microbial group is:

$$\frac{\partial X}{\partial t} = \left.\frac{\partial X}{\partial t}\right|_{growth} + \left.\frac{\partial X}{\partial t}\right|_{decay} \qquad (7)$$

with microbial growth simulated using a standard Monod-type growth model and a first-order biomass decay term:

$$\left.\frac{\partial X}{\partial t}\right|_{growth} = \nu_{\max} X \frac{C_{As(III)}}{K_{As(III)} + C_{As(III)}} * \frac{C_{NO3-}}{K_{NO3-} + C_{NO3-}} \qquad (8)$$

$$\left.\frac{\partial X}{\partial t}\right|_{decay} = -\nu_{decay} X \qquad (9)$$

where X , $C_{As(III)}$ and C_{NO3-} are the microbial arsenite and nitrate concentrations respectively, and v_{decay} and $v_{\max}$ are the decay and uptake rate constants, respectively. More details are discussed elsewhere (Prommer et al. 2002).

The biologically mediated and abiotic arsenic oxidation model variants also included the previously described mechanisms for initial arsenic release from pyrite and its subsequent removal by the complexion to ferrihydrite. Rate constants for kinetic processes are based on literature values, where applicable, and used as fitting parameters during model calibration (Table A-2, Appendix A). Thus, the kinetic rate constants are relevant for the site specific conditions at the Langerak site, but may not be transferable to other environments.

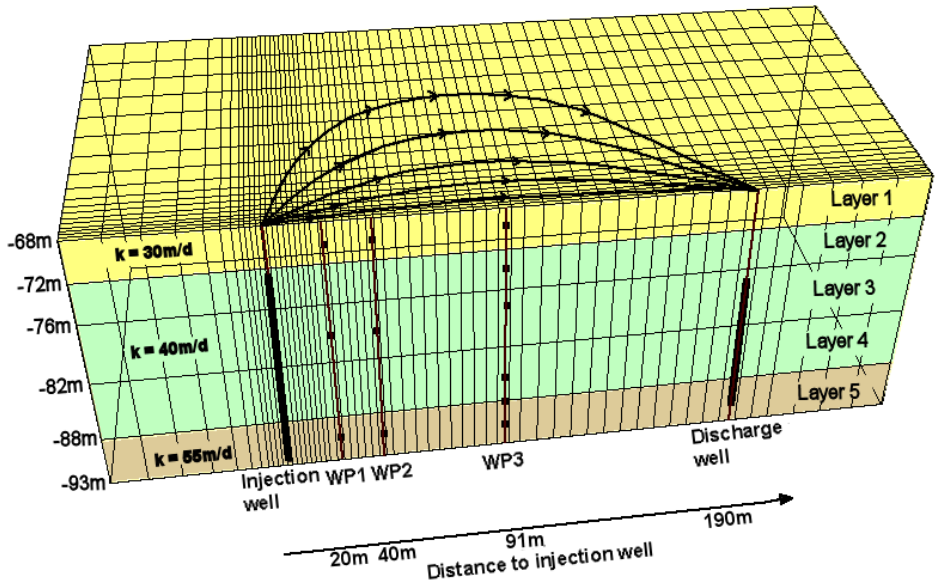

Figure 2-1 Schematized cross section of the modeled aquifer, showing position of injection, abstraction and monitoring wells (WP1-3) and their well screens. Also shown are model discretization and hydrostratigraphic zones with their permeability distributions. Projected pathlines with arrowheads for every 100 days of travel time indicate groundwater flow direction between injection and abstraction well.

2.3 RESULTS AND DISCUSSION

2.3.1 NONREACTIVE TRANSPORT

The calibrated nonreactive transport model replicates the observed chloride concentrations closely (Figure A-2, Appendix A). Hydrodynamic dispersion leads to the downstream dissipation of the chloride peak, which resulted from the temporary addition of NaCl to the injection water. Calibration of the nonreactive transport model was achieved with only minor changes to the originally proposed distribution of hydraulic conductivities at the field site and adjustment of dispersivities, confirming the validity of the conceptual hydrogeological model.

2.3.2 MAJOR ION AND REDOX CHEMISTRY

After model calibration, the comparison of simulated and observed breakthrough curves at various depths and distances from the injection well showed a close agreement for most aqueous components, illustrating that the model provides a good representation of the key processes that influenced the major ion and redox chemistry during the experiment. Oxidation of pyrite exerts the strongest influence on solution redox chemistry, as exhibited by diminishing O_2 and NO_3^- and increasing SO_4^{2-} concentrations. A comparison of nonreactive and reactive simulation results (Figure 2.2) shows that breakthrough of nitrate was substantially affected by denitrification, leading to complete nitrate removal within short distances from the injection well. Similarly, the comparison indicates the extent to which SO_4^{2-} concentrations were impacted by pyrite oxidation. SO_4^{2-} release is well described by the model in all observation wells at all depths.

Following pyrite oxidation, ferrous iron that was present in the groundwater, but also freshly produced, became oxidised and precipitated as ferric hydroxides in the expanding oxidized zone of the aquifer. Simultaneously, cation exchange resulted in desorption of Fe^{2+}, Mn^{2+} and NH_4^+. Comparison of breakthrough curves of redox sensitive species shows good agreement for NH_4^+, methane and Fe^{2+}. However, ferrous iron concentrations in the groundwater vary spatially up to one order of magnitude and an accurate simulation for all bores was difficult. Reactions involving carbonates were of lesser importance overall, and were well reproduced by the model and are not further discussed here.

2.3.3 ARSENIC RELEASE AND TRANSPORT

Initial model runs included only stoichiometric release of As during pyrite dissolution, but no attenuation by sorption. For this base case, the simulated As breakthrough is shown in Figure 2.3a. The modelled concentration of As mirrors that of SO_4^{2-} as both parameters reflect the temporally varying pyrite oxidation rates in response to nitrate input variations in the injectant.

2.3.4 EQUILIBRIUM SORPTION OF AS TO FRESHLY PRECIPITATING FERRIHYDRITE

Assuming equilibrium-controlled arsenic speciation, arsenic complexation to freshly precipitated iron oxides was implemented, following its stoichiometric release from pyrite. In stark contrast to the observed data, which shows arsenic to be high initially, before decreasing substantially, the inclusion of surface complexation reactions resulted in strong arsenic affinity for the aquifer sediments and subsequently rapid and complete removal from solution (Figure 2.3a). Through comparative simulations it was found, that neither changes in sorption sites, sorption densities nor pyrite-bound arsenic content would allow the model to reproduce observed concentrations. However, when sorption onto ferrihydrite was assumed to be delayed by a pre-defined lag-time, the model correctly describes both, the appearance and disappearance of arsenic as well as its peak concentrations (Figure 2.3a).

An explanation for delayed sorption of arsenic onto ferrihydrite could be slow sorption kinetics as described in Fuller et al. (1993). However given the comparatively long solute residence times in relation to the adsorption process, the relatively low arsenic concentrations at the site and the fact that sorption takes place to freshly precipitated HFO rather than aged oxides this appears unlikely. The well documented slow redox transformation of arsenic (e.g., Cutter 1992, Plant et al. 2007) however, are a more likely explanation at the Langerak site. The released As(III) with its relatively lower adsorption affinity to HFO at neutral pH and relatively low As concentrations (Dixit and Hering 2003; Stollenwerk et al. 2007) would have allowed arsenic to remain in solution until As(V) became the prevalent chemical species under the progressively more oxidising conditions. As(V) would have readily adsorbed onto the steadily increasing amount of neoformed HFOs, and thus immobilized. This was tested through kinetically controlled arsenic oxidation models, as described below.

2.3.5 KINETICALLY CONTROLLED AS(III) OXIDATION

Kinetically controlled arsenic oxidation was simulated in two different scenarios as (i) abiotic oxidation by iron or manganese oxides and (ii) biologically mediated As(III) oxidation. The results of the final calibrated models are presented in Figure 2.3b. Both models showed arsenic concentrations increased synchronously with the arrival of the aerated water. As(III) initially remained the dominant species after its release from pyrite due to the slow, kinetically controlled transformation of As(III) to As(V). Following arsenic breakthrough, concentrations decreased successively as As(V) adsorbed to the neoformed ferrihydrite. Arsenic which escaped sorption by migrating past the HFO-containing zone dissipated during aquifer passage and the initially sharp arsenic front flattened successively with increasing travel distance. In this case the simulated As breakthrough behavior correlated with the observations (Figure 2.3b).

While the principle behaviour could be reproduced with the initial model parameterization, the model fit was improved when (i) the molar ratio of As to FeS_2 was increased to 0.0083, attaining higher peak concentrations and (ii) the surface complexation constant for arsenate adsorption to ferrihydrite ($HFO\_wOH + AsO_4^{-3} = HFO\_wOHAsO_4^{-3}$) was adjusted from 10.58 (Dzombak and Morel 1990) to 11.88. A similar modification of the reaction constant was required in the work of Moldovan and Hendry (2005), who investigated arsenic solubility at field-scale.

2.3.6 EVALUATION AND IMPLICATIONS

The reactive transport simulations provided a detailed description of the processes affecting the spatial and temporal hydrochemical changes that occurred during the deep-well injection experiment, in particular those induced by pyrite oxidation. This provided a solid foundation to evaluate and quantify the hydrochemical processes that are likely to control the observed fate of arsenic during the field experiment. The simulation results demonstrated that arsenic sorption at the start of the injection trial was delayed. Redox equilibrium-controlled arsenic speciation in conjunction with sorption to ferrihydrite was unable to explain this breakthrough behavior at the monitoring wells. In contrast, model results indicated, that sluggish redox transformation of As is a possible explanation for the increased mobility of As at the start of the injection trial. Both models involving kinetically controlled As redox transformations (i.e. biotic and abiotic) reproduced the general pattern of observed concentrations.

An obvious shortcoming of the present study is that simulations could only be constrained by total arsenic concentrations. Kinetic redox transformation had to be inferred based on the well documented slow redox kinetics of arsenic in natural environments and presents the most likely explanation for delayed attenuation of arsenic under the geochemical conditions at the site. However, the complexities of sorption on aquifer solids rather than synthetic minerals at environmentally relevant As concentrations and in the presence of competing anions are poorly understood at present and the assumptions employed in the model may not apply universally. Nevertheless, reactive transport modelling has proven to be a valuable tool in integrating some of the known feature of arsenic behaviour and to speculate about critical factors that can lead to elevated As concentrations. The study illustrates that arsenic behaviour can be tested and evaluated numerically for complex field scale systems, where physical transport as well as geochemical processes similarly affect concentration changes. The developed conceptual models should serve as hypotheses to be further tested and amended by future detailed field and laboratory investigations.

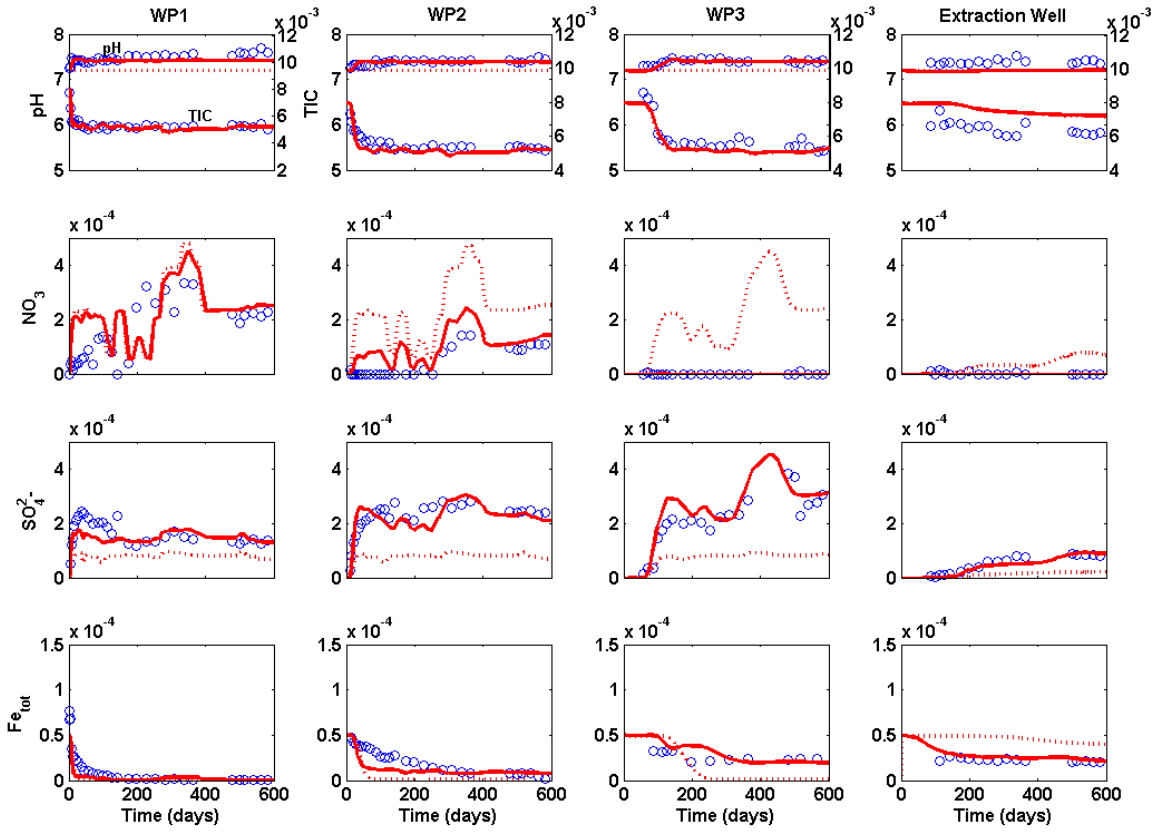

Figure 2-2 Measured (circles) and simulated (solid lines) concentrations (mol L^{-1}, except pH) of aqueous components at WP1, WP2, WP3 in centre of the aquifer (Layer 3) and in the extraction well. Dotted lines indicate simulated results of the non-reactive model.

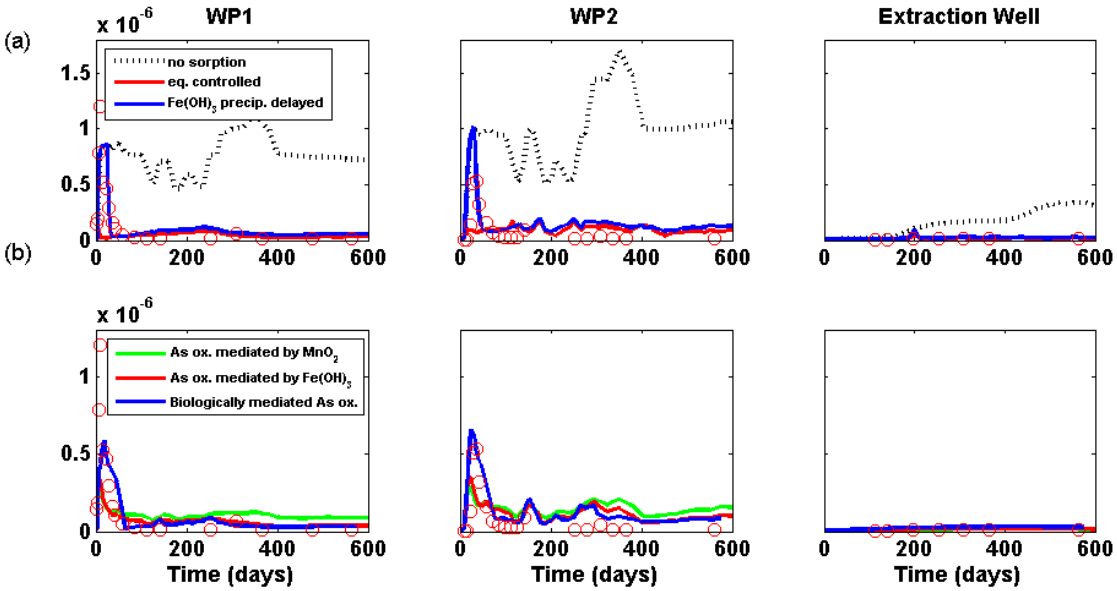

Figure 2-3 Simulated (solid lines) and observed (circles) total arsenic concentrations (mol L^{-1}) for WP1, WP2 and the extraction well for the deep part of the aquifer (Layer 5). (a) black line: no attenuation by sorption, red line: equilibrium sorption of As to $Fe(OH)_3$, blue line: sorption onto $Fe(OH)_3$ delayed by pre-defined lag-time. (b) red line: abiotic oxidation of As(III) by $Fe(OH)_3$, green line: abiotic oxidation of As(III) by MnO_2, blue line: biologically mediated As(III) oxidation.

ACKNOWLEDGEMENTS

This contribution received very valuable input from David Kinniburgh, Jim Davis, Paul Shand and Peter Franzmann. We also thank three anonymous reviewers for their constructive reviews. Financial support was provided by Land and Water Australia, Water for a Healthy Country Flagship (CSIRO Australia) and the Centre for Groundwater Studies, which is gratefully acknowledged. The authors also kindly acknowledge Schlumberger Water Services for GUI support.

Chapter 3. A PROCESS-BASED REACTIVE TRANSPORT MODEL TO QUANTIFY ARSENIC MOBILITY DURING AQUIFER STORAGE AND RECOVERY OF POTABLE WATER

ABSTRACT

Aquifer storage and recovery (ASR) is an aquifer recharge technique in which water is injected in an aquifer during periods of surplus and withdrawn from the same well during periods of deficit. It is a critical component of the long-term water supply plan in various regions, including Florida, USA. Here, the viability of ASR as a safe and cost-effective water resource is currently being tested at a number of sites due to elevated arsenic concentrations detected during groundwater recovery. In this study, we developed a process-based reactive transport model of the coupled physical and geochemical mechanisms controlling the fate of arsenic during ASR. We analyzed multi-cycle hydrochemical data from a well-documented affected southwest Floridan site and evaluated a conceptual/numerical model in which (i) arsenic is initially released during pyrite oxidation triggered by the injection of oxygenated water (ii) then largely complexes to neo-formed hydrous ferric oxides before (iii) being re-mobilized during recovery as a result of both dissolution of hydrous ferric oxides and displacement from sorption sites by competing anions.

3.1 INTRODUCTION

Aquifer storage and recovery (ASR) is an aquifer recharge technique in which potable, reclaimed or other water sources are injected into aquifers during periods of surplus and withdrawn from the same well during periods of deficit. In cases where oxic water is recharged into reducing aquifers, however, mobilization of trace metals may occur as a result of the oxidation of iron-sulfides or other reductants.

The interest in ASR as a critical component of long-term water supply strategies has increased in recent years. For example in Florida there are more than 50 ASR facilities in operation or permitted for construction (ASRSystems 2007) to compensate for seasonal imbalances between water supply and demand. Typically, these ASR operations involve the periodic injection of oxygenated water into the anoxic upper Floridan Aquifer System (FAS) and its later withdrawal. The viability of ASR as a safe and cost-effective water resource is currently being tested due to elevated arsenic (As) concentrations found at many sites

(Stuyfzand 2008). While in general, neither the injected water nor the native groundwater has any appreciable concentrations of As, concentrations in the recovered water are reported to be elevated, often above the U.S. drinking water standard of 10 µg L^{-1} (Arthur et al. 2002).

A range of conceptual/numerical models for arsenic release and attenuation during ASR or similar push-pull operations were previously proposed. For example Appelo and de Vet (2003) reported elevated As concentrations during *in-situ* iron removal operations in the Netherlands, where oxygenated water was recharged into an anoxic siliclastic aquifer. The results of their geochemical modeling suggested that at their site competitive displacement of As by native groundwater containing phosphate was the most likely As release mechanism during the recovery phases. The same mechanism was suggested by Vanderzalm et al. (2011) for an ASR site in Australia where reclaimed water was injected into a reducing carbonate aquifer. Studies by Stuyfzand and Timmer (1999) and Wallis et al. (2010) investigated elevated As concentrations at an aquifer storage transfer and recovery (ASTR) site in a siliclastic aquifer. Here, As release was closely associated with the oxidation of pyrite upon injection of oxygenated water. Under the progressively expanding oxic conditions, ferrous iron released during pyrite dissolution oxidized and precipitated as hydrous ferric oxides (HFO), thereby providing a successively increasing number of sorption sites for As. This was thought to be the key attenuation mechanism that caused elevated As concentrations to diminish to background concentrations after an initial period of elevated As concentrations close to the injection well.

For the aquifers selected by ASR operations in Florida, mineralogical and geochemical studies by Price and Pichler (2006) and Jones and Pichler (2007), also suggested As-bearing pyrite to be the most likely source of As and sorption to neo-precipitated HFO to be the most likely arsenic attenuation mechanism during injection. However, the reversal of flow during the recovery phase causes a reversal to anoxic conditions that is thought to be responsible for the observed remobilization of arsenic (Stuyfzand 2008; Mirecki 2006; Norton 2007). Several alternative or complementary processes explaining this remobilization have been postulated. Mirecki (2006) suggested the liberation of As to be associated with reductive dissolution of neo-precipitated HFO under sulfate-reducing conditions and the associated destruction of sorption sites. The instability of HFO during recovery was supported by inverse geochemical modeling. However, the calculated mass of HFO was minor, questioning the capacity of the aquifer material to effectively sorb and release the arsenic concentrations measured during cycle testing (Mirecki 2006). It was also

speculated that arsenate may transform into arsenite under the reducing conditions, thus enhancing arsenic mobility due to diminished sorption affinity of As(III) on aquifer material compared to As(V). Stuyfzand (2008) suggested the displacement of sorbed As by competing anions as a possible additional release mechanism.

For future design and operation of efficient and sustainable ASR facilities it is essential to have a clear understanding of the fundamental geochemical processes that control the mobility of As during ASR operations. In this study our aim was (i) to develop a numerical model that provides a process-based description of the physical and geochemical processes controlling the fate of arsenic during ASR and (ii) to test it for a comprehensive long-term field data set collected at an affected site in Florida.

3.2 MATERIALS AND METHODS

3.2.1 FIELD SITE USED FOR MODEL EVALUATION

Among the ASR sites reporting elevated As concentrations in the recovered water, the City of Bradenton ASR facility in southwest Florida was selected to evaluate the proposed model, because it offers a comparably comprehensive geochemical database and a well-defined site hydrogeology that is underpinned by geological and geophysical logs. The storage zone at the site is the Suwannee Limestone of the Upper Floridan Aquifer. The Suwannee Limestone is comprised primarily of carbonates, which contain clays intermixed with limestones near the formation top, and a thin layer of dolostone in the lower third (Arthur et al. 2001). Minor amounts of clay minerals and organic material, and trace amounts of quartz, gypsum, and pyrite are present (Arthur et al. 2001). Pyrite is ubiquitous throughout the Suwannee Limestone, but is most abundant in high porosity zones and is generally As-rich with concentrations between 100 and 11200 ppm (average: 2300 ppm), while iron-oxides are absent (Price and Pichler 2006). The ASR storage zone at the site is confined and separated from the overlying superficial aquifer by interbedded carbonates, sands, and clays of the Hawthorn Group and overlies the chalky, fine- to coarse-grained Ocala Limestone. Based on flow meter measurements, it can be assumed that the ASR storage zone at the study site is relatively homogenous except for a distinctly more permeable horizon at ~18 m below the top of the Suwannee Limestone (Norton 2007). The Bradenton ASR system consists of a single ASR well, and an observation well located at a distance of 68 m (Figure B-1, Appendix B). Seven ASR cycles were conducted since construction of the site in November 2003. The cycles varied considerably both in timing

and duration of the injection, storage and recovery phases (Figure B-2, Appendix B). They were documented by a monitoring program, as required by the Florida Department of Environmental Protection (FDEP) and water quality analysis followed the FDEP directions. The data are available from the FDEP (http://www.dep.state.fl.us/).

3.2.2 NUMERICAL MODEL APPROACH AND MODEL SETUP

From the hydrogeological site characterization and the records of observed hydrochemical changes during the Bradenton ASR operation, conceptual models for (i) the physical processes (flow and nonreactive transport) and (ii) the geochemical processes were formulated. They were implemented numerically using the USGS code MODFLOW in conjunction with the reactive multi-component transport code PHT3D (Prommer et al. 2003; Prommer and Stuyfzand 2005).

As (i) the native groundwater flow velocities are negligible compared to those induced by the ASR operation and (ii) the aquifer is expected to be homogeneous in lateral direction, the flow and transport conditions at the site were assumed to be radial-symmetric. In a first step, radial flow and non-reactive transport were simulated using a three-dimensional (3D) groundwater flow model that represents one-quarter of a radial-symmetric domain (Figure B-1, Appendix B). The 3D model has a lateral extension of 523.5 m in both x and y direction, selected such that boundaries were sufficiently far from the ASR well to not impact solute concentration fronts during the simulated ASR cycles. The Suwannee Limestone section targeted by the ASR operation (ca. 120 - 180 m below ground level) was separated into 7 layers (Figure B-1, Appendix B). The hydrogeological model and initial parameter estimates were based on geophysical log data and sedimentological characteristics of the aquifer (Norton 2007) (Table 3.1). The flow model was run for a simulation period of 1176 days, commencing with the start of the first ASR cycle and, therefore, pristine aquifer conditions. To represent the different phases of the ASR operation (i.e., storage, recharge and abstraction periods) the simulation time was discretized into 28 hydraulically and/or hydrochemically differing stress periods that varied in length between 5 and 423 days (Figure B-2, Appendix B). Based on this flow model, a nonreactive transport model was set up and successively improved. Sulfate was selected as the key species to identify and constrain physical transport processes. Using sulfate as a (pseudo-) conservative species was justified in this specific case because concentrations in the injectate are only approximately 20% of the native groundwater concentration and the impact of pyrite oxidation on sulfate concentration is minimal due to the high native concentrations (Figure

B-3, Appendix B). In contrast, differences in chloride concentration between the injectate and the groundwater were negligible and therefore chloride was found not to be a suitable tracer. The calibrated nonreactive model (Table 3.1) formed the basis for the subsequent reactive transport simulations. In order to reduce model execution times for the reactive transport simulations the 3D model was translated into a simpler two-dimensional quasi-radial flow/transport model (Figure B-4, Appendix B). Because the simulation of radial flow is not an explicit feature of the flow simulator MODFLOW, the radially decreasing flow velocities were obtained by a variable layer thickness that corresponds to the perimeter at the radial distance of the grid-cell centre, i.e., the distance from the ASR well, as discussed earlier by Greskowiak et al. (2005).

3.2.3 HYDROGEOCHEMICAL CHARACTERISTICS, CONCEPTUAL MODEL AND SELECTED REACTION NETWORK

The ASR operation involved the cyclic injection of oxygenated water into the reduced Suwannee Limestone aquifer. The native groundwater was clearly anoxic, as indicated by the presence of sulfide at low concentrations (~1.8×10^{-2} mmol L^{-1}). Its total dissolved arsenic concentrations (measured by ICP-MS) were below detection limit (DL) (DL varied between 1.3×10^{-6} and 3.7×10^{-5} mmol $L^{-1,}$) (Table 3.2). Concentrations of calcium (5.1 mmol L^{-1}) and bicarbonate (2.1 mmol L^{-1}) indicated mineral equilibrium with the limestone ($SI_{Calcite}$ 0.06) and the pH was found to range between 7.2 and 7.3. The injectate was sourced from surface water and pre-treated to potable quality. The chemical composition of the injectate differed clearly from the native groundwater and generally had an oxic character with dissolved oxygen concentrations varying between 0.23 and 0.34 mmol L^{-1}. NO_3 as a possible additional oxidant in the injectant water was not determined. The As concentrations in the recovered water exceeded the U.S. drinking water standard of 10 µg L^{-1} (1.3×10^{-4}mmol L^{-1}) in most cycles with maximum concentrations reaching 1.0×10^{-3} mmol L^{-1} (75 µg L^{-1}).

Three different mechanisms of arsenic release were thought to be operative. First, during injection, under progressively more oxidizing conditions, As-rich pyrite becomes unstable and releases arsenic and potentially other trace metals. Simultaneously; ferrous iron released during pyrite oxidation is oxidized and precipitates as HFO, providing sorption sites for arsenic.

Secondly, during recovery, when high TDS, reducing native groundwater passes back towards the ASR well, competition between As and other anions for the finite number of

sorption sites on HFO releases As by desorption. Finally, the third release mechanism is the reductive dissolution of HFO under the progressively more reducing redox conditions. Potential reductants of iron oxides are hydrogen sulphide as well as dissolved organic carbon (DOC). However, the latter, where present, was thought to be largely recalcitrant given that despite the presence of sulfate in the ambient water, neither sulfate reduction nor an increase in TIC over time can be observed. Also, measured TOC concentrations during recovery were similar to the concentrations measured in the injectant (average of 0.22 mmol L^{-1} and 0.27mmol L^{-1}, respectively). Thus, water-sediment interactions were considered to be the key reactions affecting water chemistry evolution at the Bradenton site, while homogeneous reactions, as they could occur for example in the presence of labile DOC, were assumed to be of minor importance. Based on this hypothesized conceptual model derived from the hydrochemical monitoring results and the geochemical characterization of the Suwannee Limestone (Price and Pichler 2006), a corresponding reaction network of mixed equilibrium and kinetic reactions was formulated.

MINERAL REACTIONS

The mineral assemblage considered in the reactive transport simulations included calcite ($CaCO_3$), siderite ($FeCO_3$), pyrite (FeS_2) and amorphous HFO ($Fe(OH)_3$), based on the results of sediment analysis (Price and Pichler 2006), and on calculated saturation indices of the native water. Pyrite oxidation by oxygen was modeled as a kinetic reaction following Williamson and Rimstidt (1994), while all other minerals were included as equilibrium reactions (thermodynamic data taken from the PHREEQC standard database). The release of As was stochiometrically linked to pyrite oxidation, as described in Wallis et al. (2010) and Descourvieres et al. (2010), with the molar ratio of As to FeS_2 based on data by Price and Pichler (2006) (Table 3.1, Figure B-5, Appendix B).

SURFACE COMPLEXATION AND ION EXCHANGE REACTIONS

The dynamic changes in the sorption capacity that result from the precipitation and dissolution of HFO play a key role in explaining the observed As behavior. This process was modeled by coupling the moles of the surface complex sites to the mass of HFO in the aquifer (Wallis et al. 2010). The database of Dzombak and Morel (1990) for sorption on HFO was employed, extended by reactions for Fe^{2+} and HCO_3^- (Appelo et al. 2002) to allow for competition of inorganic solute species for the sorption sites provided by HFO. The

properties of HFO were defined according to the values proposed by Dzombak and Morel (1990). However, the amount of sorption sites on HFO in the sediment is not known and it is probably not identical for amorphous oxides and more crystalline aged oxides (Appelo et al. 1999). The number of sorption sites on HFO was therefore used as a fitting parameter. In addition, one cation exchanger site was included to account for the exchange of cations and hydrogen on clay surfaces.

REACTION PARAMETER CALIBRATION

The selected reaction network was kept as simple as possible and was mainly based on equilibrium reactions. Thus, the model only includes a limited number of adjustable parameters (Table 3.1). These include the stoichiometric ratio of As within pyrite, the initial concentrations of pyrite in the aquifer matrix and the sorption site density of HFO. Matching simulated and measured oxygen, ferrous iron and total As concentrations served as the main constraint for the estimation of these parameters. In case of the initial pyrite concentration and the As-FeS_2 stoichiomtric ratio trialed values were kept within the range reported by Price and Pichler (2006) (Table 3.1, Figure B-5, Appendix B).

3.2.4 NATIVE GROUNDWATER, INJECTATE AND AQUIFER MATRIX COMPOSITION

The physicochemical composition of the waters were based on the data published by the FDEP. The reported analyses were obtained during cycle tests primarily to assess ASR system performance and to ensure that recovered water meets state and federal drinking-water-quality criteria (Norton 2007). The Bradenton site geochemical dataset was comprehensive in comparison to other ASR facilities in southwest Florida, but still exhibited data gaps. For example, not all major and minor ions were consistently analyzed and sampling frequencies differed between the ASR and observation well. Thus, native groundwater chemistry was inferred from the water composition measured at the monitoring well at the end of prolonged extraction periods (abstracted volumes $\geq$ injected volumes), when the measured concentrations indicated convergence towards a constant water quality. The modeled injectate water composition was generally based on the average of the water compositions measured at the ASR well during injection, although the documented variability of the oxygen concentrations in the injectate was considered. Water compositions were charge-balanced with PHREEQC-2 by adjusting the chloride

concentration. The measured and model input concentrations of the native water and injectate together with initial mineral and exchanger compositions are listed in Table 3.2.

Table 3-1 Calibrated Values of Adjustable Flow and Reaction Model Parameters and Parameter Values Reported in the Literature

Parameter	Unit	Value	Literature Values	Source[1)]
Flow model				
Hydraulic conductivity	[m d^{-1}]	4.75 (layer 1-2) 35 (layer 3-5) 1.6 (layer 6-7)	0.98 - 30	(1), (2)
Longitudinal dispersivity	[m]	1	-	model calibration
Vert./long. dispersivity ratio	-	0.1	-	model calibration
Effective porosity	-	0.2	0.19	(3)
Reactive Transport model				
Sorption site density on HFO: (1) weak sites (2) strong sites	[mol/mol HFO]	 (1) 0.06 (2) 0.0015	 (1) 0.2 – 0.066 (2) 0.005 – 0.00165	(4), (5)
Pyrite concentration (aquifer average)	[mg/kg]	819	276 – 32406	(6)
As in pyrite	[wt%]	0.5	0.01 – 1.12	(6)

References: (1): Norton (2007); (2) Pyne (2007); (3) Stuyfzand (2008), (4) Dzombak and Morel (1990); (5) Appelo et al (1999); (6) Price and Pichler (2006)

Table 3-2. Measured and modeled injectant and initial (i.e., native groundwater) concentrations of aqueous components, minerals and exchanger composition.

	Measured concentration [mmol L^{-1}][(1)]		Equilibrated and charge balanced initial model concentration [mmol L^{-1}][1)]	
	Native groundwater	Injectant [3)]	Native groundwater	Injectant
Aqueous components				
pH	7.2-7.3	7.3 – 7.9	7.3	7.7
pe	-	-	-3.7	13.0
C(4)	2.0– 2.1[4)]	0.97 – 1.2[4)]	2.38	1.04
C(-4)	-	-	$7.8x10^{-6}$	0.0
Ca	4.3-5.5	1.0 – 1.5	5.24	1.1
Na	1.0-1.1	2.0 – 2.3	1.09	2.0
Cl	0.93-1.3	0.73 – 1.0	1.00	0.91
Fe(2)	$<2x10^{-4}$-$<5.2x10^{-4}$	$<2x10^{-4}$-$<5.2x10^{-4}$	0.0	0.0
Fe(3)	-	-	0.0	0.0
K[5)]	0.09 – 0.1	0.049	0.098	0.049
Mg	2.8-3.3	0.33 – 0.63	3.2	0.354
O(0)	$3.1x10^{-4}$-$3.8x10^{-3}$	0.23 – 0.34	0.0	0.25 – 0.36
S(6)	6.5-7.5	1.5 – 2.1	7.4	1.56
S(-2)	$<1x10^{-2}$-$4.7x10^{-2}$	$<1x10^{-2}$	$1.8x10^{-2}$	0.0
As	$<4x10^{-5}$	$<4x10^{-5}$	0	0
Tmp.	26.0 -26.7	17.1 - 29.8	26.0	22.4
Initial exchanger composition (model)				
CaX2	18.1			
MgX2	6.6			
NaX	0.29			
KX	0.13			
FeX2	0.0			
Initial mineral concentrations (model)				
Pyrite (FeS_2)	0.000175 (layer 1-2) 0.016 (layer 3-5) 0.018 (layer 6-7)			
Calcite ($CaCO_3$)	0.53			
Ferrihydrite ($Fe(OH)_3$)	0.0			
Siderite ($FeCO_3$)	0.0			

1)Except temperature in [°C], minerals in [mol L^{-1} of bulk aquifer volume] and pH, pe
2) measured at observation well SZMW-1 at the end of abstraction, where abstraction volume > injection volume
3) measured at ASR well at the end of injection periods
4)HCO_3^-
5)K data from Jones and Pichler (2007)

3.3 RESULTS AND DISCUSSION

3.3.1 NATIVE GROUNDWATER, INJECTATE AND AQUIFER MATRIX COMPOSITION

The clear contrast between higher native and lower injectate sulfate concentrations was used to constrain the flow and physical transport behavior. Hydraulic conductivities as well as longitudinal and vertical dispersivities were adjusted until the simulated sulfate breakthrough curves fitted the corresponding observation data from both the ASR and the observation well (Table 3.1). In the calibrated model the simulated dynamic concentration changes are in good agreement with the measured data (Figure 3.1), including the rapid breakthrough of low sulfate water at the observation well. This rapid breakthrough is a result of the high permeability horizon that is present in the storage zone (35 m/d, model layers 3 to 5). In the calibrated model ~55% of the injected water penetrates through this section of the aquifer and accordingly the injectant plume front moves faster through this horizon during injection and recovery. The penetration distances of the plume (50% of ΔSO_4) during the longest injection cycle (cycle 6) is ~240 m within the high conductivity horizon while it is only ~120 m and ~70 m in the lower conductivity horizons above and below this zone, respectively. During the first four ASR cycles, all of which had similar injection/abstraction volumes, a freshening of the storage zone is evident from the successively lower measured and modeled sulfate concentrations at the observation well during injection.

3.3.2 REDOX ZONATION

The model simulations illustrate how aerobic water penetrated into the aquifer during the injection phase, thereby displacing the reducing native groundwater. With time pyrite oxidation consumed the oxygen of the injectate and caused the release of ferrous iron, which was subsequently oxidized and precipitated as HFO (Figure 3.2). The oxygen consumption rates and the resulting redox zonation varied as a result of the physical and chemical heterogeneity of the aquifer, i.e., the variability of the hydraulic conductivity and the estimated initial pyrite content. During the first five ASR cycles no oxygen breakthrough occurred at the observation well, as shown by both, measurements and simulations (Figure 3.1). However, during cycle 6, where injection continued for several months (total injected volume = 453×10^6 L) model simulations showed the breakthrough of low concentrations of oxygen (5.8×10^{-2} mmol L^{-1}). While oxygen breakthrough at the observation well was not detected, the simulated breakthrough corresponds with a distinct increase in measured

oxidation reduction potential (ORP) of up to 100 mV, which occurred during this cycle, while measured ORP values remained consistently below 0 mV during all other ASR cycles. We speculate that oxygen may have been diluted during sample recovery due to mixing within the well with water received from the more reducing aquifer sections. In the initial periods of each simulated recovery phase the recovered water consisted mainly of the oxygen depleted injectate, followed by a period during which increasing proportions of even more reducing native groundwater migrated back towards the ASR well. During recovery $Fe(OH)_3$ was partially depleted as a result of its reductive dissolution. Where the dissolution upon contact with the anoxic groundwater occurred, ferrous iron was released (Figure 3.1). It then complexed with carbonates and precipitated as siderite. In model simulations that did not consider siderite precipitation dissolved iron concentrations were considerably overestimated compared to the measured concentrations (results not shown). Overall the calibrated reactive transport model reproduced closely the observed redox patterns in both the ASR and the observation well.

3.3.3 ANALYSIS OF ARSENIC FATE

During the injection of aerated water, kinetically controlled oxidation of pyrite occurred where oxygen was not depleted. As was simultaneously released at a rate proportional to the simulated pyrite oxidation rate. The extent of the zone where pyrite oxidation and simultaneous As release occurred varied depending on aquifer transmissivity and pyrite content, i.e., over ~15 to 50 m at the end of the shorter injection cycles 1 to 4 (injected volume of 35 - 39 $\times$ 10^6 L/cycle) and over ~50 to 120 m at the end of the prolonged injection cycle 6. This is illustrated in Figure 3.2, which shows the simulated concentration profiles for oxygen and the corresponding simulated zone of pyrite oxidation for the high conductivity horizon. During injection, under predominantly oxic conditions the released As is transported as arsenate in radial direction away from the ASR well. Its migration, however, is strongly affected by sorption to HFO. This attenuation mechanism is effective in limiting the lateral migration of As and in maintaining dissolved As concentrations at a low level throughout the aquifer over the entire injection period. Over the duration of the 7 simulated ASR cycles, arsenic found in solution accounted on average for only 22% of the As released due to pyrite oxidation.

During the first and the following recovery phases, when the previously displaced anoxic native groundwater was drawn back towards the ASR well, the dissolution of HFO caused the release of sorbed As, mainly as arsenite, under the progressively more reducing

conditions. This resulted in increased total As concentrations in the recovered water, as illustrated in Figure 3.3. The plots show the simulated cumulative As mass as well as dissolved As concentrations at the ASR well for the first 4 ASR cycles and provides a detailed assessment of As partitioning among mineral phases, surface complexes and the aqueous phase and how the partitioning changes between injection, storage and recovery. During each cycle As concentrations continued to rise at the ASR well until the end of recovery, i.e., the maximum As concentrations were attained at abstraction/injection ratios of close to 100% or above. A survey of 52 ASR wells (ASRSystems 2007) shows this to be a common response at As affected ASR sites. However, comparative simulations (not shown) suggest the timing of the As peak to be strongly related to the redox conditions of the native groundwater, i.e., the more reducing the ASR target aquifer, the faster HFO dissolves during recovery events with As peak concentrations attained at recovery/injection ratios below 100%, a trend also commonly reported from affected sites (ASRSystems 2007).

The model simulations suggest that not all of the freshly accumulated HFO during injection phases became dissolved during recovery, except when abstraction volumes exceeded injected volumes. Subsequently, the total mass of HFO and, thus, the associated sorption capacity successively increased over time (Figure B-6, Appendix B). This resulted in an increased attenuation of As due to sorption to (i) neo-formed HFO surfaces and (ii) to previously precipitated but not subsequently dissolved HFO surfaces (Figure 3.3). Therefore the ratio of As mass mobilized during injection and that discharged during recovery varied. At the end of the model simulation, i.e., the end of ASR cycle 7, when ~116% of the total injected water volume was recovered, over 70 % (~48 mol) of the mobilized As mass was extracted. However, this amounts to only a small reduction of the total As mass prevailing in the target zone, as estimated based on the (initial) pyrite concentration. At the end of cycle 7, a predicted reduction of 6% of the total As mass occurred, from within a radius of 1.5 m around the ASR well, declining to ~0.5 % for a radial distance of 30 m (Figure B-7, Appendix B). This implies that slow “As flushing” of the target zone via repeated ASR cycles is in principle possible, but not very effective.

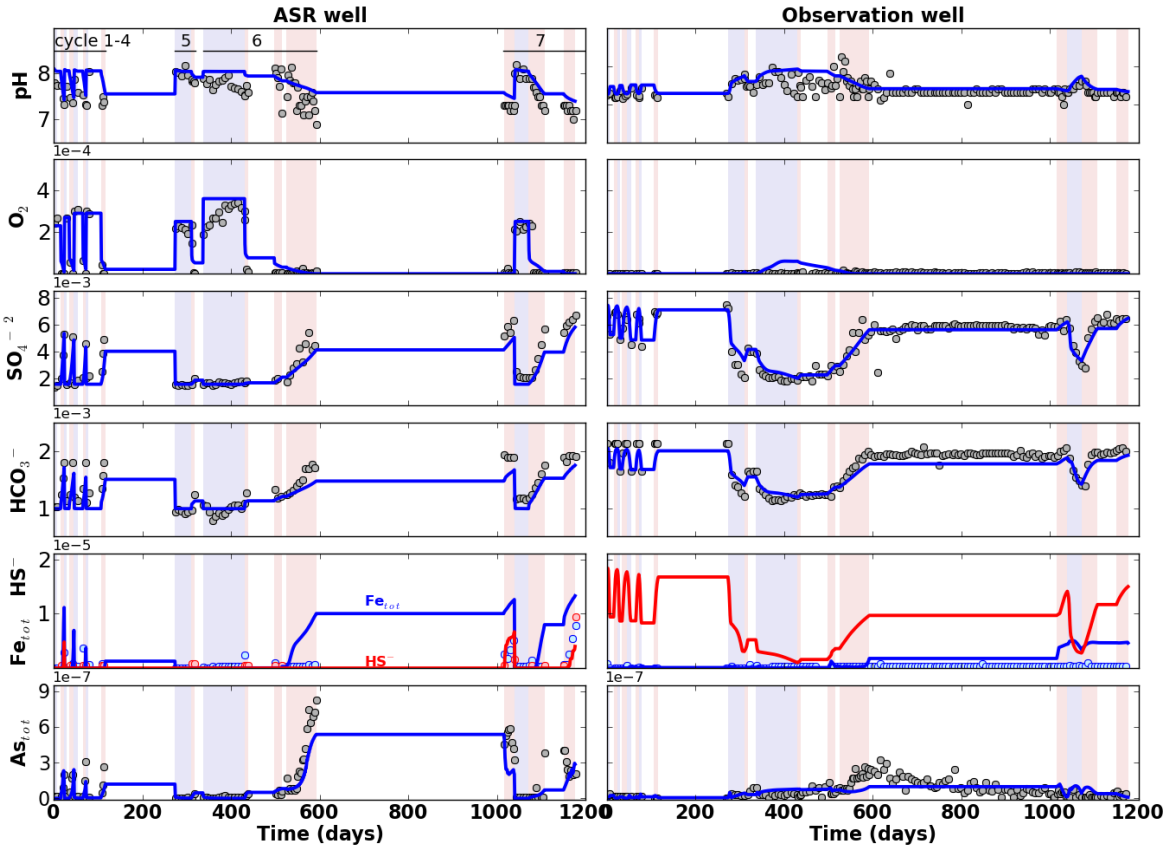

Figure 3-1. Measured (circles) and simulated (solid lines) aqueous concentrations of pH and selected ions for the 7 simulated ASR cycles. Injection periods are marked in light blue, recovery phases in light red and inter-cycle storage periods in white. Concentrations are in mol L^{-1}, except pH.

3.3.4 TRANSFERABILITY OF CONCEPTUAL/NUMERICAL MODEL TO OTHER ASR SITES

The numerical model developed based on the data collected at the Bradenton site describes a system where oxic potable water is injected into an aquifer characterized by anoxic and brackish (TDS ~ 1200 mg L^{-1}) native conditions. While these conditions are comparable to many other ASR sites, particularly in Florida, differences in the quality of the injectate, the redox conditions and salinity of the native groundwater will determine the extent to which the model is transferrable to other ASR operations. The most distinct differences are expected for sites where more nutrient and organic-rich, e.g., reclaimed water rather than drinking water is injected. Depending on the concentration and reactivity of the organic carbon, its presence will, besides pyrite oxidation, become an increasingly important driving force for geochemical changes. In this case more reducing conditions may develop within aquifer zones occupied by the injectate, thereby reducing As attenuation by sorption to HFO, compared to the present study site.

At those ASR sites where the native groundwater has higher TDS concentrations, physical and geochemical processes may differ and density-driven flow patterns may develop (Ward et al. 2007) with associated impacts on arsenic breakthrough behavior. Secondly, As mobilization by desorption from HFO may become more important. While we conclude that destruction of sorption sites was the main As release mechanism at the Bradenton site, comparative simulations where HFO was not allowed to dissolve demonstrate that competitive displacement of As from sorption sites by other inorganic solutes is an equally effective As release mechanism (Figure B-8, Appendix B). Model results suggest, that the high alkalinity of the native groundwater compared to the injectate was thereby the major driving force for As displacement from HFO. The simulations imply that a displacement of the sorbed arsenic by the major anions contained in the relatively saline ambient water is sufficient to mobilize arsenic. Importantly, dissolution of HFO, while likely under the redox conditions observed at the Bradenton site, is not necessarily required to obtain elevated arsenic concentrations during recovery. It follows that arsenic re-mobilization will generally be the combined effect of (a) a reduction in sorptive capacity of As on HFO due to elevated TDS in the native groundwater and (b) reductive dissolution of HFO. Both models are not mutually exclusive and which one takes priority depends on the prevailing redox conditions and the salinity of the native groundwater.

3.3.5 UNCERTAINTIES

Despite the complexity of the model, several assumptions are likely to be substantial oversimplifications of the subsurface system. The dissolved As concentrations, which were reasonably well described for the Bradenton site are strongly controlled by solubilities and mineral reaction rates of pyrite and HFO and by competing pH-dependent adsorption reactions. These processes and their respective parameters are highly nonlinear and will be affected by non-uniqueness and uncertainty, in particular where measured data were incomplete (e.g. NO_3, DOC, PO_4, microbial concentrations) or not available at the required density (H_2S, Fe^{2+}). Open bore construction and subsequent depth integrated sampling also contributed to the uncertainty in process/parameter identification. Future studies at other affected ASR sites with more detailed geochemical/hydrogeological data and multiple observation bores will provide additional constraints to test and improve our conceptual model. Despite these limitations, the present model is capable of providing valuable insights into the coupled flow and reaction patterns that affect arsenic fate during ASR of potable water. This quantification framework will provide a useful tool for the assessment and optimization of operational conditions and their impact on As mobility at affected sites.

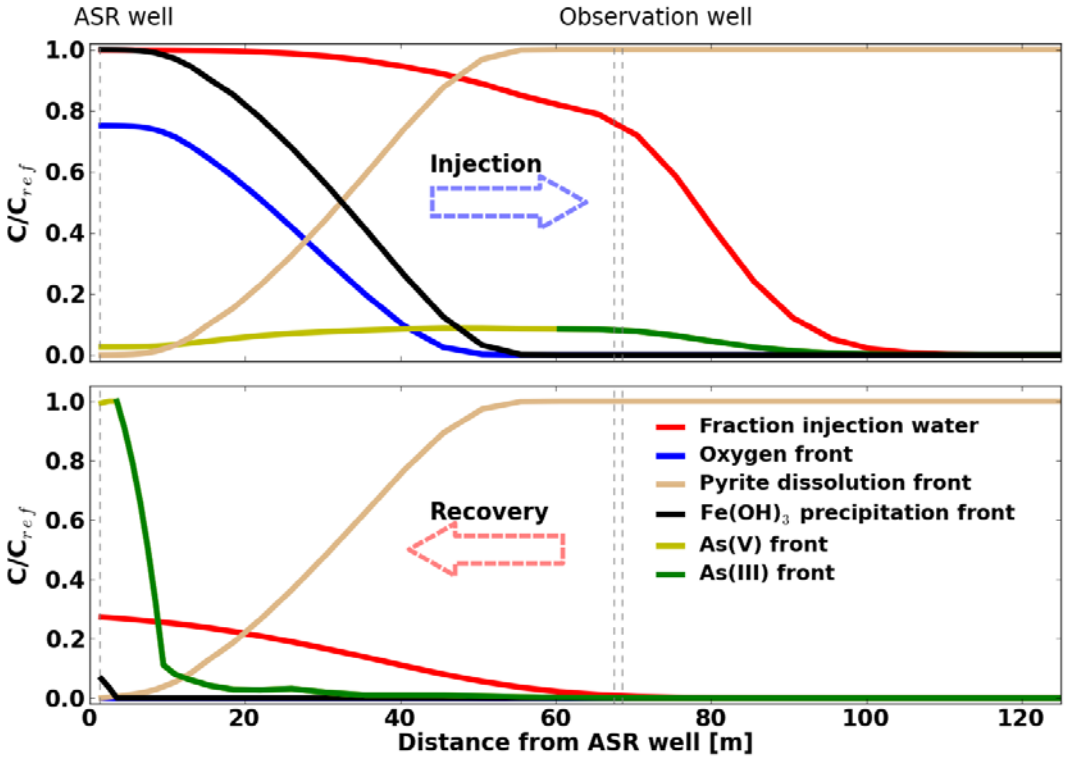

Figure 3-2. Concentration fronts of oxygen, As(III) and As(V), $Fe(OH)_3$ and extent of injected water (SO_4^{2-}) and pyrite dissolution during ASR cycle 1; a) at the end of injection b) at the end of abstraction in the high permeability horizon (model layer 4). C_{ref} = reference concentration. For concentration O_2, SO_4^{2-}: C_{ref} = injectant concentration; for As, $Fe(OH)_3$, ΔC pyrite: maximum concentration during ASR cycle 1.

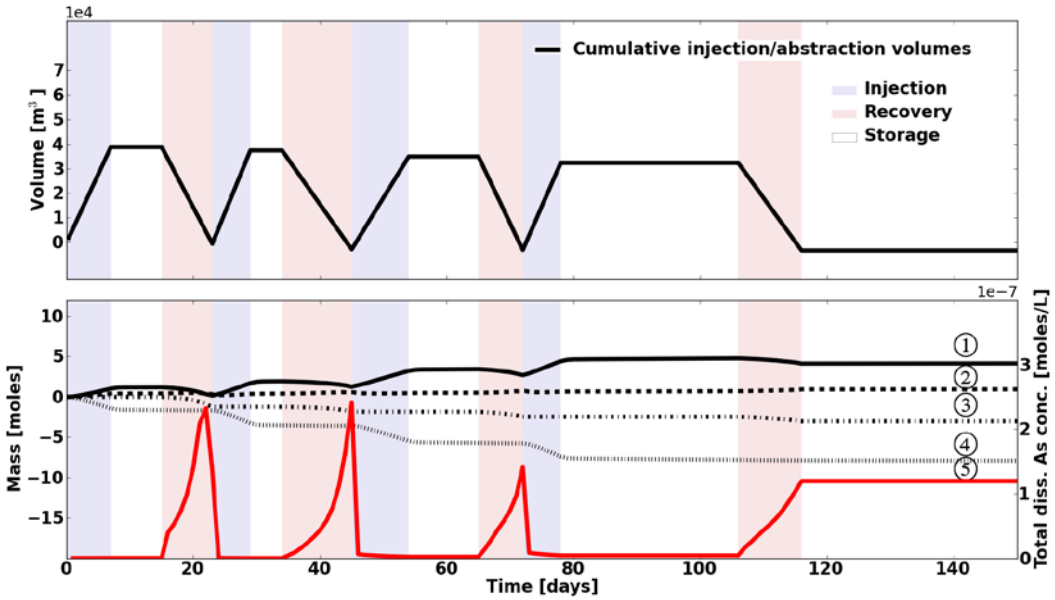

Figure 3-3. Temporal variation of the integrated mass of total dissolved and complexed arsenic in the aquifer, discharge of As from the ASR well, and As released from pyrite during oxidation for the first 4 ASR cycles. Simulated As concentrations are also shown as well as cumulative injection and abstraction volumes. 1: As complexed to HFO, 2: Total dissolved As, 3: As discharged through well, 4: As mobilized through pyrite oxidation, 5: Total dissolved As conc. at ASR well.

ACKNOWLEDGEMENTS

We gratefully acknowledge Don Ellison (South West Florida Water Management District) and Rommy Lahera (FDEP Tampa) for providing geochemical data for the Bradenton ASR site. We also thank Janek Greskowiak for kindly providing valuable input and computational resources and Greg Davies, Peter Dillon, Joanne Vanderzalm and Carlos Descourvieres for their reviews of earlier versions of the manuscript. The financial support provided by Land and Water Australia is gratefully acknowledged. Henning Prommer was supported by the Western Australian Water Foundation.

Chapter 4. SIMULATING MODFLOW-BASED REACTIVE TRANSPORT UNDER RADIALLY-SYMMETRIC FLOW CONDITIONS

ABSTRACT

Radially-symmetric flow and solute transport around point sources and sinks is an important specialized topic of groundwater hydraulics. Analysis of radial flow fields is routinely used to determine heads and flows in the vicinity of point sources or sinks. Increasingly, studies also consider solute transport, biogeochemical processes and thermal changes that occur in the vicinity of point sources/sinks. Commonly, the analysis of hydraulic processes involves numerical or (semi-) analytical modeling methods. For the description of solute transport, analytical solutions are only available for the most basic transport phenomena. Solving advanced transport problems numerically is often associated with a significant computational burden. However, where axis-symmetry applies computational cost can be decreased substantially in comparison to full 3D solutions.

In this paper, we explore several techniques of simulating conservative and reactive transport within radial flow fields using MODFLOW as the flow simulator, based on its widespread use and ability to be coupled with multiple solute and reactive transport codes of different complexity. The selected transport simulators are MT3DMS and PHT3D. Computational efficiency and accuracy of the approaches are evaluated through comparisons to full 2D/3D model simulations, analytical solutions and benchmark problems. We demonstrate that radial transport models are capable of accurately reproducing a wide variety of conservative and reactive transport problems provided that an adequate spatial discretization and advection scheme is selected. For the investigated test problems, the computational load was substantially reduced, with the improvement varying, depending on the complexity of the considered reaction network.

4.1 INTRODUCTION

Radially-symmetric flow to/from a source/sink is an important specialized topic of ground-water hydraulics. Most reported applications have been for aquifer tests and the determination of hydraulic characteristics of the groundwater regime. Radial flow applies to cases where the regional groundwater flow is negligible compared to that induced by the point source or sink over the considered time-scale. Routinely, the quantitative description of the radial flow field and the analysis of the hydraulic heads in such systems involves

numerical or (semi-) analytical modeling methods (e.g., Barlow and Moench 1999; Kruseman and de Ridder 1990; Veling and Maas 2009). The type of numerical modeling tools used ranges from generic, widely used flow simulators such as FEFLOW (Diersch 2002) and MODFLOW (McDonald and Harbaugh 1988; Harbaugh et al. 2000; Harbaugh 2005) which uses Cartesian geometry, to purpose built models (e.g., Johnson et al. 2001; *Bohling and Butler 2001; Mansour et al. 2007;* Louwyck et al. 2011) that implement a radial coordinate system. Finite-element (FE) models allow for an effective implementation for the simulation of radial flow fields through an appropriate refinement of the FE grid around point sources/sinks. The model setup for local-scale simulations of radial flow-fields with finite difference models is less efficient. Commonly, multi-dimensional models (2D/3D) are developed with a horizontal plane centred around the point source/sink using a fine discretization (e.g., cell width equal to the well radius). Cell widths then expand logarithmically with distance from the well (Langevin 2008, Louwyck et al. 2011, Barrash and Doherty, 1997) to allow approximation of cylindrical flow (Anderson and Woessner, 1991). Alternatively, axi-symmetric models may be used. These account for the actual increase in aquifer volume with distance from the point source/sink through either model parameter adjustments or manipulation of the model geometry. Computationally they are a more efficient alternative as long as the assumption of radial flow is sufficiently justified (Langevin 2008; Anderson and Woessner 1991; Halford and Yobbi 2006; Samani et al. 2004). While the initial setup of such models is still somewhat cumbersome, the numerical solution of the groundwater flow equation is usually relatively efficient, even for full three dimensional multi-layered model configurations.

Increasingly, studies also need to investigate the solute transport behaviour, as well as the biogeochemical or thermal changes that evolve in the vicinity of the point source/sink. Typical applications include, for example, tracer injection experiments (Seaman et al. 2007; Huang et al. 2010), single-well injection and withdrawal tests, e.g., push-pull tests (Istok et al. 1997; Schroth et al. 2001; Senko et al. 2002; Vandenbohede et al. 2008; Phanikumar and McGuire 2010), in-situ iron removal operations (Appelo and de Vet 2003), aquifer storage and recovery (ASR) systems (Greskowiak et al. 2005; Culkin et al. 2008, Descourvieres et al. 2010; Wallis et al. 2011), aquifer thermal energy storage (ATES) systems (Dwyer and Eckstein 1987; Griffioen and Appelo 1993; Kim et al. 2010), in-situ bioremediation (Oya and Valocchi 1998) or coal bed methane recovery (van Wageningen et al. 2009). Analytical or semi-analytical solutions are only available for highly simplified transport problems (e.g., Gelhar and Collins 1971; Valocchi 1986; Hsieh 1986; Goltz and Oxley 1991; Wang and Crampon 1995; Becker and Charbeneau 2000). The solution of the transport equations

using numerical techniques is, however, often associated with significant computational costs, even for systems where the flow model alone is solved with little effort. This can severely restrict the application of reactive transport models, in particular where a manual or automatic model calibration may require hundreds or thousands of model runs.

Among the previously published MODFLOW-based solutions for the simulation of radial flow problems, several of the solutions involve modifications of the MODFLOW code (Samani et al. 2004; Romero and Silver 2006). Others are based on unmodified versions of MODFLOW (Anderson and Woessner 1991; Reilly and Harbaugh 1993; Barrash and Dougherty 1997; Langevin 2008; Halford and Yobbi 2006; Louwyck et al. 2011). One major advantage of the latter approach is that the compatibility with the various transport simulators in the MODFLOW-family of codes such as MT3DMS (Zheng and Wang 1999), SEAWAT (Guo and Langevin 2002; Langevin and Guo 2006), RT3D (Clement 1997) and PHT3D (Prommer et al. 2003) is preserved.

The radially-symmetric approaches published to date, have focussed on the accurate simulation of the flow field. None of the methods have been rigorously evaluated for their applicability and accuracy of the transport equations. With the present paper, we aim to close this gap and (i) explore several techniques of simulating conservative and reactive solute transport around point sources and sinks under radially-symmetric flow conditions and (ii) evaluate and demonstrate the applicability of these approaches and assess their accuracy and potential for reducing the computational burden by comparing them to 2D/3D model simulations, analytical solutions and previously published benchmark problems. The focus is on methods for simulating reactive transport in radial flow fields using MODFLOW as the flow simulator, based on its widespread use and ability to be coupled with multiple solute and reactive transport codes of different complexity. The selected transport simulators areMT3DMS (Zheng and Wang 1999) and PHT3D (Prommer et al. 2003).

4.2 MODEL DISCRETIZATION APPROACHES

The conventional and probably most commonly employed method of approximating radial flow with a finite-difference scheme is to discretize a horizontal plane centred on the point source/sink. The model may encompass the full circumference of the radial flow domain ($2\pi r$), or it may represent a fraction thereof. Because of the underlying radial symmetry, the fraction of aquifer represented by the model is arbitrary and does not affect the solution.

However the injection/abstraction rates of the well need to be scaled to the simulated proportion of the model domain. The boundaries of the model should be positioned at sufficient distance from the well, that they have minimal impact on the model solution over the time-scales of interest using, e.g., a constant head boundary condition (Dirichlet boundary) or a general head boundary (Cauchy boundary). If only a proportion of the full radial flow domain is simulated, no-flow boundary conditions are applied to the model boundaries along the two symmetry axes.

This multi-dimensional Cartesian model approach (2D/3D) was applied in the present paper to compare to axi-symmetric methods. The model domain was chosen to represent one-quarter of the full radially-symmetric domain, with the well placed into one corner of the model grid. In the following, three axi-symmetric model approaches are described. These are then compared to the 2D/3D Cartesian model simulations for a variety of analytical and benchmark problems to test their accuracy and ability to reduce computational burden.

4.2.1 RADIALLY-SYMMETRIC MODEL APPROACH 1: REDUCTION OF DIMENSION BY PARAMETER SCALING AFTER LANGEVIN (2008)

The two horizontal dimensions of models describing axi-symmetric flow using Cartesian coordinates can be effectively reduced to one dimension through adjustment of model input data. Model parameters thereby become a function of the increase in aquifer and storage volume with radial distance from the sink/source. The approach was originally proposed by Anderson and Woessner (1991) for flow simulations alone, but was later extended and described in detail by Langevin (2008) (hereafter referred to as the "*Langevin method*").

In this method a numerical model setup of *k* layers, *j* columns and a single row is used, whereby the width of the row is set to 1 m. The well is assumed to be located in one or more layers in column 1 (r_{well}, Figure 4.1 a). The outer vertical boundary of the well cell represents the centre of the radial flow field. The discretisation in column direction can be chosen freely depending on the required radial resolution. Each of the grid cells in column direction corresponds to a concentric ring around the well centre. The grid cell centres in each column are located at radii r_j and the column width corresponds to the width of the concentric ring (Figure 4.1 a). As each column corresponds to an ever greater aquifer volume with increasing distance from the well, the aquifer parameters (*X*) of each cell become a function of the radial distance from the point source/sink:

$$X_{k,j} = r_j 2\pi X_k^r \quad (1)$$

where X_k^r is the aquifer parameter value of the k^{th} layer in radial direction, r_j the radial distance to the cell centre of the j^{th} column and $X_{k,j}$ is the adjusted model parameter in the k^{th} layer and j^{th} column.

For flow simulations the conductivities (K_h and K_v), storage properties as well as recharge and evapotranspiration increase with radial distance according to eq. (1). As eq. (1) assumes laterally homogeneous parameter values, the logarithmic mean is used within MODFLOW to calculate the interblock conductivities (Goode and Appel 1992, Langevin 2008).

4.2.2 RADIALLY-SYMMETRIC MODEL APPROACH 2: REDUCTION OF DIMENSION BY PARAMETER SCALING AFTER LOUWYCK ET AL. (2011)

An alternative technique of simulating radial flow with MODFLOW was recently presented by Louwyck et al. (2011) (hereafter referred to as the "*Louwyck method*"). It is also based on the adjustment of model parameters as a function of the radial distance from the injection/extraction well. In contrast to the *Langevin method* this technique allows laterally heterogeneous aquifer properties (e.g., well skin) to be considered.

The Louwyck method requires aquifer parameters to be scaled on the basis of a radial grid consisting of a series of *nc* concentric rings with radii r_j around a well. The radii r_j of the rings is thereby defined as the geometric mean of inner ring radius $r_{j-0.5} = r_j a_r^{-0.5}$ and outer ring radius $r_{j+0.5} = r_j a_r^{+0.5}$ (Figure 4.1 b). For flow simulations, where the emphasis is on efficient and accurate simulation of heads around point sources and sinks, Louwyck et al. (2011) proposed the following logarithmic scaling of the radial distance r_j:

$$r_j = r_0 {a_r}^{j-1} \quad j = 1,2,\dots,nc \quad (2)$$

with the expansion factor for the radii of the concentric rings being $1<a_r<2$, r_0 being the radius of the first concentric ring and *nc* the total number of rings.

Besides a logarithmic scaling, a flexible lateral discretization of the aquifer can also be applied as long as the geometric mean of the radii of inner and outer ring boundaries is used for the calculation of the radii of the concentric rings.

Eq. (2) defines a series of nc concentric rings on which basis aquifer parameters are increased radially to account for the expansion in aquifer volume. The full discussion of the derivation of the scaling factors is provided in Louwyck et al. (2011). The horizontal conductivity $K^h_{k,j}$ of the k^{th} layer and j^{th} column becomes:

$$K^h_{k,j} = \frac{2\pi K^r_{k,j}}{\ln(r_{(j+0.5)}/r_{(j-0.5)})} \quad (3)$$

where $K^r_{k,j}$ is the radial horizontal conductivity, $K^h_{k,j}$ is the adjusted horizontal conductivity for input to the model and $r_{j-0.5}$ and $r_{j+0.5}$ are the inner and outer radius of the j^{th} column. Vertical conductivity and storage properties are calculated by multiplying these with the horizontal surface area of the circular element represented by column *j*:

$$X_{k,j} = A_j * X^r_{k,j} \quad (4)$$

$$\text{where: } A_j = \pi[(r^2_{(j+0.5)}) - (r^2_{(j-0.5)})] \quad (5)$$

The scaled aquifer parameters are input to a MODFLOW model grid, which consists of a single row, *j* columns and *k* layers. The number of model columns (*nc*) correspond to the series of *nc* concentric rings around the well. MODFLOW model column widths are thereby pre-set to 1m along both row and column direction, i.e. the MODFLOW model, which follows the Louwyck approach requires fixed cell sizes.

The *Louwyck method* is based on the assumption that the transmissivity within a cell is constant, but that it may vary from cell to cell. Thus, laterally heterogeneous aquifer properties can be accommodated. As a consequence, the harmonic mean is used within MODFLOW to calculate the interblock conductivities (Harbaugh et al. 2000).

4.2.3 RADIALLY-SYMMETRIC MODEL APPROACH 3: REDUCTION OF DIMENSION BY MANIPULATION OF MODEL GEOMETRY

An alternative approach to simulating axi-symmetric flow is to represent the cylindrical flow field by a one-layer model tilted on its side. Aquifer properties remain unchanged, but instead the geometry of the model grid is modified (Greskowiak et al. 2005, Wallis et al. 2011) (hereafter referred to as the "*geometry method*"). To account for the increase in aquifer volume with radial distance, the model layer thickness (Δz) increases radially as:

$$\Delta z_j = r_j 2\pi \tag{6}$$

The variable thickness of the profile is thereby based on the chosen angle of the simulated wedge (2π in case of simulation of the full radial flow field). The value of Δz_j numerically equals the perimeter of a circle at the radial distance at the centre of each grid cell (r_j), i.e., the distance from the point sink/source. To discretise the system vertically, multiple rows are used, with the actual layer thicknesses being input to the model as the widths of the model rows (Δy_k) (Figure 4.1 c).

As this approach does not require any model parameters besides the model layer thickness to be adjusted, the parameter assignment of flow and transport models is straightforward. However, this approach is restricted to simulating confined systems and it is not suitable for model simulations that require the correct layer top and bottom elevations, such as with SEAWAT.

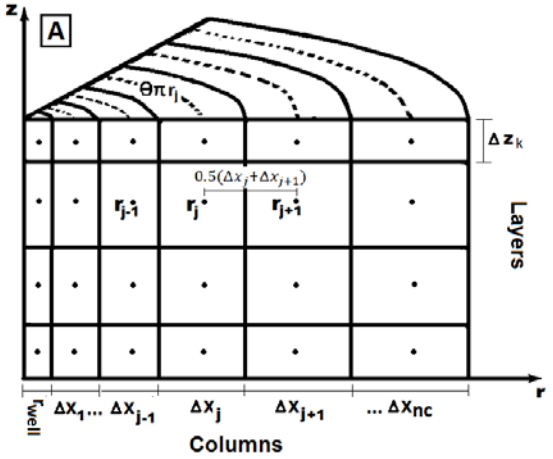

$\Delta x_j = width\ of\ column\ j$
$\Delta z_k = thickness\ of\ layer\ k$

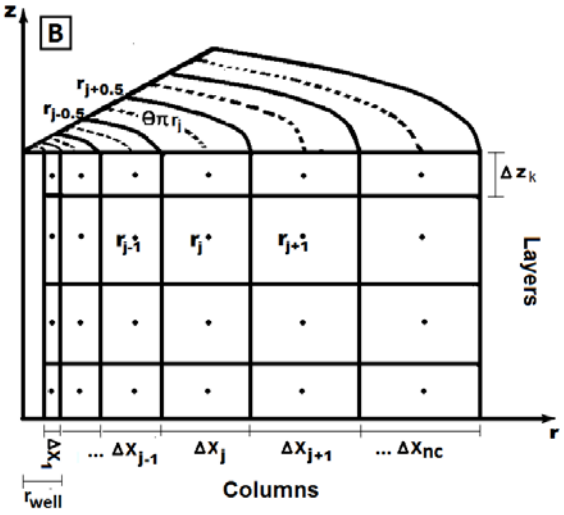

$r_j = \sqrt{r_{j-0.5} * r_{j+0.5}}$
$r_{j-0.5} = r_j * a_r^{-0.5}$
$r_{j+0.5} = r_j * a_r^{0.5}$

$\Delta x_j = width\ of\ column\ j$
$\Delta z_k = thickness\ of\ layer\ k$

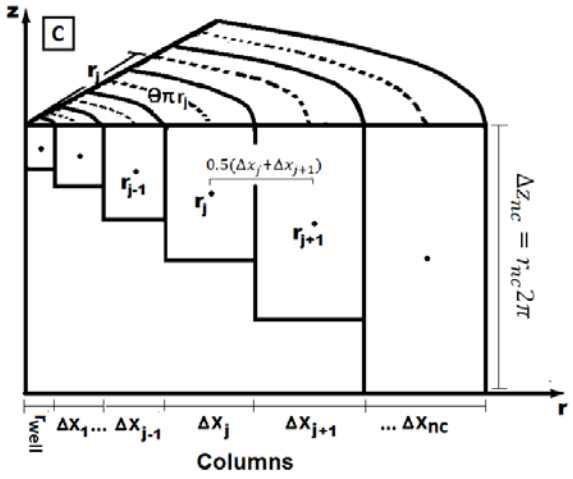

$\Delta x_j = width\ of\ column\ j$
$\Delta y_k = thickness\ of\ layer\ k$

Figure 4-1. Model discretization following the methods of a) Langevin (2008), b) Louwyck (2011) and c) manipulation of the model geometry.

4.2.4 SOLUTE TRANSPORT PARAMETER RESCALING

Transport parameter scaling is not required if an axi-symmetric model is developed based on the *geometry method*, as the manipulation of the model grid accounts for the radially increasing aquifer volume. However, for both, the *Langevin* and the *Louwyck method*, scaling of transport parameters is required to all input values used in equations and their numerical solutions that contain an area or volume analogous to the flow parameter adjustments (Langevin 2008). Scaling of the transmissive and storage properties, as discussed in the previous sections, ensure that the *Langevin* and the *Louwyck methods* calculate the correct Darcy fluxes, which in MODFLOW are obtained by multiplying the conductance with the head difference across the cell faces (McDonald and Harbaugh 1988). For the simulation of advective solute transport by MT3DMS (Zheng and Wang 1999), these Darcy fluxes need to be converted into linear groundwater flow velocities by division with the effective porosity. Accordingly, the effective porosity needs to be rescaled and the adjustment follows the same procedure as for the flow model input parameters, i.e. using eq. (1) and eq. (4) for the *Langevin* and the *Louwyck* methods, respectively.

After incorporation of these adjustments the computed velocity field, which forms the basis for the transport simulations, will be equal to the respective velocity field calculated with the *geometry method* as well as the Cartesian model equivalents. Computed flow velocities are compared in Figure 4.2a to results from the respective analytical solution, which for steady state horizontal radial flow is found to be:

$$v(r) = \frac{Q}{2\pi r \theta \Delta z} \tag{7}$$

where *v(r)* is the flow velocity [L/T] , ϑ is the porosity [-], *Q* is the injection/abstraction rate [L^3/T] and Δz is the thickness of the domain.

When, as it generally is the case, dispersive transport is considered, the dispersivity requires rescaling only if the *Louwyck method* is used. This compensates for the prefixed MODFLOW column and row width of 1 m, through division by the width of the radial rings ($r_{j+0.5} - r_{j-0.5}$) corresponding to each model column.

If, in addition to advective and dispersive transport, reactive processes are considered, the parameters used to describe chemical reactions may also require adjustment, depending

on the type and the complexity of the reactions that are included in the reaction network of the transport model. For instance, if sorption is modelled via the appropriate MT3DMS reaction package, the bulk density of the aquifer material requires scaling to account for the increase in mass with radial distance from the point source/sink in accordance to the flow parameter adjustements, i.e., using eq. (1) and eq. (4) for the *Langevin* and the *Louwyck* methods, respectively.

The necessary input data modifications may also be code-specific. For example, if the multi-component reactive transport code PHT3D is used, mineral concentrations, ion exchange capacities and surface complexation parameters are by convention expressed in moles per litre of bulk aquifer volume. Internally, the code divides these concentrations in each cell by the porosity of that cell in order to scale them relative to one kilogram of water. Thus, without parameter input adjustments according to eq. (1) (*Langevin method*) and eq. (4) (*Louwyck method*), this internal conversion step would result in incorrect proportions of mineral or sorbed solute mass relative to solute concentrations. For other codes, however, other conventions and thus different scaling rules may apply.

4.3 PERFORMANCE ASSESSMENT OF RADIALLY-SYMMETRIC MODEL APPROACHES

A number of representative benchmark problems of different complexity were selected from the literature to assess the accuracy and computational efficiency (i.e., run-times) of the three axi-symmetric model approaches discussed above in comparison to the equivalent 2D/3D Cartesian model solutions for both conservative and reactive transport.

4.3.1 CONSERVATIVE SINGLE SPECIES TRANSPORT

The numerical solution obtained with MT3DMS is compared to the analytical solution developed by Gelhar and Collins (1971) for the case of a conservative solute front that propagates from a fully-penetrating injection well into a confined aquifer:

$$\frac{C-C_0}{C_{inj}-C_0} = 0.5erfc\left\{\frac{r^2-{r_i}^2}{2\left[\left(\frac{4}{3}\alpha_L\right){r_i}^3+\left(\frac{D}{A}\right){r_i}^4\right]^{0.5}}\right\} \quad (8)$$

where

$$r_i = (2At)^{0.5} \tag{9}$$

and $$A = \left(\frac{Q}{2\pi\Delta z\theta}\right) \tag{10}$$

where t is the time, α_L the longitudinal dispersivity [L] and D the molecular diffusion [L^2/T].

In this test case (*TC1*), fluid is injected at a rate Q_{inj} with a solute concentration of $C_{inj.}$ The aquifer initially contains water with solute concentration C_o. For the numerical solution, the model domain of the 2D/3D Cartesian model and its equivalent three axi-symmetric model approaches was discretized into (i) a first 1m wide cell that represents the well ($\Delta x_{well} = 1m$), (ii) additional cells increasing in width according to an expansion factor ($a_r = 1.05$) up to a maximum column width of 5m and (iii) a regular discretization of 5m for larger radial distances (Table 4.1). As this discretization scheme differs from the commonly applied logarithmic scaling used for radial flow problems (Langevin 2008, Louwyck et al. 2011, Reilly and Harbaugh 1997), an additional model was set up applying logarithmic scaling in conjunction with the *Louwyck approach*. The spatial discretization followed a logarithmic increase of column width, as defined in eq. (2). All relevant numerical model parameters and their values used in the simulation are listed in Table 4.1.

As a measure of the accuracy of the numerical solution a relative error was defined based on the equation presented by Langevin (2008) and Samani et al. (2004):

$$RE = (X_{num} - X_{analytical})/M * 100 \tag{11}$$

where *RE* is the relative error [%], X_{num} is the simulated value. $X_{analytical}$ is the corresponding value determined with the analytical solution. *M* is a reference value, which is based on the maximum change in *X,* which for this problem is for example the maximum difference between injected and initial concentration, maximum change in mass or velocity.

The method of characteristics (MOC) solution technique was employed for the present example as it was expected to perform best under the given advection dominated conditions (Peclet numbers ranging from 1 to 5). For the selected spatial discretization the MOC scheme provides sufficient accuracy without excessive computational demand. Note that the absolute model run times as well as the relative errors are, however, a function of both the model discretization and the selected advection scheme.

Table 4-1 Numerical model parameters to simulate radial transport of a conservative solute (*TC1*)

Model	2D model	1D_axi-symmetric Langevin 2008	1D_axi-symmetric Louwyck 2011 log discretization[3]	1D_axi-symmetric Louwyck 2011	1D_axi-symmetrix Geometry adjusted
Model cells	78 * 78	78	78	78	78
Radial extent of model (radius of cell 78) [m]	302.56	302.56	301.8	303.05	302.56
Discretization x direction [1]	$\Delta x(well)$: 1m $\Delta x\ col.2-33$: $\Delta x(well)*a_r^{(j-1)5)}$; $\Delta x\ col.34-78$: 5m	see 2D model	$r_j = r_0 a_r^{j-1}$; $a_r = 1.086$ $r_0 = 0.5\text{m}$ [2]	$r_0 = 0.866\text{m}$; $\Delta x(1)$: 1m, $r_j\ col.2-78$: $r_j = \sqrt{r_{j-0.5} * r_{j+0.5}}$; $r_{j-0.5} = r_j * a_r^{-0.5}$;[6] $r_{j+0.5} = r_j * a_r^{0.5}$	see 2D model
Resulting width of columns	Columns 1:33: 1 to 4.7m Columns 34:78: 5m	see 2D model	0.041 to 25.1m	see 2D model	see 2D model
Discretization y direction[1]	78 rows, discretisation as in x direction	1 row: 1m	1 row: 1m	1 row: 1m	1 row: 60m
Discretization z direction	1 layer: 60m	1 layer: 60m	1 layer: 60m	1 layer: 60m	1 layer: $\Delta z_j = r_j 2\pi$
Time	1 sp[4]: 200days; 400 ts[4]	1 sp[4]: 200days; 400 ts[4]	1 sp[4]: 200days; 400 ts[4]	1 sp[4]: 200days; 400 ts[4]	1 sp[4]: 200days; 400 ts[4]
Advection scheme	MOC	MOC	MOC	MOC	MOC
Solver; conc. closure criterion	GCG, $1*10^{-9}$	GCG, $1*10^{-9}$	GCG, $1*10^{-9}$	GCG, $1*10^{-9}$	GCG, $1*10^{-9}$
Horiz. hydraulic conductivity *(k)* [m/d]	8.64	$k_j = r_j 2\pi k^r$	$k_j^h = \frac{2\pi k_j^r}{\ln(r_{(j+0.5)}/r_{(j-0.5)})}$	$k_j^h = \frac{2\pi k_j^r}{\ln(r_{(j+0.5)}/r_{(j-0.5)})}$	8.64
Porosity (ϑ)	0.2	$\theta_j = r_j 2\pi k\theta^r$	$\theta_j = \pi(r_{(j+0.5)}^2 - r_{(j-0.5)}^2)\theta^r$	$\theta_j = \pi(r_{(j+0.5)}^2 - r_{(j-0.5)}^2)\theta^r$	0.2
Long. dispersivity [m]	1	1	$1/(r_{(j+0.5)} - r_{(j-0.5)})$	$1/(r_{(j+0.5)} - r_{(j-0.5)})$	1
C_o	1	1	1	1	1
C_{inj}	0.5	0.5	0.5	0.5	0.5

1) The 2D model domain represents one-quarter of a full radial-symmetric domain (i.e. 2πr/4), with the well emplaced in one grid corner
2) $j = (2,3,..,nc)$
3) Logarithmic expansion of space as described in Louwyck et al. (2011)
4) sp=stress periods; ts: time steps
5) a_r = expansion factor for spatial discretization; $a_r = 1.05$; $j = (2,3,..,nc)$
6) $a_r = variable$; $1 < a_r < 2$

The comparison of the modeling results shown in Figure 4.2 indicates that all three methods described above agree well with both the full 2D model and the analytical solution. The maximum *RE* for dissolved solute concentrations is shown to be below 5% for both the *geometry method* and the *Langevin method.* It is below 7% for the *Louwyck method*. Close agreement is also achieved for the total simulated solute mass over time,

which lies within 5% of the analytical solution for all axi-symmetric model approaches and the 2D Cartesian model (results not shown). In contrast, the axi-symmetric model that applies the logarithmic-based spatial discretization (*Louwyck method* with log discretisation) is unable to reproduce the concentration breakthrough curves with sufficient accuracy (Figure 4.2 b/c). This discretization scheme is beneficial for the flow solution as it provides increased efficiency and accuracy for the calculation of groundwater heads around point sources and sinks (Louwyck et al. 2011). However, it leads to rapidly increasing Peclet numbers with distance from the point sink/source. As a result the transport solution is sufficiently accurate in the vicinity of the injection point (Figure 4.2 b/c) but, breakthrough curves are poorly resolved at greater distances from the well. There, depending on the applied MT3DMS advection scheme, the solution may be plagued by numerical dispersion. Therefore, logarithmic scaling as commonly applied for radial flow problems was not further considered in the following transport test cases.

The axi-symmetric models that follow the other three approaches are ~90 times (*Langevin method*, *geometry method)* and ~370 times faster (*Louwyck method*) than the full 2D model (Table 4.3).

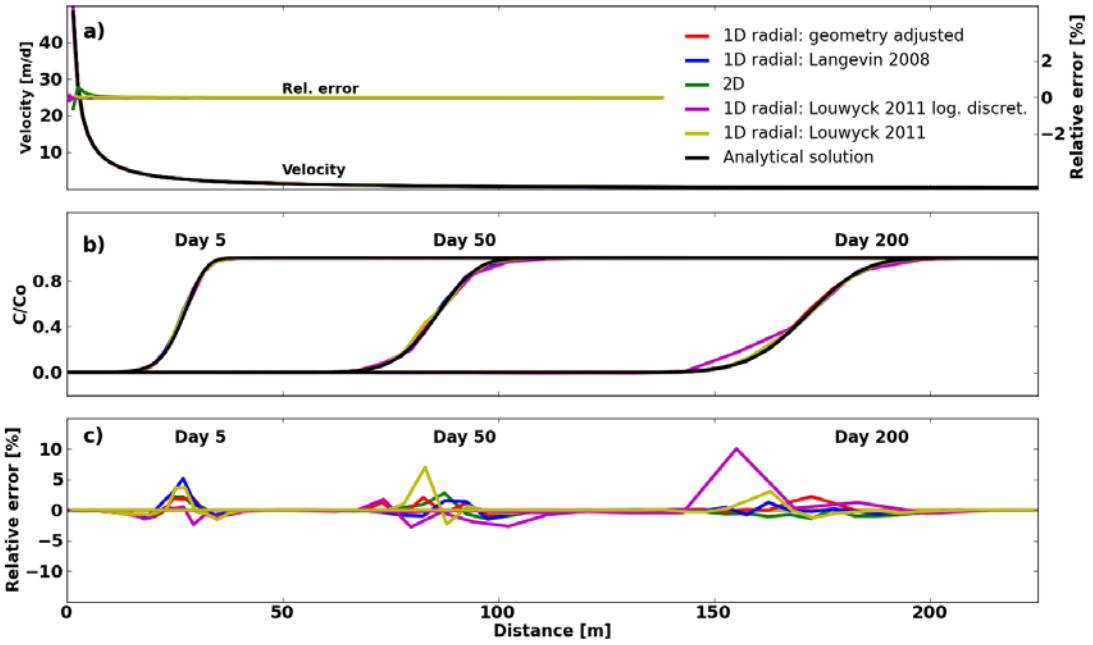

Figure 4-2. a) Simulated flow velocities by four axi-symmetric models and the equivalent full 2D model and their error to the analytical solution; b) comparison of simulated concentrations for all model approaches at three timesteps (5days, 50days, 200days of injection); and c) the corresponding error to the analytical solution.

4.3.2 SINGLE-COMPONENT REACTIVE TRANSPORT AND DUAL DOMAIN MODELS

Extending from the previous conservative case the applicability and accuracy of the various radially-symmetric model approaches was investigated for cases that additionally employ the reaction capabilities as provided by the MT3DMS code. In the first step, the transport of a sorbing solute was analyzed for a test case (*TC2*) in which linear equilibrium sorption was included (Karickhoff 1981), i.e.:

$$S = K_d * C, \tag{12}$$

where K_d is the distribution coefficient [L^3/M] and S the mass of the solute species adsorbed on the aquifer solids [M/M].

To correctly account for the sorbed mass within axi-symmetric models based on model parameter adjustements (*Langevin* and *Louwyck method*), the bulk density of the aquifer material requires scaling to account for the increase in mass with radial distance from the point source/sink according to eq. 1 (*Langevin method*) and eq. 4 (*Louwyck method*) (Table 4.2, *TC2*). The numercial solution for *TC2* is compared with the corresponding analytical solution for one-dimensional advective transport with linear soprtion by incorperating the retardation factor (R) into the solution of Gelhar and Collins (1971), eq(8):

$$\frac{C-C_0}{C_{inj}-C_0} = 0.5erfc\left\{\frac{r^2-{r_i}^2}{2\left[\left(\frac{4}{3}\alpha_L\right){r_i}^3+\left(\frac{D}{A\frac{1}{R}}\right){r_i}^4\right]^{0.5}}\right\} \tag{13}$$

In a variation of this case (*TC3*) it was assumed that the local equilibrium assumption was not valid, and that sorption is described through a first-order reversible kinetic reaction:

$$\rho_b \frac{\partial S}{\partial t} = \beta\left(C - \frac{S}{K_d}\right) \tag{14}$$

where ρ_b is the bulk density of the subsurface medium [M/L^3], β is the first-order mass transfer rate [1/T] between the liquid and solid phases (Table 4.2, *TC3*).

The test case *TC3* was further expanded through inclusion of an irreversible first-order reaction (*TC4*). First-order reactions are often employed to represent (bio)degradation or other mass-loss mechanisms in cases where either (i) a first order reaction represents a

good approximation of the mass-loss behaviour or (ii) where insufficient process understanding and/or aquifer characterisation does not warrant a more complex and more process-based model formulation. The loss in mass in the sorbed and solute phase is described through a rate constant, which generally represents the half-life of the degradable phase (Table 4.2).

The final MT3DMS-based test problem (*TC5*) involves a case in which the classic advection-dispersion model is replaced by a dual domain approach. The dual domain mass transfer model partitions the aquifer's pore space into two separate domains: a mobile domain, where transport is dominated by advection and a second domain, where transport is controlled by diffusion or (very) slow advection (Feehley and Zheng 2000, Culkin et al. 2008). Correspondingly the total porosity is partitioned into a mobile fraction (ϑ_m) and an immobile fraction (ϑ_{im}). The mass exchange between the two domains is controlled through a mass transfer rate (β_{dd}) that is proportional to the concentration difference between the two domains:

$$\theta_{im} \frac{\partial C_{im}}{\partial t} = \beta_{dd} (C_m - C_{im}) \quad (15)$$

where ϑ_{im} is the porosity of the immobile domain, β_{dd} is the mass transfer rate coefficient [1/T], C_m and C_{im} are the solute concentrations [M/L^3] in the mobile and immobile domain, respectively.

The relevant transport parameters together with their respective adjustments for axi-symmetric models required to simulate linear and kinetic sorption, first-order irreversible rate reactions and dual porosity models are detailed in Table 4.2. These parameters are input to the model in addition to the parameters listed in Table 4.1.

Table 4-2. Flow and transport model parameters (test cases 2 to 7)

Model	2D model	1D_axi-symmetric Langevin (2008)	1D_axi-symmetric Louwyck (2011)	1D_axi-symmetric Geometry adjusted
TC2: Linear sorption (MT3DMS)				
Bulk density (ρ) [kg/m^3]	2000	$\rho_j = r_j 2\pi\rho^r$	$\rho_j = \pi(r^2_{(j+0.5)} - r^2_{(j-0.5)})\rho^r_j$	2000
Kd [m^3/kg]	1e^{-4}	1e^{-4}	1e^{-4}	1e^{-4}
TC3: Kinetic sorption (MT3DMS)				
Bulk density (ρ) [kg/m^3]	2000	$\rho_j = r_j 2\pi\rho^r$	$\rho_j = \pi(r^2_{(j+0.5)} - r^2_{(j-0.5)})\rho^r_j$	2000
Mass transfer rate (β) [1/s]	0.005	$\beta_j = r_j 2\pi\beta^r$	$\beta_j = \pi(r^2_{(j+0.5)} - r^2_{(j-0.5)})\beta^r_j$	0.005
TC4: Decay (MT3DMS)				
Bulk density (ρ) [kg/m^3]	2000	$\rho_j = r_j 2\pi\rho^r$	$\rho_j = \pi(r^2_{(j+0.5)} - r^2_{(j-0.5)})\rho^r_j$	2000
Mass transfer rate (β) [1/s]	0.005	$\beta_j = r_j 2\pi\beta^r$	$\beta_j = \pi(r^2_{(j+0.5)} - r^2_{(j-0.5)})\beta^r_j$	0.005
Rate const. dissolved phase (λ)	0.0025	0.0025	0.0025	0.0025
Rate const. sorbed phase (λ)	0.001	0.001	0.001	0.001
TC5: Dual domain (MT3DMS)				
Mass transfer rate (β) [1/s]	0.005	$\beta_j = r_j 2\pi\beta^r$	$\beta_j = \pi(r^2_{(j+0.5)} - r^2_{(j-0.5)})\beta^r_j$	0.005
Immobile porosity (θ_{im})	0.05	$\theta_{im\,j=} r_j 2\pi\theta^r_{im}$	$\theta_j = \pi(r^2_{(j+0.5)} - r^2_{(j-0.5)})\theta^r_j$	0.05
TC6: Ion-exchange (PHT3D)				
Discretization x direction	see TC1, table 4.1	see TC1, table 4.1	see TC1, table 4.1	see TC1, table 4.1
Discretization y direction	78 rows, discretisation as in x direction	1 row: 1m	1 row: 1m	1 row: 1.25m
Discretization z direction	1 layer: 1.25m	1 layer: 1.25m	1 layer: 1.25m	1 layer: $\Delta z_j = r_j 2\pi$
C and C_o [1)] [x mol/L]	x [mol/L]	x [mol/L]	x [mol/L]	x [mol/L]
Exchanger CaX (E) [mol/l_{bulk}]	0.0306	$E_j = r_j 2\pi E^r$	$E_j = \pi(r^2_{(j+0.5)} - r^2_{(j-0.5)})E^r_j$	0.0306
Exchanger NaX (E) [mol/l_{bulk}]	0.03189	$E_j = r_j 2\pi E^r$	$E = \pi(r^2_{(j+0.5)} - r^2_{(j-0.5)})E^r_j$	0.03189
Exchanger MgX (E) [mol/l_{bulk}]	0.0285	$E_j = r_j 2\pi E^r$	$E_j = \pi(r^2_{(j+0.5)} - r^2_{(j-0.5)})E^r_j$	0.0285
TC7: 3D multicomp. reactive transport (PHT3D)				
	3D model [2)]	**2D_axi-symmetric** Langevin (2008)	**2D_axi-symmetric** Louwyck (2011)	**2D_axi-symmetric** Geometry adjusted
Cell nr.	3 * 78 * 78	3 * 78	3 * 78	3 * 78
Discretization – x direction [2)]	see TC1, table 4.1	see TC1, table 4.1	see TC1, table 4.1	see TC1, table 4.1
Discretization – y direction [2)]	discretization as in x direction	1 row. Δy = 1m	1 row. $\Delta y = 1\text{m}$	3 rows. 20m each
Discretization – z direction	3 layers 20m each	see 3D model	see 3D model	1 layer: $\Delta z_j = r_j 2\pi$
Time	1 sp:83days; 830 ts	see 3D model	see 3D model	see 3D model
Horiz. hydr. cond. Layer1 (k) [m/d]	4	$k_{k,j} = r_j 2\pi k^r_k$	$k_{k,j} = \frac{2\pi k^r_{k,j}}{\ln(r_{(j+0.5)}/r_{(j-0.5)})}$	4
Horiz. hydr. cond. Layer2 (k) [m/d]	8	$k_{k,j} = r_j 2\pi k^r_k$	$k_{k,j} = \frac{2\pi k^r_{k,j}}{\ln(r_{(j+0.5)}/r_{(j-0.5)})}$	8
Horiz. hydr. cond. Layer3 (k) [m/d]	13.92	$k_{k,j} = r_j 2\pi k^r_k$	$k_{k,j} = \frac{2\pi k^r_{k,j}}{\ln(r_{(j+0.5)}/r_{(j-0.5)})}$	13.92
Vert. hydr. cond. Layer1 (k^v) [m/d]	4	$k^v_{k,j} = r_j 2\pi k^v_k$	$k^v_{k,j} = \pi(r^2_{(j+0.5)} - r^2_{(j-0.5)})k^v_{k,j}$	4
Vert. hydr. cond. Layer2 (k^v) [m/d]	8	$k^v_{k,j} = r_j 2\pi k^v_k$	$k^v_{k,j} = \pi(r^2_{(j+0.5)} - r^2_{(j-0.5)})k^v_{k,j}$	8
Vert. hydr. cond. Layer3 (k^v) [m/d]	13.92	$k^v_{k,j} = r_j 2\pi k^v_k$	$k^v_{k,j} = \pi(r^2_{(j+0.5)} - r^2_{(j-0.5)})k^v_{k,j}$	13.92

Table 4.2. continued

TC7: 3D multicomp. reactive transport (PHT3D)

	3D model [2]	2D_axi-symmetric	2D_axi-symmetric	2D_axi-symmetric
Long. dispersion [3] [m]	1	1	$1/(r_{(j+0.5)} - r_{(j-0.5)})$	1
Initial/ injection water [mol/L][1]	x [mol/L]	x [mol/L]	x [mol/L]	x [mol/L]
Minerals:				
Calcite (*M*) [mol/l_{bulk}]	0.53	$M_{k,j} = r_j 2\pi M_k^r$	$M_{k,j} = \pi(r_{(j+0.5)}^2 - r_{(j-0.5)}^2)M_k^r$	0.53
Pyrite (*M*) [mol/l_{bulk}]	0.018	$M_{k,j} = r_j 2\pi M_k^r$	$M_{k,j} = \pi(r_{(j+0.5)}^2 - r_{(j-0.5)}^2)M_k^r$	0.018
$Fe(OH)_3$; $FeCO_3$ (*M*) [mol/l_{bulk}]	0	$M_{k,j} = r_j 2\pi M_k^r$	$M_{k,j} = \pi(r_{(j+0.5)}^2 - r_{(j-0.5)}^2)M_k^r$	0
[4] nr of strong sites/mole (*S*)	0.06	$S_{k,j} = r_j 2\pi S_k^r$	$S_{k,j} = \pi(r_{(j+0.5)}^2 - r_{(j-0.5)}^2)S_k^r$	0.06
[4] nr of weak sites/mole (*S*)	0.0015	$S_{k,j} = r_j 2\pi S_k^r$	$S_{k,j} = \pi(r_{(j+0.5)}^2 - r_{(j-0.5)}^2)S_k^r$	0.15

1) Initial and injection water concentration is given in Valocchi et al. (1981) and Appelo (1994) for *TC6* and Wallis et al. (2011) for *TC7*.
2) The 3D model domain represents one-quarter of a full radial-symmetric domain (i.e. 2πr/4), with the well emplaced in one grid corner
3) Long. dispersion = 10* trans. dispersion
4) Surface connected to kinetic reactant $Fe(OH)_3$

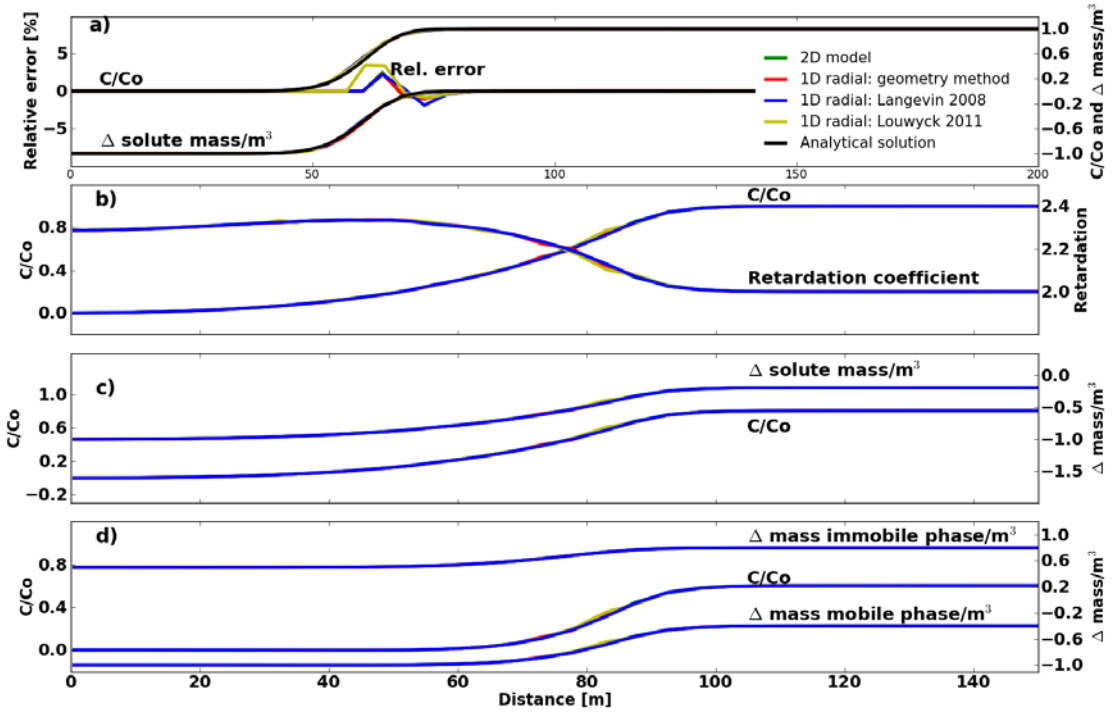

Figure 4-3 Comparison between full 2D and axi-symmetric model results (t=50days). Solute concentrations are shown as dimensionless ratio of injection to initial concentration (C/C_o). Mass of sorbed and dissolved phases are graphed as the change in mass/m^3 of aquifer at t=50days ($\Delta(mass_{initial}\text{-}mass_{actual})/m^3_{bulk\ aquifer}$); a) linear sorption: C/Co and relative error to the analytical solution is shown, as well as Δsolute mass/m^3; b) kinetic sorption: C/Co and retardation coefficient is shown; c) first-order irreversible rate reaction: C/Co and Δsolute mass/m^3; d) dual domain mass transfer: The change in mass of solute in the immobile and mobile phase per m^3 of bulk aquifer is shown as well as C/Co for the mobile domain.

Comparisons between axi-symmetric transport solutions and the corresponding 2D Cartesian model approach as well as the analytical solution for *TC2* are shown in Figure 4.3. It can be seen that dissolved species concentrations are in close agreement for all of the considered transport test cases. Where the RE could be established in relation to the analytical solution (*TC2*), it is below 5% for all model approaches (Figure 4.3a). The absolute mass of dissolved and sorbed phases within the aquifer also matches the full 2D solutions closely in all cases. Computing times for axi-symmetric models are reduced ~50 to 400-fold compared to the respective 2D Cartesian approach (Table 4.3). The *Louwyck method* is thereby consistently faster by a factor of 3 to 4 compared to the alternative radial model set-ups. The *Langevin* and *geometry method* generally yield model run times of similar duration irrespective of the transport problem. Overall, the radially-symmetric models prove to be an efficient alternative to the corresponding 2D Cartesian approach, without any loss of accuracy.

4.3.3 MULTI-COMPONENT REACTIVE TRANSPORT MODELS

Using the transport simulator PHT3D we extend the single species transport models of the previous section to include multi-component reactive transport. The first of the two investigated problems is a frequently used benchmark problem that was originally presented by Valocchi et al. (1981) (*TC6*). It involves the injection of treated municipal effluent water at a rate of 21m^3/hr into an alluvial brackish aquifer, creating a radial flow field around the recharge well. The resulting dilution front was monitored in a well at 16m distance from the injection point. Chloride served as a conservative tracer, while the breakthrough curves of the exchangeable cations (Mg^{2+}, Ca^{2+} and Na^{+}) illustrate the chromatographic separation of cations that occurs during transport.

The model parameters for this reactive transport case are noted in Table 4.2. The principal model discretization and parameterisation of the flow model remained unchanged from the previous examples (Table 4.1). However, the aquifer thickness was reduced to 1.25 meters to match the earlier reported radial flow velocities between the injection and observation point (Valocchi et al 1981). The native and injected water compositions are listed in Valocchi et al. (1981) and Appelo (1994).

The axi-symmetric model solutions are compared to the equivalent 2D PHT3D model results as well as to the solution computed by PHREEQC (Valocchi et al. 1981). All radial model

approaches allow for an accurate description of the conservative solute front as well as for the chromatographic pattern of the exchangeable cations and match the 2D model and PHREEQC solutions well (Figure 4.4). A ~70-110 fold reduction in computational time is achieved compared to the corresponding 2D Cartesian model (Table 4.3).

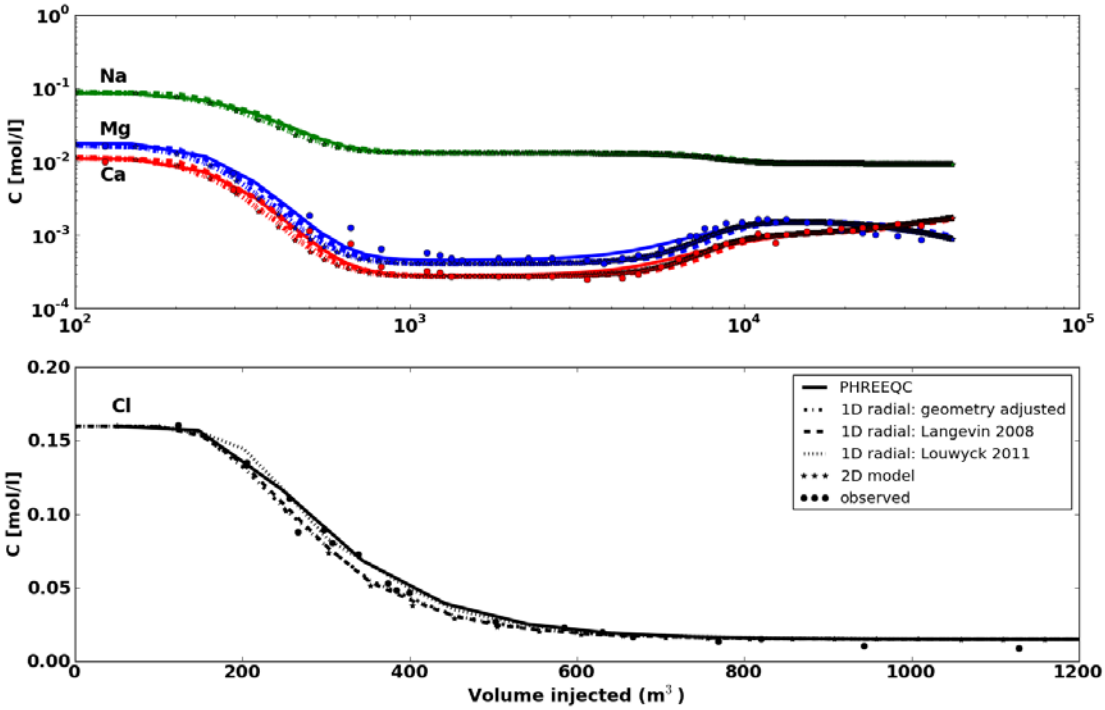

Figure 4-4 Match between axi-symmetric models and the corresponding 2D model version as well as the PHREEQC solution and the observation data by Valocchi et al. (1981) for three exchangeable cations: Na^{+} (green), Mg^{2+} (blue), Ca^{2+} (red) and chloride (black symbols, conservative).

In a final test case (TC7) the applicability and accuracy of axi-symmetric models for more comprehensive three dimensional multi-component reactive transport problems was examined. The test case was based on the conceptual model underlying a previously developed and described reactive transport model for an aquifer storage and recovery (ASR) operation in South-West Florida (Wallis et al. 2011). The reaction network of this numerical model includes redox reactions, mineral dissolution/precipitation reactions (equilibrium based and kinetically controlled) and surface complexion reactions of As and other competing ions onto $Fe(OH)_3$. The ASR operation involved the cyclic injection of oxygenated water into a reducing, pyritic aquifer before later recovery. During injection, arsenic (As) associated with pyrite, which becomes unstable under the progressively more

oxidizing conditions, is released into the aqueous solution. Simultaneously, the ferrous iron that is released during pyrite oxidation is oxidized and precipitates as $Fe(OH)_3$. The neo-precipitated $Fe(OH)_3$ provides additional sorption sites for ions and thus also for As. During recovery, when high TDS (total dissolved solids), reducing native groundwater passes back towards the ASR well, competition between As and other anions for the finite number of sorption sites on $Fe(OH)_3$ releases As by desorption. Simultaneously reductive dissolution of $Fe(OH)_3$ under the progressively more reducing conditions increases As and ferrous iron concentrations further.

The flow model that underlies this transport simulation is principally based on *TC1* (Table 4.1). However, in addition a hypothetical vertical conductivity distribution was introduced to create a heterogeneous three-dimensional flow field. The parameters that define the transport problem and their required axi-symmetric adjustments are listed in Table 4.2. Ambient and injected water compositions are given in Wallis et al. (2011).

The model comparison shows a very good agreement between the 3D Cartesian model and the respective 2D axi-symmetric models for all three model layers for conservative and reactive solutes, kinetic and equilibrium controlled minerals and solutes undergoing surface complexation reactions (Figure 4.5). The computational burden associated with the 3D Cartesian version of this problem is substantial, despite the fact that only one quarter of the full radial flow field is simulated. Run times are reduced by a factor of ~40 to 60 through the use of axi-symmetric models (Table 4.3). The above examples illustrate that axi-symmetric models are an efficient alternative to the equivalent 2D/3D model solutions for more complex transport cases. However, extreme care is required to ensure that the model inputs for the *Langevin* and *Louwyck methods* are correct, depending on the employed transport code and the reaction network considered. Therefore they typically require to be test/benchmarked against full 2D or 3D Cartesian models prior to their application.

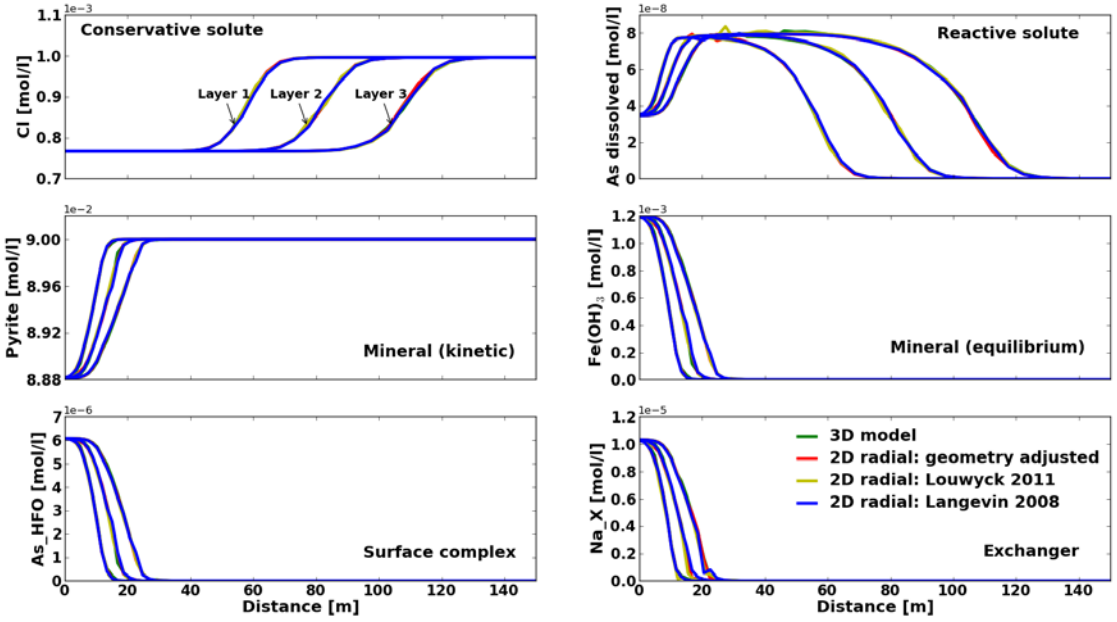

Figure 4-5 Comparison of simulated concentrations for conservative and reactive solutes, kinetic and equilibrium controlled mineral concentrations and exchanger and surface complexation sites for the full 3D model and three corresponding 2D axi-symmetric models for three model layers (t=50days).

4.3.4 EFFICIENCY VS. ACCURACY

The examples described above and the summary in Table 4.3 illustrate that the computational costs of the radially-symmetric models are substantially lower when compared to their 2D or 3D Cartesian equivalents. Depending on the implemented reaction network the radial models were ~40 to 400 times faster. Considering the two dimensional multi-component reactive transport problem (example *TC6*) this translates into a reduction from 1 day run time to about 14 minutes. However, for each simulation problem, the absolute model run times as well as the relative errors are simultaneously a function of both the model discretization, i.e., Peclet numbers and for MT3DMS-based models also of the selected advection scheme. A more strict comparison of model run times therefore needs to consider the accuracy of the numerical solution.

Comparative simulations for conservative single species transport (*TC1*) using the standard explicit finite-difference (FD) method with upstream weighting, the particle-tracking based Eulerian-Lagrangian methods (MOC, HMOC, MMOC) and the higher-order finite-volume

(TVD) scheme for the advection term are shown in Figure 4.6 for different spatial discretizations. All of these numerical schemes are available within MT3DMS and are typically implemented in many MT3DMS-based reactive transport codes such as RT3D (Clement 1997) and PHT3D (Prommer et al. 2003).

The chosen spatial model discretization plays a key role in the accuracy and efficiency of the radial transport solution (Figure 4.6). Generally, a fine discretization is required to adequately resolve steep concentration gradients commonly encountered in radial flow domains. Inherently, this increases computational demand and there is a trade-off between accuracy and efficiency. Considering the FD based model solution of *TC1*, for instance, halving the integrated relative numerical error quadruples computational demand (Figure 4.6). However, with increasing grid resolution the reduction in relative error diminishes, yet, the computational burden increases further. Consequently, there is a limit beyond which a reduction in cell size produces no more substantial gain in accuracy, but may lead to impractical run times. For the MOC based transport solution of *TC1* this limit is encountered beyond 75 model cells, when the numerical error of the transport solution remains stagnant while computational burden increases further by a factor of 6 (Figure 4.6). Numerical algorithms plagued by numerical dispersion under advection-dominated conditions (e.g., FD) generally require a finer discretization to adequately reduce the numerical error in a radial flow domain. As exact analytical solutions are not available for most field problems, testing the numerical accuracy of the transport solution vs. its computational efficiency for the chosen discretization can only be achieved by trial and error. This involves a successive refinement of the grid size and time step until convergence is achieved.

The chosen advection scheme further influences the accuracy and efficiency of the radial transport solution (Figure 4.6). Due to the radially decreasing velocities away from the point sink/source, the transport processes are likely to be advection dominated close to the injection/abstraction point and diffusion controlled where the radial flow velocity is low. Consequently, none of the numerical solution algorithms is optimal within the entire flow domain. However, the TVD, HMOC and MOC methods, which are more accurate in solving the transport solution over a relatively wide range of Peclet numbers (Figure 4.6), perform well for the majority of radial transport problems. For a given spatial discretization, they are computationally more demanding than the alternative FD or MMOC methods (Zheng and Wang, 1999). For example for *TC1* the FD scheme is approximately 5 times faster than the MOC method. However, the TVD, HMOC and MOC schemes achieve the same accuracy

with a coarser grid resolution, and therefore are overall more efficient for a given accuracy. This is illustrated in Figure 4.6, where the FD based transport solution of *TC1* required an 8 times finer grid, which resulted in 50 times longer model run times to achieve the same absolute error compared to the MOC based solution. It should, however, be noted, that the TVD scheme induces mass balance errors if layer thicknesses vary spatially and the scheme produces erroneous results if used with the model geometry.

Table 4-3. CPU model run times. The computation times cited are computer clock times on an Intel Core 1,73 GHz PC.

Model	**2D/3D model[1)]**	**1D/2D axi-symmetric**	**1D/2D axi-symmetric**	**1D/2D axi-symmetric**	**1D/2D axi-symmetric**
		Langevin (2008)	Louwyck (2011) log discretization	Louwyck (2011)	Geometry adjusted
TC1: Conservative single species transport (MT3DMS)	55min, 23sec	0min, 37 sec	12min, 18sec	0min, 9sec	0 min, 36sec
TC2: Linear sorption (MT3DMS)	20min, 20sec	0min, 13.7sec	-	0min, 6sec	0min, 26sec
TC3: First order kinetic sorption (MT3DMS)	60min, 19sec	0min, 35sec	-	0min, 12sec	0min, 37sec
TC4: First-order irreversible rate reaction (MT3DMS)	40min, 13 sec	0min, 54sec	-	0min, 16sec	0min, 50sec
TC5: Dual domain mass transfer (MT3DMS)	61min, 24sec	0min, 36sec	-	0min, 9sec	0min, 35sec
TC6: Ion-exchange (PHT3D)	245min, 7 sec	2min, 31sec	-	2min, 10sec	3min, 32sec
TC7: Multi-component reactive transport – 3D (PHT3D)	2008 min, 18sec	48min, 52sec	-	34min, 8sec	48min, 35sec

1) The 2D/3D model domain represents one-quarter of a full radial-symmetric domain (i.e. $2\pi r/4$)

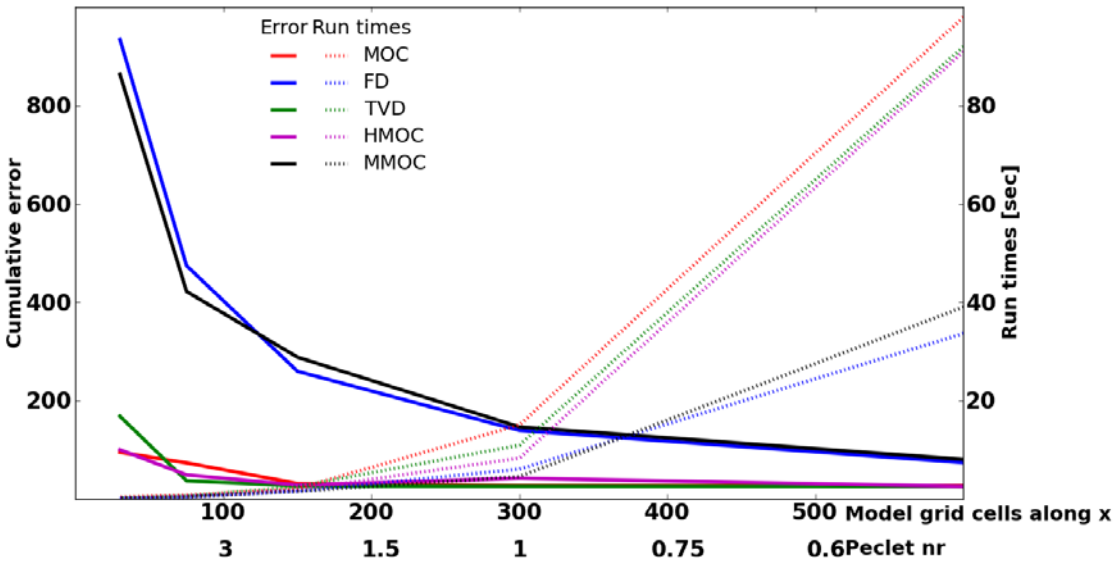

Figure 4-6 Model run times and numerical error (integrated absolute RE) to the analytical solution as a function of advection scheme and Peclet number (TC1). The cumulative error is the integrated error over the extent of the model at t=50days.

4.4 SUMMARY AND CONCLUSIONS

In this paper we presented three approaches for simulating axi-symmetric flow and transport using two MODFLOW-based solute and reactive transport model codes, i.e.; MT3DMS and PHT3D. The methods were evaluated using benchmark and analytical solutions. Our evaluation demonstrated that after the appropriate modifications of the geometry and parameters all approaches were capable of accurately reproducing a wide variety of non-reactive and reactive transport problems of different complexity. In all cases the computational burden was significantly reduced by factors ranging between ~40 to 400 when compared to the equivalent 2D/3D Cartesian model. The *Louwyck method* was consistently the most efficient approach. For the tested cases involving MT3DMS it was 2 to 3 times faster compared to the alternative *Langevin* and *geometry methods*, without any loss of numerical accuracy. However, a less pronounced difference in run-times was observed between the methods for more complicated reaction networks that were solved with PHT3D.

For the axially symmetric model approaches that rely on parameter adjustments (i.e., the *Langevin* and *Louwyck method*), the required modifications to the input parameters can make the application of these models rather cumbersome. The data input is further

dependent on the applied transport code, as well as the reaction network selected. For complex reactive transport problems, extreme care is required to ensure that the model input is free of errors. Complex manipulations will therefore typically require those axi-symmetric models to be tested/benchmarked against full 2D or 3D Cartesian models prior to their application. Radial models developed on the basis of manipulation of the model geometry (i.e., the *geometry method*) require by far less complicated input modifications. Here, only the layer thickness requires adjustment prior to any flow or transport simulation. However, the latter method is only applicable for confined aquifers and cannot be used in conjunction with codes that require layer elevations to be defined explicitly.

Discretization schemes that are optimal for the calculation of heads may not be suitable for the simulation of solute concentrations in a radial flow field. This was demonstrated through application of the prescribed logarithmic spatial discretization, as suggested in Louwyck et al. (2011) for the simulation of heads. The method was unable to provide a transport solution of sufficient accuracy. The logarithmic expansion of column width means Peclet numbers increase rapidly with distance from the point sink/source and breakthrough curves are insufficiently resolved away from the well. Depending on the advection scheme, this may also lead to excessive numerical dispersion. While the method provides increased efficiency and accuracy for the calculation of groundwater heads around point sources and sinks, it is not advisable to adopt this approach for flow modeling, if the obtained head solution is intended to be used during transport simulations. A fine discretization is generally required to adequately resolve sharp concentration fronts commonly encountered in radial flow domains, and to minimize numerical errors of the transport solution.

Advection schemes capable of accurately solving the transport solution over a relatively wide range of Peclet numbers (e.g. MOC) were shown to be most successful in balancing total computational cost and achieved numerical accuracy of radial transport test cases.

Overall, the axi-symmetric model approaches investigated have a general applicability to a broad range of radial solute transport problems subject to a great variety of chemical reactions available within the modeling framework of common transport codes. They constitute an effective way to reduce model run times, without having to compromise the complexity in the considered reactions. While the study focussed on MODFLOW-based models, similar results would be expected for other flow and transport simulators, which are based on Cartesian coordinates.

Acknowledgements

We gratefully acknowledge Simone Seibert, Evelien Martens (CSIRO) and James McCallum (Flinders University) for their reviews of earlier versions of the manuscript. Financial support for IW was provided by Land and Water Australia and Water for a Healthy Country Flagship (CSIRO Australia), which is gratefully acknowledged. Alexander Vandenbohede is supported by the Fund for Scientific Research — Flanders (Belgium).

APPENDIX A SUPPORTING INFORMATION FOR CHAPTER 2

Additional information on the setup and definition of the numerical model of the Langerak site and simulated breakthrough curves for As(III), As(V) and major and minor ions are provided in this supporting information. This material is also available via the Internet at http://pubs.acs.org.

MODEL SETUP

Injection and recovery of water at the Langerak ASTR site was assumed to establish a symmetrical flow field, allowing the numerical model to be set up as a half-model of 340m length, oriented along the axis between injection and recovery well. The model is 150m wide and no-flow boundaries were defined for the central symmetry axis and its parallel axis at 150m distance. Fixed head boundaries were defined perpendicular to the flow direction and symmetry axis. Vertically, the model domain was discretized into 5 layers over a depth ranging from -68m to -93m b.g.l. corresponding to the extent of the target aquifer. The resolution of the model grid in the horizontal direction ranged between 1m around the injection well to 15m at the model boundaries. Vertically, the discretization ranged between 4 and 6 metres.

Initial estimates of aquifer parameters and the conceptual hydrogeological model were adopted from Stuyfzand and Timmer (1999). Horizontal conductivities ranged between 15m d^{-1} and 55m d^{-1}, with vertical conductivities assumed to be 1/10 thereof (Table A-1).

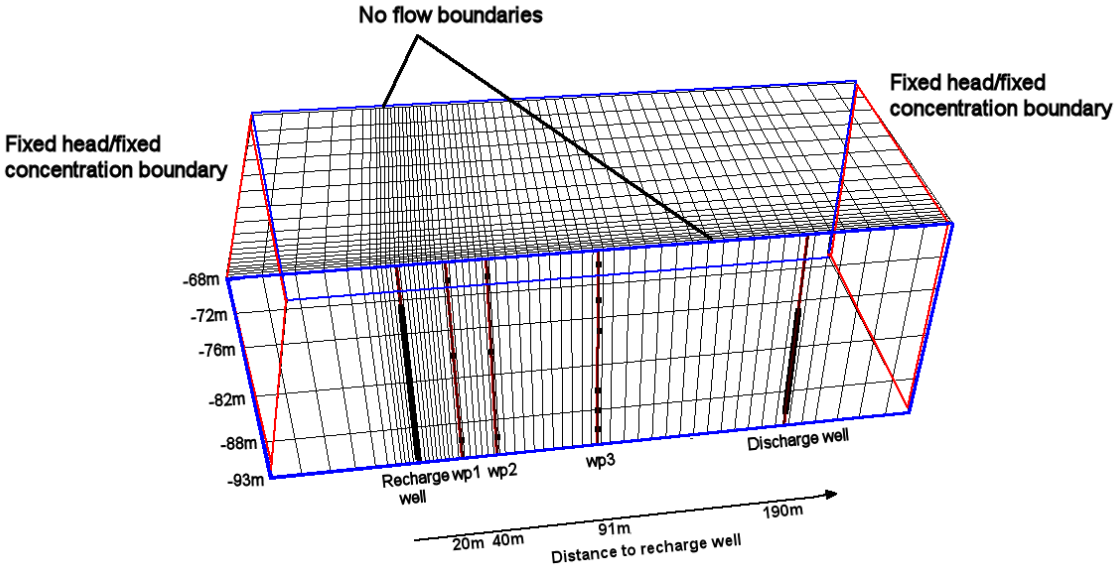

Figure A-1 Model domain with discretization and boundary conditions. Also shown are the positions of injection, abstraction and monitoring wells (wp1-3) and their well screens.

The flow and reactive transport model was run for a total simulation time of 600 days. Commencing with the start of the injection trial, the simulation time was divided into 29 stress periods. The stress periods varied in length between 2 and 42 days to accurately represent the variability of chloride input in the injection water. During model calibration, hydraulic conductivities of the stratified aquifer and the dispersivity were adjusted until the non-reactive transport model accurately reproduced the dissipation of the chloride peak, which resulted from the addition of NaCl during the first 30 days of the injection trial (Table A-1, Figure A-2).

Table A-1 Parameters of calibrated flow and non-reactive transport model. In cases where parameter estimates were changed during model calibration, initial estimates are given in brackets.

Parameter	Layer 1	Layer2-4	Layer 5	Source
Hydraulic conductivity [m d^{-1}][a)]	30 (15)	40	55 (65)	Stuyfzand and Timmer (1999), model calibration
Effective porosity []	0.31	0.31	0.31	Stuyfzand and Timmer (1999)
Longitudinal dispersivity [m][b)]	1 (0.3-5.5)	1 (0.3-5.5)	1 (0.3-5.5)	Stuyfzand and Timmer (1999), model calibration

a) Vertical to horizontal conductivity = 1:10

b) Horizontal = vertical transverse dispersivity; Horizontal/longitudinal dispersivity = 1:10

Table A-2 Parameter values used in calibrated reactive transport model

	unit	Equation	Value	Source
$k_{(Fe(II)\ ox)}$	$mol^{-2}\ atm^{-1} s^{-1}$	(1)	2.0×10^{-12}	Singer and Stumm (1970), model calibration
$k_{k(MnCO3)}$	$mol\ L^{-1}\ s^{-1}$	(2)	1.0×10^{-12}	Matsunaga et al. (1993), model calibration
$k_{O2;}$ $k_{NO3-;}$ k_{SO42-}	$mol\ L^{-1}\ s^{-1}$	(3)	1.57×10^{-9}; 1.67×10^{-11}, 1.0×10^{-13}	Parkhurst and Appelo (1999)
A_{pyr}/V	$dm^{-1}\ mol^{-1}$	(4)	300	Prommer and Stuyfzand (2005), model calibration
$k_{(Fe(OH)3)}$	$mol\ L^{-1}\ s^{-1}$	(5)	5.0×10^{-2}	Asta et al. (2009), model calibration
$k_{(MnO2)}$	$mol^{-}\ L^{-1}\ s^{-1}$	(5)	2.0	model calibration
$v_{max,}$ v_{decay}	d^{-1}	(8), (9)	0.3, 0.26	model calibration

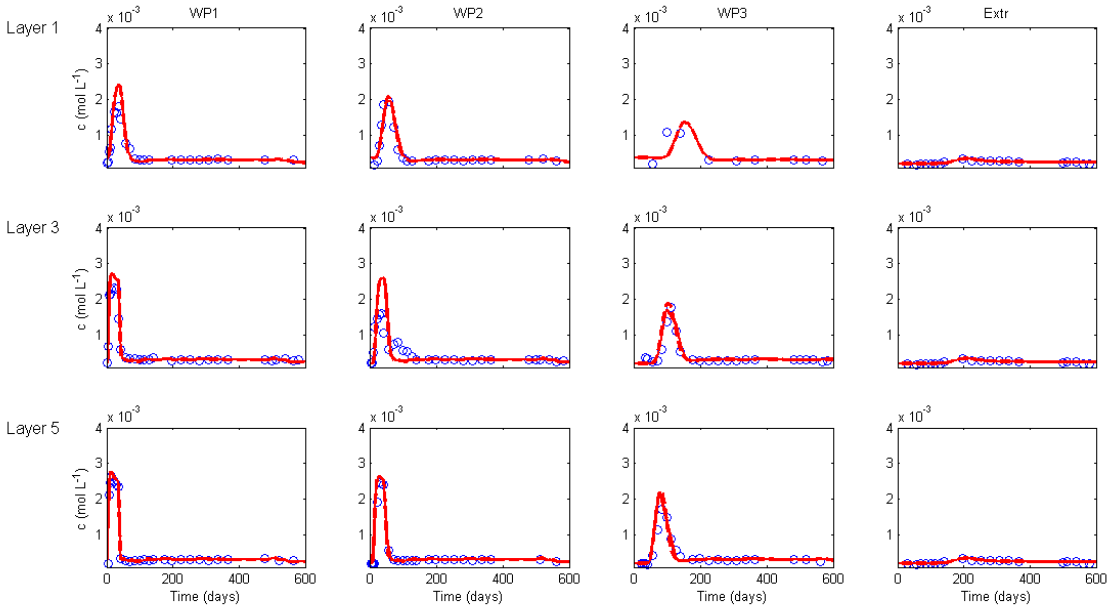

Figure A-2. Measured and simulated chloride concentrations for WP1, WP2, WP3 at different depth and at the recovery well. Simulated concentrations are indicated by solid lines, circles indicate measured chloride concentrations.

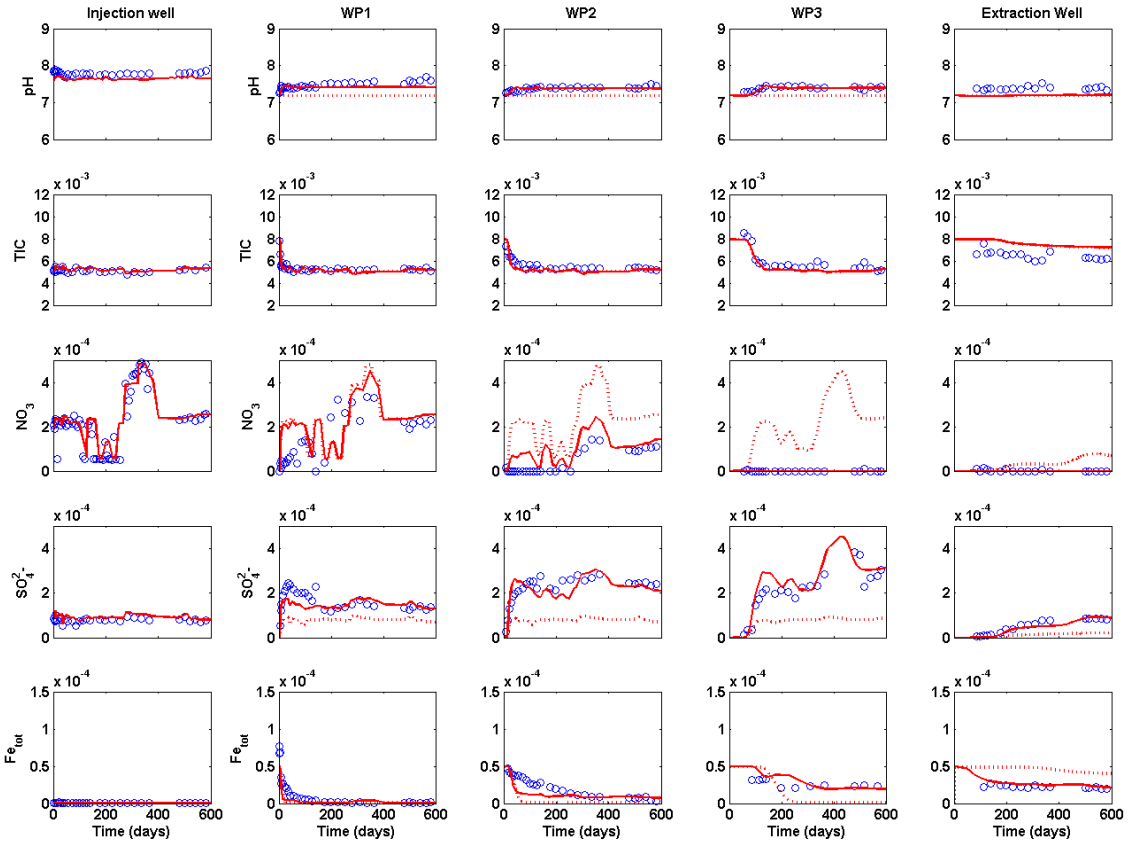

Figure A-3. Measured (circles) and simulated (solid lines) concentrations (mol L^{-1}, except pH) of aqueous components at WP1, WP2, WP3 in centre of the aquifer (Layer3) and in the extraction and injection well. Dotted lines indicate simulated results of the non-reactive model.

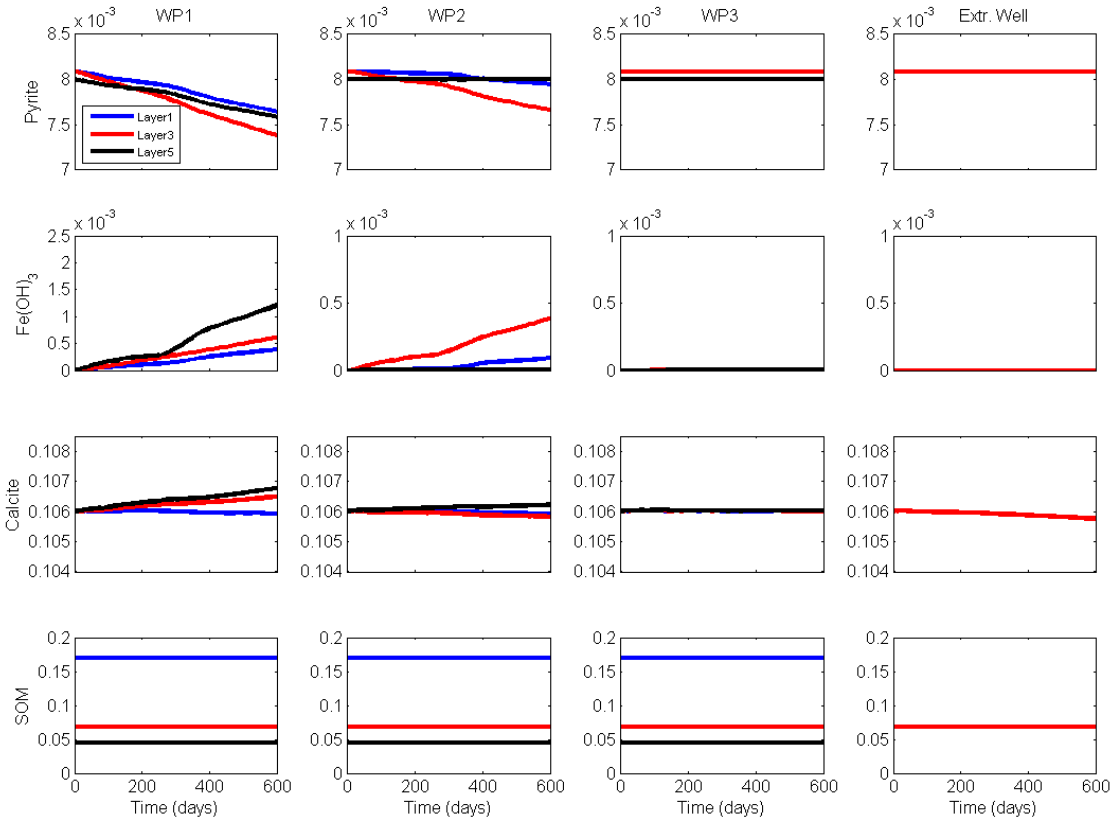

Figure A-4. Mineral and organic matter concentrations for WP1, WP2, WP3 and in the extraction well. Concentrations in mol L^{-1} bulk (concentration for pyrite in Layer 5 = C_{pyr}* 0.2).

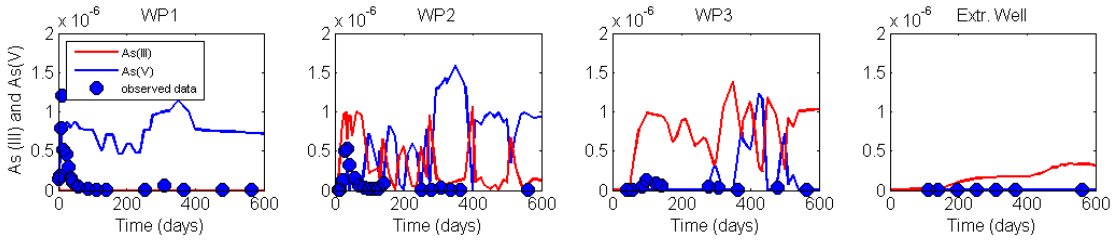

Figure A-5. Base case model run of stoichiometric release of As during pyrite dissolution assuming equilibrium-controlled arsenic speciation with no attenuation by sorption. Blue line: As(V), red line: As(III), circles indicate measured total arsenic concentrations for WP1, WP2, WP3 and the recovery well for the deep part of the aquifer (Layer5). Concentrations in mol L^{-1}.

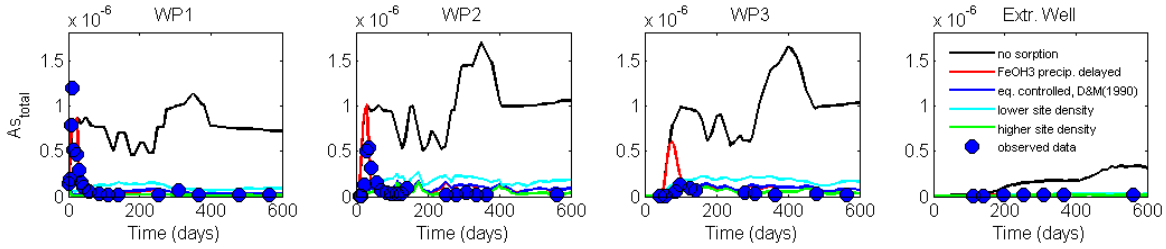

Figure A-6. Simulated (solid lines) and observed (dots) total arsenic concentrations for WP1, WP2, WP3 and the recovery well for the deep part of the aquifer (Layer5). Black line: no sorption, dark blue line: properties of HFO according to Dzombak and Morel (1990), light blue line: site densities of HFO reduced by 1/3 (i.e. weak and strong site densities 0.13 and 0.00375 mol/mol of HFO, respectively), light blue line: site densities of HFO increased by 1/3 (i.e. weak and strong site densities 0.3 and 0.0075 mol/mol of HFO, respectively), red line: forced delay in $Fe(OH)_3$ precipitation.

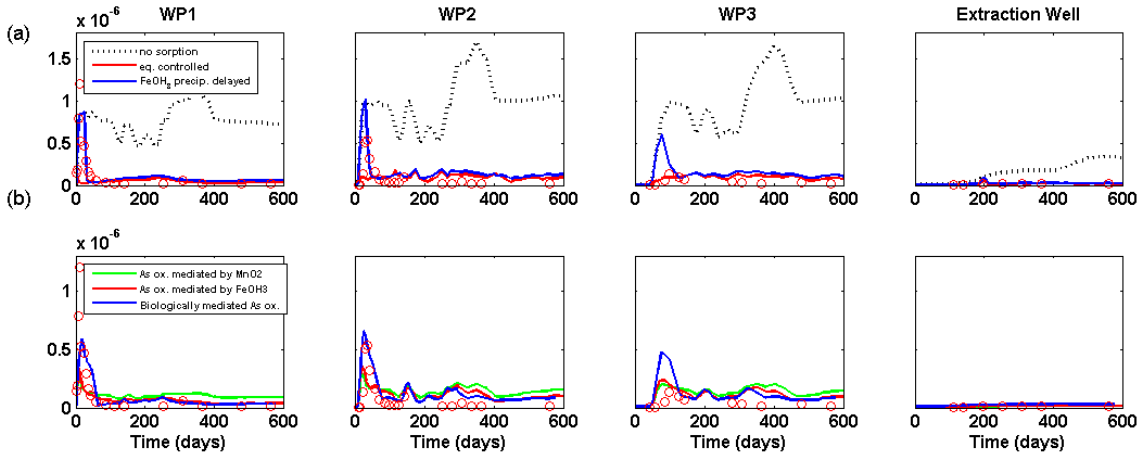

Figure A-7. Simulated (solid lines) and observed (circles) total arsenic concentrations (mol L^{-1}) for WP1, WP2, WP3 and the extraction well for the deep part of the aquifer (Layer 5). (a) black line: no attenuation by sorption, red line: equilibrium sorption of As to $Fe(OH)_3$, blue line: sorption onto $Fe(OH)_3$ delayed by pre-defined lag-time. (b) red line: abiotic oxidation of As(III) by $Fe(OH)_3$, green line: abiotic oxidation of As(III) by MnO_2, blue line: biologically mediated As(III) oxidation.

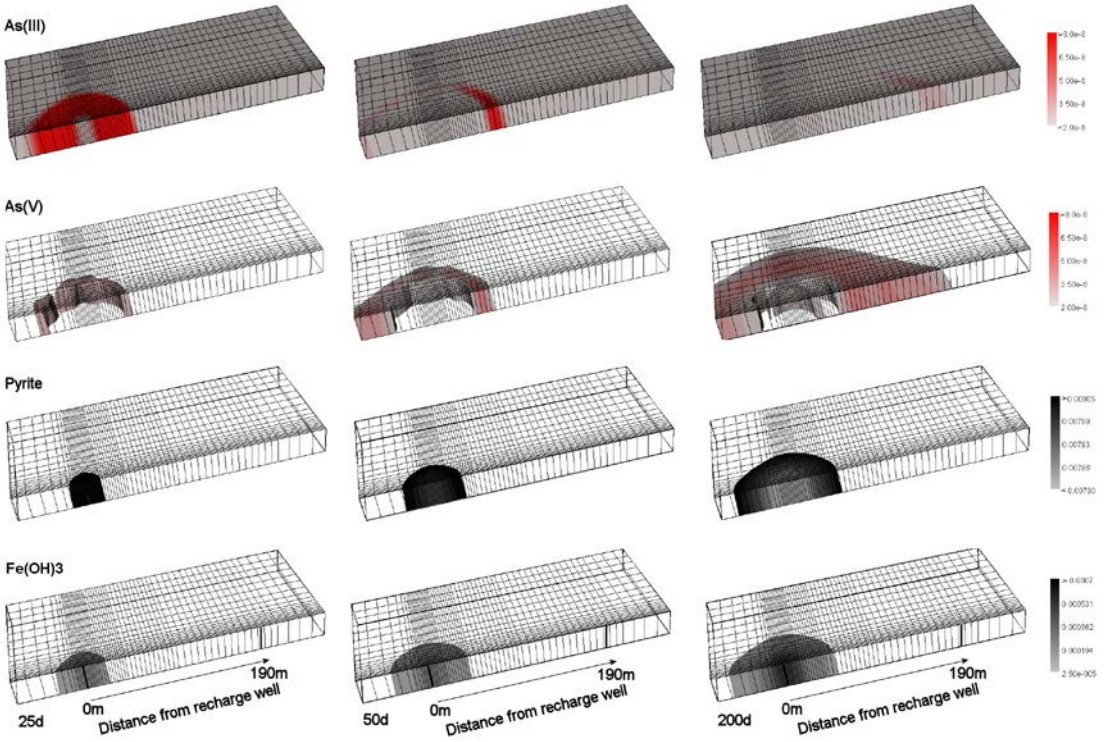

Figure A-8. Spatial distribution of As(III) and As(V) between injection and abstraction well over time in the middle of the target aquifer (Layer 3). Also shown are the area of pyrite dissolution, i.e. area in which > 0.5% of the initial pyrite mass is oxidised, and the zone of $Fe(OH)_3$ precipitation, i.e. the area in which the $Fe(OH)_3$ mass is > 1mg/kg.

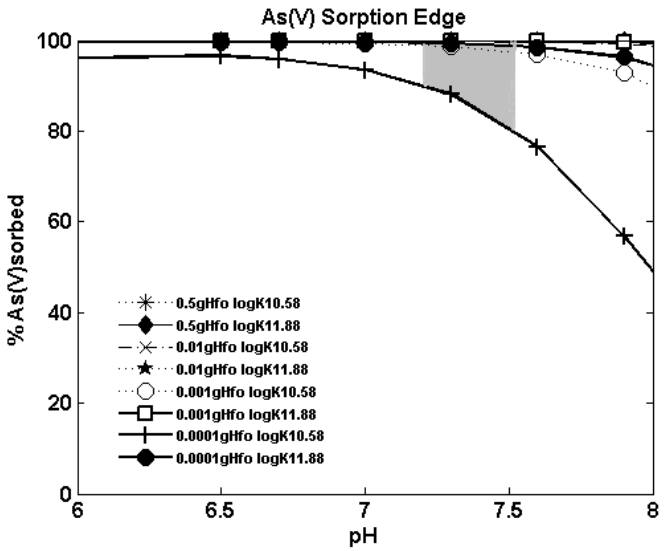

Figure A-9. pH dependent sorption of As(V) on HFO. The figure illustrates the impact of a change in the surface complexation constant for arsenate adsorption to ferrihydrite ($Hfo\_wOH + AsO_4^{-3} = Hfo\_wOHAsO_4^{-3}$) from 10.58 (Dzombak and Morel 1990) to 11.88. Sorption of As(V) onto HFO is modelled for the range of arsenic and HFO concentrations simulated for the site, i.e. concentrations of $As_{tot} = 1e^{-7}M$ and total mass of surface material varying between 0.0001 to 0.5g. HFO. For the pH range observed at the Langerak site (grey area in A-9), a difference in the amount sorbed is observable only at low HFO concentrations.

APPENDIX B SUPPORTING INFORMATION FOR CHAPTER 3

Additional information on operational conditions at the Bradenton ASR site, model set up, simulated breakthrough curves and mass balances for Arsenic and other selected species are provided in this supporting information. This material is also available via the Internet at http://pubs.acs.org.

NUMERICAL MODEL SETUP.

The 3D model has a lateral extension of 523.5 m in both x and y direction, selected such that boundaries were sufficiently far from the ASR well to not impact solute concentration fronts during the simulated ASR cycles. Selected grid cell-sizes increase from 1m near the ASR well to 20 m near the outer model fringes. The Suwannee Limestone section targeted by the ASR operation (ca. 120 - 180 m below ground level) was separated into 7 layers. A constant head boundary was implemented at all grid cells at a radial distance of 515 m from the ASR well.

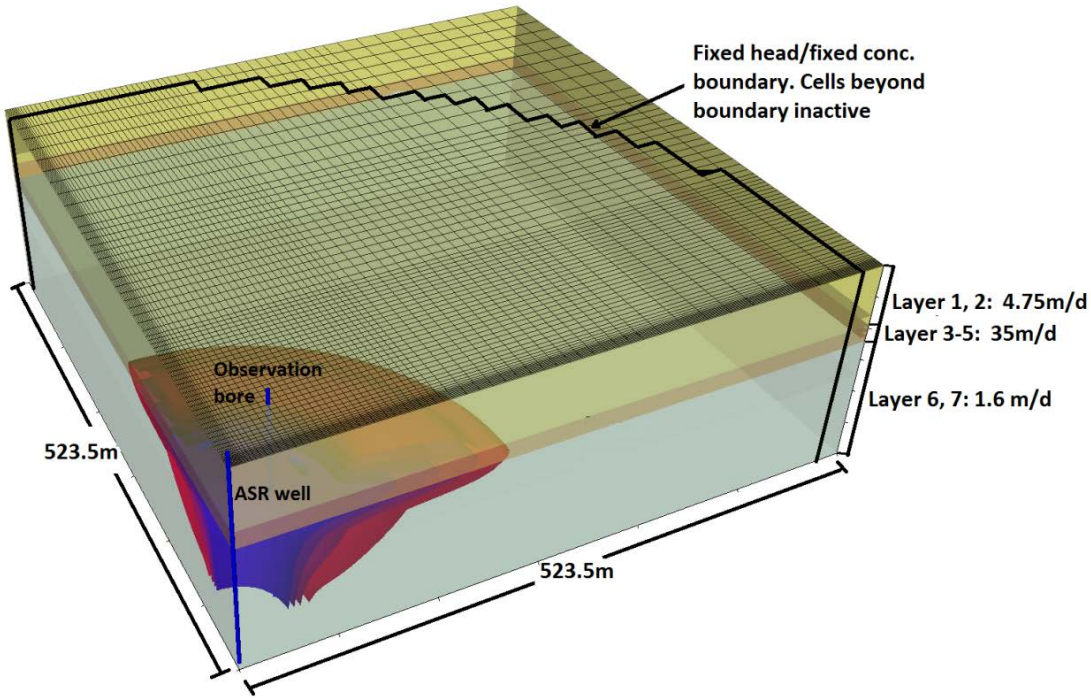

Figure B-1: Schematic illustration of the three-dimensional model, showing layering, boundaries, positions of wells and the model extent. Also shown is the simulated sulfate concentration during injection (cycle 6).

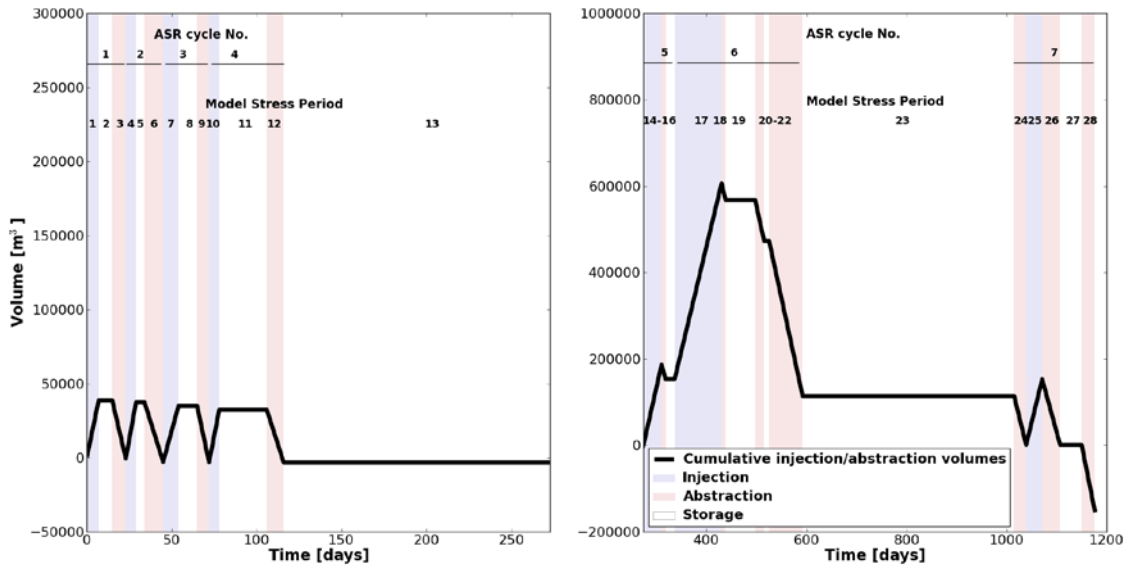

Figure B-2: Cumulative volume of injected and abstracted water of the simulated 7 ASR cycles (November 2004 to January 2008) as well as their translation into hydraulically and/or hydrochemically differing model stress periods.

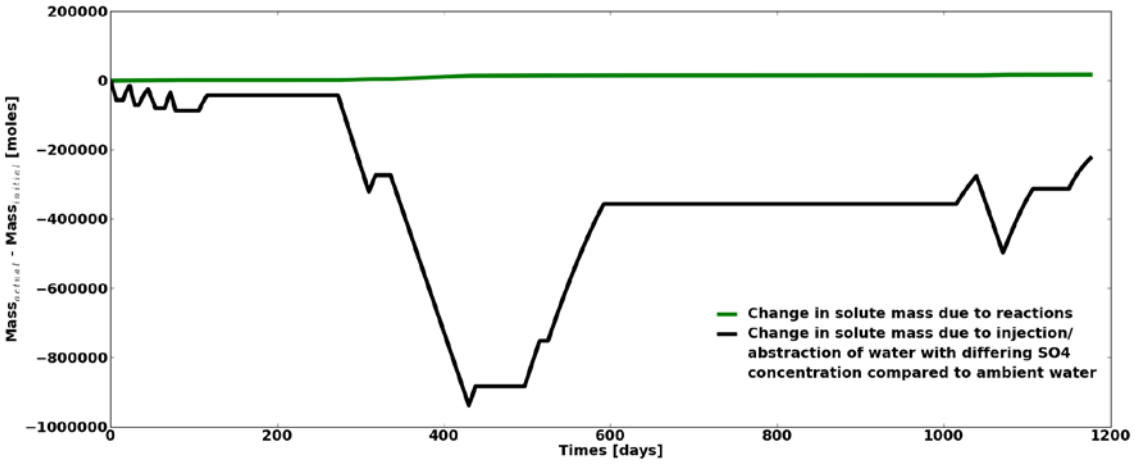

Figure B-3: Sulfate mass balance over time, illustrating freshening of the aquifer during recharge due to lower SO_4^{2-} concentrations in the injectant compared to the ambient groundwater and a return towards background water quality during recovery (black line). The contribution of reactions (e.g. pyrite dissolution) to the overall change in SO_4 mass in the aquifer is illustrated by the green line and is insignificant compared to SO_4 changes due to injection/abstraction, supporting the assumption, that SO_4 can be used as a pseudo-conservative tracer for calibration of the non-reactive transport model.

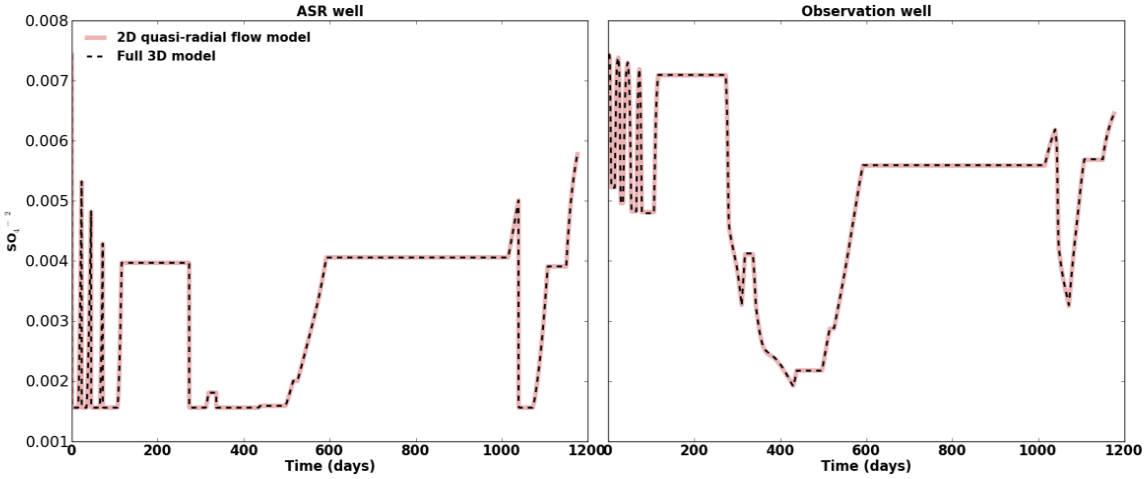

Figure B-4: Comparison of model results obtained through the full 3D model and the 2D quasi-radial flow and non-reactive transport model.

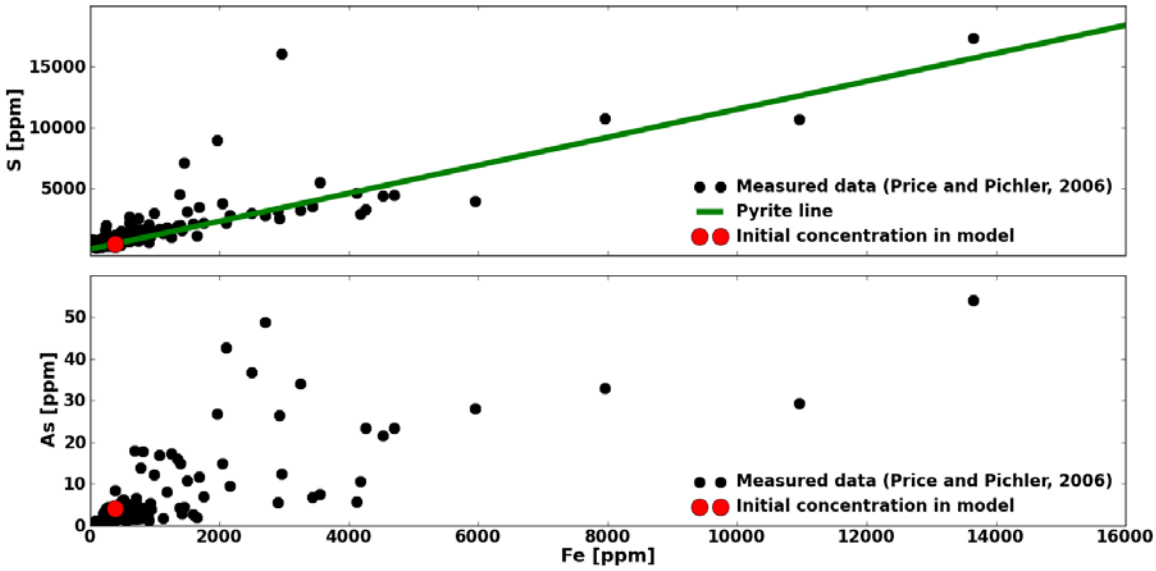

Figure B-5: Comparison between measured pyrite concentrations and initial pyrite concentrations adopted in the model based on Fe vs. S concentrations for all Suwannee Limestone core samples analyzed by Price and Pichler (2006). The "Pyrite Line" represents Fe = 2S, i.e., FeS_2. Also shown is As vs. Fe as analysed by Prize and Pichler (2006) in comparison to the initial As values in the model based on the adopted As to FeS_2 molar ratio.

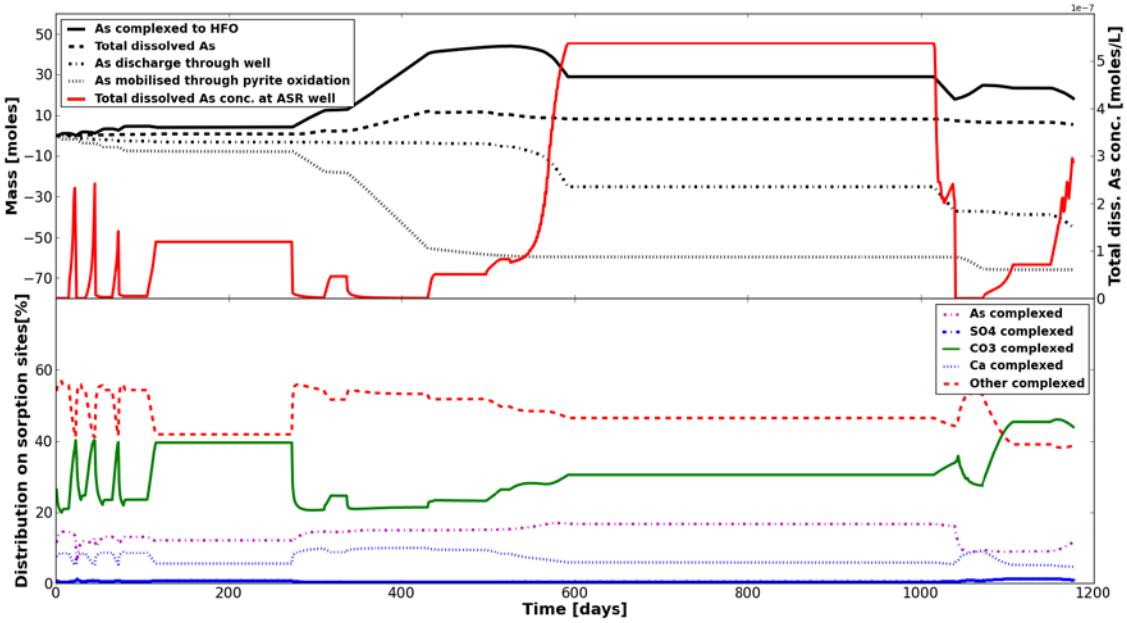

Figure B-6: Temporal variation of the integrated mass of total dissolved and surface-complexed arsenic in the aquifer, discharge of As from the ASR well, and As released from pyrite during oxidation for the entire model run (ASR cycle 1 to 7). Simulated As concentrations at the ASR well are also shown.

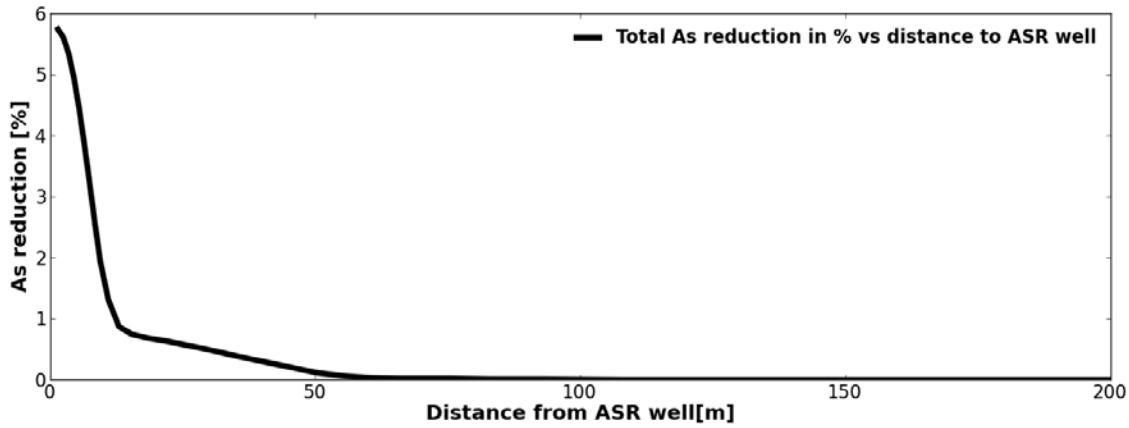

Figure B-7 Reduction in initial As mass in % at the end of cycle 7 with distance from the ASR well

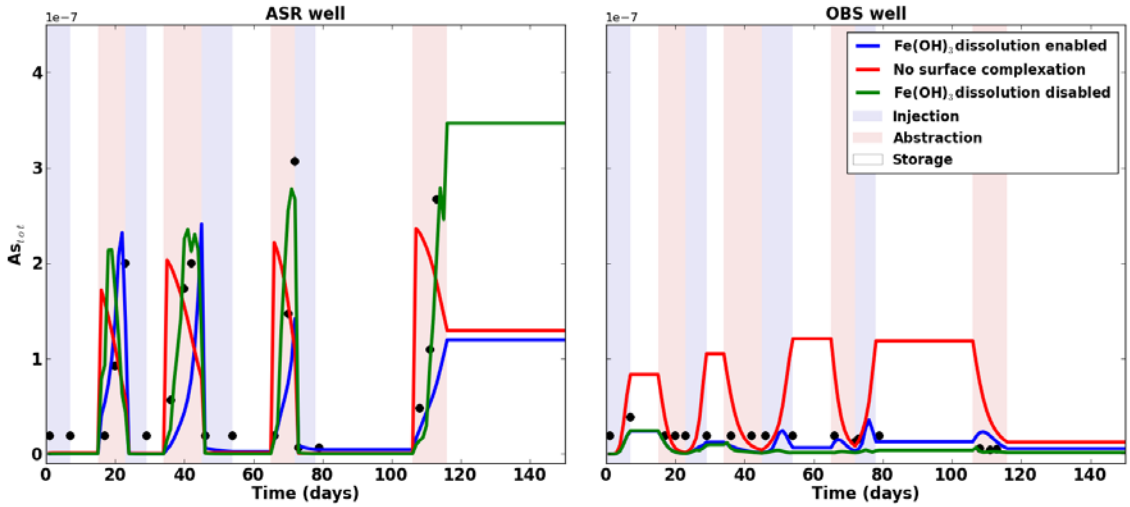

Figure B-8 Comparison of model results for the first 4 ASR cycles: Blue line: reductive dissolution of $Fe(OH)_3$ as well as competitive displacement of As from sorption sites is enabled; green line: reductive dissolution of $Fe(OH)_3$ is disabled and As mobilisation during recovery is through competitive displacement from sorption sites only; red line: Sorption onto HFO is disabled, i.e. As is not attenuated and breakthrough occurs at the observation well. Subsequently, As peak concentrations in the ASR well occur at the start of the recovery and decline towards the end.

APPENDIX C EXAMPLE INPUT DATA FOR THE GEOMETRY, LANGEVIN AND LOUWYCK METHODS

C1 GEOMETRY METHOD

Cell nr x direction	Cell width [m]	Cum. Width [m]	Midpoint of cell [m]	Radial distance [m]	Layer bot. [m]
1	1.00	1.00	0.50	3.14	-0.79
2	1.05	2.05	1.53	9.58	-2.40
3	1.10	3.15	2.60	16.34	-4.09
4	1.16	4.31	3.73	23.44	-5.86
5	1.22	5.53	4.92	30.90	-7.72
6	1.28	6.80	6.16	38.73	-9.68
7	1.34	8.14	7.47	46.95	-11.74
8	1.41	9.55	8.85	55.58	-13.89
9	1.48	11.03	10.29	64.64	-16.16
10	1.55	12.58	11.80	74.16	-18.54
11	1.63	14.21	13.39	84.15	-21.04
12	1.71	15.92	15.06	94.64	-23.66
13	1.80	17.71	16.82	105.65	-26.41
14	1.89	19.60	18.66	117.22	-29.30
15	1.98	21.58	20.59	129.36	-32.34
16	2.08	23.66	22.62	142.11	-35.53
17	2.18	25.84	24.75	155.50	-38.88
18	2.29	28.13	26.99	169.56	-42.39
19	2.41	30.54	29.34	184.32	-46.08
20	2.53	33.07	31.80	199.82	-49.96
21	2.65	35.72	34.39	216.10	-54.02
22	2.79	38.51	37.11	233.18	-58.30
23	2.93	41.43	39.97	251.13	-62.78
24	3.07	44.50	42.97	269.96	-67.49
25	3.23	47.73	46.11	289.75	-72.44
26	3.39	51.11	49.42	310.52	-77.63
27	3.56	54.67	52.89	332.33	-83.08
28	3.73	58.40	56.54	355.23	-88.81
29	3.92	62.32	60.36	379.27	-94.82
30	4.12	66.44	64.38	404.52	-101.13

C2 LANGEVIN METHOD

Cell nr x direction	Cell width [m]	Cum. Width [m]	Midpoint of cell [m]	Radial distance [m]	Hydr. Cond. [m/d] 8.64	Porosity 0.2
1	1.00	1.00	0.50	3.14	6.79	0.16
2	1.05	2.05	1.53	9.58	20.70	0.48
3	1.10	3.15	2.60	16.34	35.30	0.82
4	1.16	4.31	3.73	23.44	50.64	1.17
5	1.22	5.53	4.92	30.90	66.74	1.54
6	1.28	6.80	6.16	38.73	83.65	1.94
7	1.34	8.14	7.47	46.95	101.41	2.35
8	1.41	9.55	8.85	55.58	120.05	2.78
9	1.48	11.03	10.29	64.64	139.62	3.23
10	1.55	12.58	11.80	74.16	160.18	3.71
11	1.63	14.21	13.39	84.15	181.76	4.21
12	1.71	15.92	15.06	94.64	204.42	4.73
13	1.80	17.71	16.82	105.65	228.21	5.28
14	1.89	19.60	18.66	117.22	253.19	5.86
15	1.98	21.58	20.59	129.36	279.42	6.47
16	2.08	23.66	22.62	142.11	306.96	7.11
17	2.18	25.84	24.75	155.50	335.88	7.78
18	2.29	28.13	26.99	169.56	366.25	8.48
19	2.41	30.54	29.34	184.32	398.13	9.22
20	2.53	33.07	31.80	199.82	431.61	9.99
21	2.65	35.72	34.39	216.10	466.77	10.80
22	2.79	38.51	37.11	233.18	503.68	11.66
23	2.93	41.43	39.97	251.13	542.43	12.56
24	3.07	44.50	42.97	269.96	583.12	13.50
25	3.23	47.73	46.11	289.75	625.85	14.49
26	3.39	51.11	49.42	310.52	670.72	15.53
27	3.56	54.67	52.89	332.33	717.82	16.62
28	3.73	58.40	56.54	355.23	767.29	17.76
29	3.92	62.32	60.36	379.27	819.22	18.96
30	4.12	66.44	64.38	404.52	873.76	20.23

C3 LOUWYCK METHOD

Well radius 0.1
Width first cell 0.01
Width second cell 0.1
Width of other cells increase with factor alpha= 10^0.1

Cell nr x direction	width x direc. MODFLOW	width conc. rings	r(j-0.5)	rj	r(j+0.5)	Hydr. Cond. [m/d] 1	Porosity 0.2
1	1	0.01	0.09	0.09	0.10	59.64	0.00
2	1	0.10	0.10	0.14	0.20	9.06	0.02
3	1	0.13	0.20	0.26	0.33	12.87	0.04
4	1	0.16	0.33	0.40	0.48	15.85	0.08
5	1	0.20	0.48	0.58	0.68	18.21	0.15
6	1	0.25	0.68	0.80	0.94	20.09	0.26
7	1	0.32	0.94	1.08	1.25	21.57	0.43
8	1	0.40	1.25	1.44	1.65	22.75	0.73
9	1	0.50	1.65	1.88	2.15	23.68	1.20
10	1	0.63	2.15	2.45	2.78	24.42	1.96
11	1	0.79	2.78	3.15	3.58	25.01	3.17
12	1	1.00	3.58	4.05	4.58	25.48	5.12
13	1	1.26	4.58	5.17	5.83	25.85	8.23
14	1	1.58	5.83	6.58	7.42	26.15	13.20
15	1	2.00	7.42	8.36	9.41	26.38	21.11
16	1	2.51	9.41	10.60	11.93	26.57	33.68
17	1	3.16	11.93	13.42	15.09	26.72	53.68
18	1	3.98	15.09	16.96	19.07	26.83	85.45
19	1	5.01	19.07	21.43	24.08	26.93	135.89
20	1	6.31	24.08	27.05	30.39	27.00	215.96
21	1	7.94	30.39	34.13	38.33	27.06	343.01
22	1	10.00	38.33	43.05	48.33	27.11	544.56
23	1	12.59	48.33	54.27	60.92	27.14	864.25
24	1	15.85	60.92	68.39	76.77	27.17	1371.21
25	1	19.95	76.77	86.17	96.73	27.20	2175.09
26	1	25.12	96.73	108.56	121.84	27.22	3449.62
27	1	31.62	121.84	136.74	153.47	27.23	5470.22
28	1	39.81	153.47	172.23	193.28	27.24	8673.43
29	1	50.12	193.28	216.89	243.40	27.25	13751.12
30	1	63.10	243.40	273.13	306.49	27.26	21799.94

APPENDIX D PUBLISHED CONFERENCE PROCEEDINGS RESULTING FROM THE RESEARCH WORK

D1 NUMERICAL EVALUATION OF ARSENIC MOBILISATION DURING DEEPWELL INJECTION OF AEROBIC GROUNDWATER INTO A PYRITIC AQUIFER

Presented at the Goldschmidt conference 2009, Davos, Switzerland

Ilka Wallis[1*], Henning Prommer [2],Vincent Post[3], Pieter Stuyfzand[4], Craig Simmons[1]

[1]Flinder University, Adelaide, South Australia

[2]CSIRO Land and Water, Western Australia

[3]Vrije Universiteit Amsterdam, The Netherlands

[4]Kiwa Water Research, The Netherlands

Managed aquifer recharge is being widely promoted as an attractive technique to meet growing water demands. It involves the injection of, for example, treated or reclaimed water into permeable formations for later withdrawal. An impediment for all applications, where oxygenated water is recharged into anoxic aquifers, can be the mobilization of trace metals, including arsenic. While conceptual models for the fate of arsenic under such circumstances exist, they are generally not rigorously tested through translation into numerical modelling approaches and subsequent application to field data sets.

In this study, geochemcial data from a deepwell injection trial in The Netherlands, where arsenic mobilization resulted from the introduction of oxygenated water into an anoxic aquifer, was used to test several conceptual models of arsenic mobilization under natural flow conditions. A reactive transport model was developed to explore physical, chemical, and biochemical interactions that influence arsenic mobility under transient geochemical conditions at the field scale.

The first part of the study focussed on the simulation of the non-reactive transport behaviour. In the subsequent part of the study, a calibration for the major ion and redox chemistry was performed, where pyrite oxidation and the formation of amorphous iron-oxides were shown to be key chemical processes for water quality changes. In the final part of the study various models for arsenic release and sorption were tested. In the model that best reproduced field observations the fate of arsenic could be explained by (i) release/mobilisation via co-dissolution of arsenopyrite, stoichiometrically linked to pyrite

oxidation (ii) kinetically controlled oxidation of dissolved As(III) to As(V) and (iii) As adsorption via surface complexation on neo-precipitated amorphous iron oxides.

D2 EVALUATION OF CONCEPTUAL AND NUMERICAL MODEL FOR ARSENIC MOBILISATION DURING MANAGED AQUIFER RECHARGE

Presented at the 2010 Ground Water Summit and 2010 Ground Water Protection Council Spring Meeting, Denver, Colorado, US

Ilka Wallis[1], Henning Prommer[2], Craig T. Simmons[1], Pieter J. Stuyfzand[3], Vincent Post[4] and Thomas Pichler[5],

(1)School of Chemistry, Physics and Earth Sciences, Flinders University, Adelaide, Australia,

(2)Land and Water, CSIRO, Wembley, Western Australia 6913, Australia,

(3)KWR Watercycle Research Institute, Amsterdam, Netherlands,

(4)Faculty of Earth and Life Sciences, VU University, Amsterdam, Netherlands,

(5)Geochemistry/ Hydrogeology, University Bremen, Bremen, Germany

Managed aquifer recharge (MAR) is widely seen as a promising technique to meet growing water demands. It involves the injection of, for example, treated or reclaimed water into permeable formations for later withdrawal. An impediment for all applications, where oxygenated water is recharged into anoxic aquifers, can be the mobilization of trace metals, including arsenic. While conceptual models for the fate of arsenic under such circumstances exist, they are generally not rigorously tested through translation into numerical modeling approaches and subsequent application to field data sets.

In this study, we use well-documented examples of arsenic mobilization, i.e., a deepwell injection experiment in the Netherlands and ASR operations in west-central and southwest Florida for model development and evaluation. In all considered cases arsenic mobilization is induced during injection of oxygenated water into anoxic aquifers. Several conceptual models of arsenic mobilization were evaluated through field-scale reactive transport modeling. Initially observed chloride data were used to calibrate the groundwater flow and nonreactive transport behaviour in the MAR systems before subsequently the impact of reactive processes was quantified. The calibrated reactive transport models were then able to provide a detailed description of the spatial and temporal hydrochemical changes that occurred in the investigated MAR operations. Pyrite oxidation and the formation and dissolution of amorphous iron-oxides were shown to be the key chemical processes for water quality changes, which in turn controlled the observed fate of arsenic during the experiments.

D3 REACTIVE TRANSPORT MODELLING TO QUANTIFY ARSENIC MOBILIZATION AND CAPTURE DURING AQUIFER STORAGE AND RECOVERY OF POTABLE WATER

Presented at the Goldschmidt conference 2011, Prague

Ilka Wallis[1,2], Henning Prommer[2,3], Thomas Pichler[4], Vincent Post[1] and Craig Simmons[5]

(1)School of Chemistry, Physics and Earth Sciences, Flinders University, Adelaide, Australia,

(2)Land and Water, CSIRO, Wembley, Western Australia 6913, Australia,

(3)University of Western Australia, Australia,

(4)Geochemistry/ Hydrogeology, University Bremen, Bremen, Germany

(5) National Centre for Groundwater Research and Training, Flinders University, Adelaide, Australia

Aquifer storage and recovery (ASR) is an artificial recharge technique which is increasingly used as a water management tool to augment depleted groundwater resources. ASR is a critical component of the long-term water supply plan in various regions, including Florida and Australia. However, under particular, site-specific conditions the viability of ASR as a safe and cost-effective water resource may be impacted by elevated arsenic concentrations that are detected during recovery of the injectant. This study describes a conceptual and process-based reactive transport model of the coupled physical and geochemical mechanisms controlling the fate of arsenic during ASR. The conceptual/numerical model assumes that (i) arsenic is initially released following pyrite oxidation triggered by the injection of oxygenated water (ii) then largely complexed to neo-formed hydrous ferric oxides before (iii) being released again during recovery as a result of both dissolution of hydrous ferric oxides and displacement from sorption sites by competing anions. Multi-cycle hydrochemical data from an affected site where oxic, potable water was injected into a reducing pyrite-containing storage zone were used to evaluate the model. For this site a detailed assessment of the partitioning of arsenic among mineral phases, surface complexes and aqueous phases during injection, storage and recovery is given, together with an evaluation of temporal and areal extent of arsenic mobilization and capture.

D4 MODELLING OF ARSENIC FATE DURING ASR OF POTABLE WATER

Presented at the Modelcare conference 2011, Leipzig, Germany

Ilka Wallis[1,2], Henning Prommer[2,3], Vincent Post[1] , Thomas Pichler[4], Stuart Norton[5], Craig Simmons[6] and Mike Annable[5]

(1) School of Chemistry, Physics and Earth Sciences, Flinders University, Adelaide, Australia,

(2) Land and Water, CSIRO, Wembley, Western Australia 6913, Australia,

(3) University of Western Australia, Australia,

(4) Geochemistry/ Hydrogeology, University Bremen, Bremen, Germany

(5) Department of Environmental Engineering Sciences, University of Florida, FL

(6) National Centre for Groundwater Research and Training, Flinders University, Adelaide, Australia

ABSTRACT

Aquifer storage and recovery (ASR) is an artificial recharge technique in which potable or reclaimed water is injected in an aquifer during periods of surplus and withdrawn from the same well during periods of deficit. In cases where oxic water is recharged into reducing aquifers mobilization of trace metals may occur as a result of the oxidation of iron-sulfides. In this study our aim was to develop a numerical model that could provide a process-based description of the physical and geochemical processes controlling the fate of arsenic during ASR operations. Conceptual models for (i) the physical processes (flow and non-reactive transport) and (ii) the geochemical processes were formulated for a well-documented ASR site affected by arsenic mobilization. At that site, ambient groundwater flow velocities were negligible compared to those induced by the ASR operation and flow and transport conditions at the site were assumed to be radial-symmetric. In a first step, all site-specific hydrogeological information was incorporated into a three-dimensional groundwater flow and non-reactive transport model representing one-quarter of a radial-symmetric domain. The model calibration of the non-reactive model was well constrained by the comparison of results with measured sulphate concentrations. In a subsequent second step, a simpler, computationally more efficient one-dimensional flow and transport model was set-up, where the radially-decreasing flow velocities, which characterize the three-dimensional radial flow field, were implemented by using a variable layer thickness that corresponds to the perimeter at the radial distance of the centre of the grid-cell, i.e., the distance from the ASR well. The model allowed for the coupled simulation of the highly transient flow and geochemical conditions that prevail during the cyclic injection of oxygenated potable water into the reduced target aquifer. The results of the numerical modelling study provided conceptual insight into the predominating reaction patterns and their spatial variability under typical ASR operating conditions. For the test site the calibrated model was used to

provide a detailed appraisal of the arsenic partitioning among mineral phases, surface complexes and the aqueous phase during injection, storage and recovery together with temporal and areal extent of arsenic mobilization and capture.

REFERENCES

AMIRBAHMAN, A., D.B. KENT, G.P. CURTIS, AND J.A. DAVIS. 2006. KINETICS OF SORPTION AND ABIOTIC OXIDATION OF ARSENIC(III) BY AQUIFER MATERIALS. *GEOCHIMICA ET COSMOCHIMICA ACTA* 70 NO. 3: 533-547.

ANDERSON, M.P., AND W.W. WOESSNER. 1991. *APPLIED GROUNDWATER MODELING, SIMULATION OF FLOW AND ADVECTIVE TRANSPORT*. SAN DIEGO, CALIFORNIA: ACADEMIC PRESS.

APPELO, C.A.J. 1994. SOME CALCULATIONS ON MULTICOMPONENT TRANSPORT WITH CATION EXCHANGE IN AQUIFERS. *GROUND WATER* 32 NO. 6: 968-975.

APPELO, C.A.J., AND W.W.J.M. DE VET. 2003. MODELING IN SITU IRON REMOVAL FROM GROUNDWATER WITH TRACE ELEMENTS SUCH AS AS. IN *ARSENIC IN GROUNDWATER*, ED. A. H. WELCH AND K. G. STOLLENWERK, 381-401. BOSTON: KLUWER ACADEMIC.

APPELO, C.A.J., B. DRIJVER, R. HEKKENBERG, AND M. DE JONGE. 1999. MODELING IN SITU IRON REMOVAL FROM GROUND WATER. *GROUND WATER* 37 NO. 6: 811-817.

APPELO, C.A.J., M.J.J. VAN DER WEIDEN, C. TOURNASSAT, AND L. CHARLET. 2002. SURFACE COMPLEXATION OF FERROUS IRON AND CARBONATE ON FERRIHYDRITE AND THE MOBILIZATION OF ARSENIC. *ENVIRONMENTAL SCIENCE & TECHNOLOGY* 36 NO. 14: 3096-3103.

APPLEYARD, S.J., J. ANGELONI, AND R. WATKINS. 2006. ARSENIC-RICH GROUNDWATER IN AN URBAN AREA EXPERIENCING DROUGHT AND INCREASING POPULATION DENSITY, PERTH, AUSTRALIA. *APPLIED GEOCHEMISTRY* 21 NO. 1: 83-97.

ARTHUR, J.D., A.A. DABOUS, AND J.B. COWART. 2002. MOBILIZATION OF ARSENIC AND OTHER TRACE ELEMENTS DURING AQUIFER STORAGE AND RECOVERY, SOUTHWEST FLORIDA. IN *U.S. GEOLOGICAL SURVEY ARTIFICIAL RECHARGE WORKSHOP* ED. G. R. AIKEN AND E. L. KUNIANSKY, 20–32. SACRAMENTO, CALIFORNIA

ARTHUR, J.D., J.B. COWART, AND A.A. DABOUS. 2001. FLORIDA AQUIFER STORAGE AND RECOVERY GEOCHEMICAL STUDY: YEAR THREE PROGRESS REPORT. IN *OPEN FILE REPORT 83*, ED. D. O. E. PROTECTION. TALLAHASSEE: FLORIDA GEOLOGICAL SURVEY.

ASRSYSTEMS. 2007. EVALUATION OF ARSENIC MOBILIZATION PROCESSES OCCURING DURING AQUIFER STORAGE RECOVERY ACTIVITIES ED. S. F. W. M. DISTRICT.

ASTA, M.P., C. AYORA, J. CAMA, G. ROMAN-ROSS, A.G. GAULT, J.M. CHARNOCK, AND P. ACERO. 2009. ARSENIC MOBILIZATION IN ACID MINE DRAINAGE FROM THE TINTO SANTA ROSA MINE, IBERIAN PYRITE BELT, SPAIN. *GEOCHIMICA ET COSMOCHIMICA ACTA* 73 NO. 13, SUPPLEMENT 1: A1-A65.

BARLOW, P.M., AND A.F. MOENCH. 1999. WTAQ—A COMPUTER PROGRAM FOR CALCULATING DRAWDOWNS AND ESTIMATING HYDRAULIC PROPERTIES FOR CONFINED AND WATER-TABLE AQUIFERS. USGS WATER-RESOURCES INVESTIGATIONS REPORT 99-4225.

BARRASH, W., AND M.E. DOUGHERTY. 1997. MODELING AXIALLY SYMMETRIC AND NONSYMMETRIC FLOW TO A WELL WITH MODFLOW, AND APPLICATION TO GODDARD2 WELL TEST, BOISE, IDAHO. *GROUND WATER* 35 NO. 4: 602-611.

BECKER, M.W., AND R.J. CHARBENEAU. 2000. FIRST-PASSAGE-TIME TRANSFER FUNCTIONS FOR GROUNDWATER TRACER TESTS CONDUCTED IN RADIALLY CONVERGENT FLOW. *JOURNAL OF CONTAMINANT HYDROLOGY* 40 NO. 4: 299-310.

BOHLING, G.C., AND J.J. BUTLER. 2001. LR2DINV: A FINITE-DIFFERENCE MODEL FOR INVERSE ANALYSIS OF TWO-DIMENSIONAL LINEAR OR RADIAL GROUNDWATER FLOW. *COMPUTERS & GEOSCIENCES* 27: 1147-1156.

BURNOL, A., F. GARRIDO, P. BARANGER, C. JOULIAN, M.-C. DICTOR, F. BODÉNAN, G. MORIN AND L. CHARLET. 2007. DECOUPLING OF ARSENIC AND IRON RELEASE FROM FERRIHYDRITE SUSPENSION UNDER REDUCING CONDITIONS: A BIOGEOCHEMICAL MODEL. *GEOCHEMICAL TRANSACTIONS* 8 NO.12

CHARLET, L., S. CHAKRABORTY, C.A.J. APPELO, G. ROMAN-ROSS, B. NATH, A.A. ANSARI, M. LANSON, D. CHATTERJEE, S. BASU MALLIK. 2007. CHEMODYNAMICS OF AN ARSENIC ''HOTSPOT'' IN A WEST

BENGAL AQUIFER: A FIELD AND REACTIVE TRANSPORT MODELING STUDY. *APPLIED GEOCHEMISTRY* 22: 1273–1292.

CLEMENT, T.P. 1997. *RT3D - A MODULAR COMPUTER CODE FOR SIMULATING REACTIVE MULTI-SPECIES TRANSPORT IN 3-DIMENSIONAL GROUNDWATER AQUIFERS*. RICHLAND, WASHINGTON: PACIFIC NORTHWEST NATIONAL LABORATORY.

CULKIN, S.L.; SINGHA KAMINI, F.D. DAY-LEWIS. 2008. IMPLICATIONS OF RATE-LIMITED MASS TRANSFER FOR AQUIFER STORAGE AND RECOVERY. *GROUND WATER* 46 NO. 4: 591-605.

DE VITRE, R., N. BELZILE, AND A. TESSIER. 1991. SPECIATION AND ADSORPTION OF ARSENIC ON DIAGENETIC IRON OXYHYDROXIDES. *AMERICAN SOCIETY OF LIMNOLOGY AND OCEANOGRAPHY* 36 NO. 7: 1480-1485.

DESCOURVIERES, C., H. PROMMER, C. OLDHAM, J. GRESKOWIAK, AND N. HARTOG. 2010. KINETIC REACTION MODELING FRAMEWORK FOR IDENTIFYING AND QUANTIFYING REDUCTANT REACTIVITY IN HETEROGENEOUS AQUIFER SEDIMENTS. *ENVIRONMENTAL SCIENCE & TECHNOLOGY* 44 NO. 17: 6698-6705.

DIERSCH, H.J.G. 2002. *FEFLOW FINITE ELEMENT SUBSURFACE FLOW AND TRANSPORT SIMULATION SYSTEM—USER'S MANUAL/ REFERENCE MANUAL/WHITE PAPERS. RELEASE 5.0.* BERLIN: WASY LTD.

DILLON, P., P. PAVELIC, D. PAGE, H. BERINGEN, AND J. WARD. 2009. *MANAGED AQUIFER RECHARGE: AN INTRODUCTION*. CANBERRA: NATIONAL WATER COMMISSION.

DIXIT, S. AND J.G. HERING. 2003. COMPARISON OF ARSENIC (V) AND ARSENIC (III) SORPTION ONTO IRON OXIDE MINERALS: IMPLICATIONS FOR ARSENIC MOBILITY. *ENVIRONMENTAL SCIENCE & TECHNOLOGY* 37 NO. 18: 4182-4189.

DWYER, T.E., AND Y. ECKSTEIN. 1987. FINITE-ELEMENT SIMULATION OF LOW-TEMPERATURE, HEAT-PUMP-COUPLED, AQUIFER THERMAL ENERGY STORAGE. *JOURNAL OF HYDROLOGY* 95 NO. 1-2: 19-38.

DZOMBAK, D.A., AND F.M.M. MOREL. 1990. *SURFACE COMPLEXATION MODELING*. NEW YORK: WILEY AND SONS.

EARY, L.E., AND J.A. SCHRAMKE. 1990. RATES OF INORGANIC OXIDATION REACTIONS INVOLVING DISSOLVED-OXYGEN. *ACS SYMPOSIUM SERIES* 416: 379-396.

ECKERT, P., AND C.A.J. APPELO. 2002. HYDROGEOCHEMICAL MODELING OF ENHANCED BENZENE, TOLUENE, ETHYLBENZENE, XYLENE (BTEX) REMEDIATION WITH NITRATE. *WATER RESOURCES RESEARCH* 38 NO. 8.

FEEHLEY, C.E., AND C. ZHENG. 2000. A DUAL-DOMAIN MASS TRANSFER APPROACH FOR MODELING SOLUTE TRANSPORT IN HETEROGENEOUS AQUIFERS: APPLICATION TO THE MACRODISPERSION EXPERIMENT (MADE) SITE. . *WATER RESOURCES RESEARCH* 36 NO. 9: 2501-2515.

GELHAR, L.W., AND M.A. COLLINS. 1971. GENERAL ANALYSIS OF LONGITUDINAL DISPERSION IN NONUNIFORM FLOW. *WATER RESOURCES RESEARCH* 7 NO. 6: 1511-1521.

GOLDBERG, S. 2002. ADSORPTION OF ARSENATE AND ARSENITE ON OXIDES AND CLAY MINERALS. *SOIL SCI. SOC. AM. J.* 66: 413–421.

GOLTZ, M.N., AND M.E. OXLEY. 1991. ANALYTICAL MODELING OF AQUIFER DECONTAMINATION BY PUMPING WHEN TRANSPORT IS AFFECTED BY RATE-LIMITED SORPTION. *WATER RESOURCES RESEARCH* 27 NO. 4: 547-556.

GOODE, D.J., AND C.A. APPEL. 1992. FINITE-DIFFERENCE INTERBLOCK TRANSMISSIVITY FOR UNCONFINED AQUIFERS AND FOR AQUIFER HAVING SMOOTHLY VARYING TRANSMISSIVITY. USGS WATER-RESOUCES INVESTIGATIONS REPORT 92-4124. RESTON, VIRGINIA: USGS.

GOTKOWITZ, M. B., M.E. SCHREIBER, T. SIMO. 2000. DELINEATING CAUSES OF ARSENIC CONTAMINATION OF GROUNDWATER, EASTERN WISCONSIN. *EOS TRANS., AM. GEOPHYS. UNION FALL MEETING SUPPL. 81* NO. 52.

GRESKOWIAK, J., H. PROMMER, J. VANDERZALM, P. PAVELIC, AND P. DILLON. 2005. MODELING OF CARBON CYCLING AND BIOGEOCHEMICAL CHANGES DURING INJECTION AND RECOVERY OF RECLAIMED WATER AT BOLIVAR, SOUTH AUSTRALIA. *WATER RESOURCES RESEARCH* 41 NO. 10.

GRIFFIOEN, J., AND C.A.J. APPELO. 1993. NATURE AND EXTENT OF CARBONATE PRECIPITATION DURING AQUIFER THERMAL ENERGY STORAGE. *APPLIED GEOCHEMISTRY* 8 NO. 2: 161-176.

GUO, W., AND C.D. LANGEVIN. 2002. *USER'S GUIDE TO SEAWAT: A COMPUTER PROGRAM FOR THE SIMULATION OF THREE-DIMENSIONAL VARIABLE-DENSITY GROUND-WATER FLOW.* USGS TECHNIQUES OF WATER RESOURCES INVESTIGATIONS BOOK 6, CHAPTER A7. RESTON, VIRGINIA: USGS.

HALFORD, K.J., AND D. YOBBI. 2006. ESTIMATING HYDRAULIC PROPERTIES USING A MOVING-MODEL APPROACH AND MULTIPLE AQUIFER TESTS. *GROUND WATER* 44 NO. 2: 284-291.

HARBAUGH, A.W. 2005. *MODFLOW-2005, THE U.S. GEOLOGICAL SURVEY MODULAR GROUND-WATER MODEL—THE GROUND-WATER FLOW PROCESS.*: USGS OPEN-FILE REPORT. RESTON, VIRGINIA: USGS.

HARBAUGH, A.W., E.R. BANTA, M.C. HILL, AND M.G. MCDONALD. 2000. MODFLOW-2000, THE U.S. GEOLOGICAL SURVEY MODULAR GROUND-WATER MODEL: USER GUIDE TO MODULARIZATION CONCEPTS AND THE GROUND-WATER FLOW PROCESS. USGS OPEN-FILE REPORT. RESTON, VIRGINIA: USGS.

HE, Y.T., A.G. FITZMAURICE, A. BILGIN, S. CHOI, P. O'DAY, J. HORST, J. HARRINGTON, H.J., REISINGER, D.R. BURRIS AND J.G. HERING. 2010. GEOCHEMICAL PROCESSES CONTROLLING ARSENIC MOBILITY IN GROUNDWATER: A CASE STUDY OF ARSENIC MOBILIZATION AND NATURAL ATTENUATION. *APPLIED GEOCHEMISTRY* 25, NO. 1: 69-80.

Hiemstra, T. and van Riemsdijk, W. 1996. A surface Structural Approach to Ion Adsorption: The Charge Distribution (CD) Model. *J.Colloid Interface Sci.* no. 179, pp. 488-508.

HSIEH, P.A. 1986. A NEW FORMULA FOR THE ANALYTICAL SOLUTION OF THE RADIAL DISPERSION PROBLEM. *WATER RESOURCES RESEARCH* 22 NO. 11: 1597-1605.

HUANG, J.Q., J.A. CHRIST, AND M.N. GOLTZ. 2010. ANALYTICAL SOLUTIONS FOR EFFICIENT INTERPRETATION OF SINGLE-WELL PUSH-PULL TRACER TESTS. *WATER RESOURCES RESEARCH* 46. W08538, DOI:10.1029/2008WR007647.

HUG, S.J., AND O. LEUPIN. 2003. IRON-CATALYZED OXIDATION OF ARSENIC(III) BY OXYGEN AND BY HYDROGEN PEROXIDE: PH-DEPENDENT FORMATION OF OXIDANTS IN THE FENTON REACTION. *ENVIRONMENTAL SCIENCE & TECHNOLOGY* 37 NO. 12: 2734-2742.

ISLAM, F. S.,A. G. GAULT, C. BOOTHMAN, D. A. POLYA, J.M. CHARNOCK, D. CHATTERJEE AND J.R. LLOYD. 2004. ROLE OF METAL-REDUCING BACTERIA IN ARSENIC RELEASE FROM BENGAL DELTA SEDIMENTS. NATURE. 430 NO: 6995:68-71.

ISTOK, J.D., M.D. HUMPHREY, M.H. SCHROTH, M.R. HYMAN, AND K.T. O'REILLY. 1997. SINGLE-WELL, "PUSH-PULL" TEST FOR IN SITU DETERMINATION OF MICROBIAL ACTIVITIES. *GROUND WATER* 35 NO. 4: 619-631.

JANG, J .–H. AND B.A. DEMPSEY. 2008 COADSORPTION OF ARSENIC(III) AND ARSENIC(V) ONTO HYDROUS FERRIC OXIDE: EFFECTS ON ABIOTIC OXIDATION OF ARSENIC(III), EXTRACTION EFFICIENCY, AND MODEL ACCURACY. *ENVIRONMENTAL SCIENCE & TECHNOLOGY.* 42, 2893–2898.

JEPPU, G.P., T. P. CLEMENT, M. O. BARNETT AND K.-K LEE. 2010. A SCALABLE SURFACE COMPLEXATION MODELING FRAMEWORK FOR PREDICTING ARSENATE ADSORPTION ON GOETHITE-COATED SANDS. *ENVIRONMENTAL ENGINEERING SCIENCE*. 27 NO.2: 147-158.

JOHNSON, G.S., D.M. COSGROVE, AND D.B. FREDERICK. 2001. A NUMERICAL MODEL AND SPREADSHEET INTERFACE FOR PUMPING TEST ANALYSIS. *GROUND WATER* 39 NO. 4: 582-592.

JONES, G.W., AND T. PICHLER. 2007. RELATIONSHIP BETWEEN PYRITE STABILITY AND ARSENIC MOBILITY DURING AQUIFER STORAGE AND RECOVERY IN SOUTHWEST CENTRAL FLORIDA. *ENVIRONMENTAL SCIENCE & TECHNOLOGY* 41 NO. 3: 723-730.

KIM, J., Y. LEE, W.S. YOON, J.S. JEON, M.-H. KOO, AND Y. KEEHM. 2010. NUMERICAL MODELING OF AQUIFER THERMAL ENERGY STORAGE SYSTEM. *ENERGY* 35 NO. 12: 4955-4965.

KINNIBURGH, D.G., P.L. SMEDLEY, J. DAVIES, C. MILNE, I. GAUS, J.M. TRAFFORD, S. BURDEN, S.M.I. HUQ, N. AHMAD, AND K.M. AHMED. 2003. THE SCALE AND CAUSES OF THE GROUND WATER ARSENIC PROBLEM IN BANGLADESH. IN *GROUNDWATER: OCCURRENCE AND GEOCHEMISTRY* ED. A. H. WELCH AND K. G. STOLLENWERK, 211–257. BOSTON: KLUWER.

KRUSEMAN, G.P., AND N.A. DE RIDDER. 1990. *ANALYSIS AND EVALUATION OF PUMPING TEST DATA*. 2ND. ED. WAGENINGEN.

LANGEVIN, C.D. 2008. MODELING AXISYMMETRIC FLOW AND TRANSPORT. *GROUND WATER* 46 NO. 4: 579-590.

LANGEVIN, C.D., AND W. GUO. 2006. MODFLOW/MT3DMS-BASED SIMULATION OF VARIABLE DENSITY GROUND WATER FLOW AND TRANSPORT. *GROUND WATER* 44 NO. 3: 339-351.

LEUPIN, O.X., AND S.J. HUG. 2005. OXIDATION AND REMOVAL OF ARSENIC (III) FROM AERATED GROUNDWATER BY FILTRATION THROUGH SAND AND ZERO-VALENT IRON. *WATER RESEARCH* 39 NO. 9: 1729-1740.

LOUWYCK, A., A. VANDENBOHEDE, M. BAKKER, AND L. LEBBE. 2011. SIMULATION OF AXI-SYMMETRIC FLOW TOWARDS WELLS: A FINITE-DIFFERENCE APPROACH. *COMPUTERS & GEOSCIENCES*, DOI:10.1016/J.CAGEO.2011.09.004

MANNING, B.A., M.L. HUNT, C. AMRHEIN, AND J.A. YARMOFF. 2002B. ARSENIC(III) AND ARSENIC(V) REACTIONS WITH ZEROVALENT IRON CORROSION PRODUCTS. *ENVIRONMENTAL SCIENCE AND TECHNOLOGY* 36 NO. 24: 5455-5461.

MANNING, B.A., S.E. FENDORF, B. BOSTICK, AND D.L. SUAREZ. 2002A. ARSENIC(III) OXIDATION AND ARSENIC(V) ADSORPTION REACTIONS ON SYNTHETIC BIRNESSITE. *ENVIRONMENTAL SCIENCE & TECHNOLOGY* 36 NO. 5: 976-981.

MANSOUR, M.M., A.G. HUGHES, AND A.E.F. SPINK. 2007. USER MANUAL FOR THE LAYERED R-THETA NUMERICAL MODEL. BRITISH GEOLOGICAL SURVEY 59.

MATSUNAGA, T., G. KARAMETAXAS, H.R. VONGUNTEN, AND P.C. LICHTNER. 1993. REDOX CHEMISTRY OF IRON AND MANGANESE MINERALS IN RIVER-RECHARGED AQUIFERS - A MODEL INTERPRETATION OF A COLUMN EXPERIMENT. *GEOCHIMICA ET COSMOCHIMICA ACTA* 57 NO. 8: 1691-1704.

MCDONALD, M.G., AND A.W. HARBAUGH. 1988. *A MODULAR THREEDIMENSIONAL FINITE-DIFFERENCE GROUND-WATER FLOW MODEL.*: USGS OPEN-FILE REPORT. RESTON, VIRGINIA: USGS.

MIRECKI, J.E. 2004. WATER-QUALITY CHANGES DURING CYCLE TESTING AT AQUIFER STORAGE RECOVERY (ASR) SYSTEMS OF SOUTH FLORIDA. U. S. ARMY ENGINEER RESEARCH AND DEVELOPMENT CENTER ERDC TECHNICAL REPORT.

MIRECKI, J.E. 2006. GEOCHEMICAL MODELS OF WATER-QUALITY CHNAGES DURING AQUIFER STORAGE RECOVERY (ASR) CYCLE TESTS, PHASE I: GEOCHEMICAL MODELS USING EXISTING DATA. US ARMY CORPS OF ENGINEERS.

MOLDOVAN, B.J., AND M.J. HENDRY. 2005. CHARACTERIZING AND QUANTIFYING CONTROLS ON ARSENIC SOLUBILITY OVER A PH RANGE OF 1−11 IN A URANIUM MILL-SCALE EXPERIMENT. *ENVIRONMENTAL SCIENCE & TECHNOLOGY* 39 NO. 13: 4913-4920.

NORTON, S.B. 2007. QUANTIFYING THE NEAR-BOREHOLE GEOCHEMICAL RESPONSE DURING AQUIFER STORAGE AND RECOVERY: APPLICATION OF "PUSH-PULL" ANALYTICAL TECHNIQUES TO ASR CYCLE TESTING, DEPARTMENT OF ENVIRONMENTAL ENGINEERING SCIENCES, UNIVERSITY OF FLORIDA.

OREMLAND, R.S., AND J.F. STOLZ. 2003. THE ECOLOGY OF ARSENIC *SCIENCE* 300 NO. 5621: 939-944.

OSCARSON, D.W., P.M. HUANG, C. DEFOSSE, AND A. HERBILLON. 1981. OXIDATIVE POWER OF MN(IV) AND FE(III) OXIDES WITH RESPECT TO AS(III) IN TERRESTRIAL AND AQUATIC ENVIRONMENTS. *NATURE* 291 NO. 5810: 50-51.

OYA, S., AND A.J. VALOCCHI. 1998. ANALYTICAL APPROXIMATION OF BIODEGRADATION RATE FOR IN SITU BIOREMEDIATION OF GROUNDWATER UNDER IDEAL RADIAL FLOW CONDITIONS. *JOURNAL OF CONTAMINANT HYDROLOGY* 31 NO. 3-4: 275-293.

PARKHUST, D., CHRISTENSON, S. AND G.N. BREIT. 1996. GROUND-WATER-QUALITY ASSESSMENT OF THE CENTRAL OKLAHOMA AQUIFER, OKLAHOMA-GEOCHEMICAL AND GEOHYDROLOGICAL INVESTIGATIONS. U.S. GEOLOGICAL SURVEY WATER-SUPPLY PAPER 2357

PARKHURST, D., AND C. APPELO. 1999. USER'S GUIDE TO PHREEQC (VERSION 2)—A COMPUTER PROGRAM FOR SPECIATION, BATCH- REACTION, ONE-DIMENSIONAL TRANSPORT, AND INVERSE GEOCHEMICAL CALCULATIONS. US GEOLOGICAL SURVEY WATER-RESOURCES INVESTIGATIONS REPORT

PARKHURST, D., KIPP, K.L. AND S.R. CHARLTON. 2010. PHAST VERSION 2—A PROGRAM FOR SIMULATING GROUNDWATER FLOW, SOLUTE TRANSPORT, AND MULTICOMPONENT GEOCHEMICAL REACTIONS: U.S. GEOLOGICAL SURVEY TECHNIQUES AND METHODS 6–A35, 235 P.

PHANIKUMAR, M.S., AND J.T. MCGUIRE. 2010. A MULTI-SPECIES REACTIVE TRANSPORT MODEL TO ESTIMATE BIOGEOCHEMICAL RATES BASED ON SINGLE-WELL PUSH–PULL TEST DATA. *COMPUTERS & GEOSCIENCES* 36 NO. 8: 997-1004.

PLANT, J.A., D.G. KINNIBURGH, P.L. SMEDLEY, F.M. FORDYCE, B.A. KLINCK, D.H. HEINRICH, AND K.T. KARL. 2007. ARSENIC AND SELENIUM. IN *TREATISE ON GEOCHEMISTRY*, 17-66. OXFORD: PERGAMON.

PLUMMER, L.N., T.M.L. WIGLEY, AND D.L. PARKHURST. 1978. THE KINETICS OF CALCITE DISSOLUTION IN CO2-WATER SYSTEMS AT 5-60 C AND 0. 0-1.0 ATM CO2. *AMERICAN JOURNAL OF SCIENCE* 278: 179-216.

POSTMA, D., F. LARSEN, N.T. MINH HUE, M.T. DUC, P.H. VIET, P.Q. NHAN, AND S. JESSEN. 2007. ARSENIC IN GROUNDWATER OF THE RED RIVER FLOODPLAIN, VIETNAM: CONTROLLING GEOCHEMICAL PROCESSES AND REACTIVE TRANSPORT MODELING. *GEOCHIMICA ET COSMOCHIMICA ACTA* 71 NO. 21: 5054-5071.

PRICE, R.E., AND T. PICHLER. 2006. ABUNDANCE AND MINERALOGICAL ASSOCIATION OF ARSENIC IN THE SUWANNEE LIMESTONE (FLORIDA): IMPLICATIONS FOR ARSENIC RELEASE DURING WATER-ROCK INTERACTION. *CHEMICAL GEOLOGY* 228 NO. 1-3: 44-56.

PROMMER, H., AND P.J. STUYFZAND. 2005. IDENTIFICATION OF TEMPERATURE-DEPENDENT WATER QUALITY CHANGES DURING A DEEP WELL INJECTION EXPERIMENT IN A PYRITIC AQUIFER. *ENVIRONMENTAL SCIENCE & TECHNOLOGY* 39 NO. 7: 2200-2209.

PROMMER, H., D.A. BARRY, AND C. ZHENG. 2003. MODFLOW/MT3DMS-BASED REACTIVE MULTICOMPONENT TRANSPORT MODELING. *GROUND WATER* 41 NO. 2: 247-257.

PROMMER, H., D.A. BARRY, AND G.B. DAVIS. 2002. MODELLING OF PHYSICAL AND REACTIVE PROCESSES DURING BIODEGRADATION OF A HYDROCARBON PLUME UNDER TRANSIENT GROUNDWATER FLOW CONDITIONS. *JOURNAL OF CONTAMINANT HYDROLOGY* 59 NO. 1-2: 113-131.

RADU, T., A. KUMAR, T.P. CLEMENT, G. JEPPU, AND M.O. BARNETT. 2008. DEVELOPMENT OF A SCALABLE MODEL FOR PREDICTING ARSENIC TRANSPORT COUPLED WITH OXIDATION AND ADSORPTION REACTIONS. *JOURNAL OF CONTAMINANT HYDROLOGY* 95 NO. 1-2: 30-41.

REILLY, T.E., AND A.W. HARBAUGH. 1993. COMPUTER NOTE: SIMULATION OF CYLINDRICAL FLOW TO A WELL USING THE U.S. GEOLOGICAL SURVEY MODULAR FINITE-DIFFERENCE GROUND-WATER FLOW MODEL. *GROUND WATER* 31 NO. 3: 489-494.

ROBERTS, L.C., S.J. HUG, T. RUETTIMANN, M. BILLAH, A.W. KHAN, AND M.T. RAHMAN. 2004. ARSENIC REMOVAL WITH IRON(II) AND IRON(III) WATERS WITH HIGH SILICATE AND PHOSPHATE CONCENTRATIONS. *ENVIRONMENTAL SCIENCE AND TECHNOLOGY* 38 NO. 1: 307–315.

RUITER, H., AND P.J. STUYFZAND. 1998. AN EXPERIMENT ON WELL RECHARGE OF OXIC WATER INTO AN ANOXIC AQUIFER. IN *ARTIFICIAL RECHARGE OF GROUNDWATER*, ED. J. H. PETERS, ET AL., 299-304. ROTTERDAM, NETHERLANDS: A.A. BALKEMA.

SAMANI, N., M. KOMPANI-ZARE, AND D.A. BARRY. 2004. MODFLOW EQUIPPED WITH A NEW METHOD FOR THE ACCURATE SIMULATION OF AXISYMMETRIC FLOW. *ADVANCES IN WATER RESOURCES* 27 NO. 1: 31-45.

SAUNDERS, J.A., M.-K. LEE, M. SHAMSUDDUHA, P. DHAKAL, A. UDDIN, M.T. CHOWDURY, K.M. AHMED. 2008. GEOCHEMISTRY AND MINERALOGY OF ARSENIC IN (NATURAL) ANAEROBIC GROUNDWATERS. *APPLIED GEOCHEMISTRY* NO. 23: 3205–3214.

SCHROTH, M.H., J. KLEIKEMPER, C. BOLLIGER, S.M. BERNASCONI, AND J. ZEYER. 2001. IN SITU ASSESSMENT OF MICROBIAL SULFATE REDUCTION IN A PETROLEUM-CONTAMINATED AQUIFER USING PUSH–PULL TESTS AND STABLE SULFUR ISOTOPE ANALYSES. *JOURNAL OF CONTAMINANT HYDROLOGY* 51 NO. 3-4: 179-195.

SEAMAN, J.C., P.M. BERTSCH, M. WILSON, J. SINGER, F. MAJS, AND S.A. ABURIME. 2007. TRACER MIGRATION IN A RADIALLY DIVERGENT FLOW FIELD: LONGITUDINAL DISPERSIVITY AND ANIONIC TRACER RETARDATION. *VADOSE ZONE JOURNAL* 6 NO. 2: 373-386.

SENKO, J.M., J.D. ISTOK, J.M. SUFLITA, AND L.R. KRUMHOLZ. 2002. IN-SITU EVIDENCE FOR URANIUM IMMOBILIZATION AND REMOBILIZATION. *ENVIRONMENTAL SCIENCE & TECHNOLOGY* 36 NO. 7: 1491-1496.

SINGER, P.C., AND W. STUMM. 1970. THE SOLUBILITY OF FERROUS IRON IN CARBONATE-BEARING WATERS. *JOURNAL OF THE AMERICAN WATER WORKS ASSOCIATION* 62: 198-202.

SMEDLEY, P.L., AND D.G. KINNIBURGH. 2002. A REVIEW OF THE SOURCE, BEHAVIOUR AND DISTRIBUTION OF ARSENIC IN NATURAL WATERS. *APPLIED GEOCHEMISTRY* 17 NO. 5: 517568.

SRACEK, O., P. BHATTACHARYA, G. JACKS, J.-P. GUSTAFSSON, AND M.V. BRÖMSSEN. 2004. BEHAVIOR OF ARSENIC AND GEOCHEMICAL MODELING OF ARSENIC ENRICHMENT IN AQUEOUS ENVIRONMENTS. *APPLIED GEOCHEMISTRY* 19 NO. 2: 169-180.

STOLLENWERK, K. G. 2003. *ARSENIC IN GOUNDWATER*, EDS. WELCH, A. H. AND STOLLENWERK, K. G. (KLUWER, BOSTON), PP. 67–100.

STOLLENWERK, K.G., G.N. BREIT, A.H. WELCH, J.C. YOUNT, J.W. WHITNEY, A.L. FOSTER, M.N. UDDIN, R.K. MAJUMDER, AND N. AHMED. 2007. ARSENIC ATTENUATION BY OXIDIZED AQUIFER SEDIMENTS IN BANGLADESH. *SCIENCE OF THE TOTAL ENVIRONMENT* 379 NO. 2-3: 133-150.

STUYFZAND, P.J. 2008. ASR ARSENIC SURROGATE MODEL, ED. S. F. W. M. DISTRICT.

STUYFZAND, P.J., AND H. TIMMER. 1999. DEEP WELL INJECTION AT THE LANGERAK AND NIEUWEGEIN SITES IN THE NETHERLANDS: CHEMICAL REACTIONS AND THEIR MODELING. KIWA-SWE 96.006; NIEUWEGEIN, NETHERLANDS.

VALOCCHI, A.J. 1986. EFFECT OF RADIAL FLOW ON DEVIATIONS FROM LOCAL EQUILIBRIUM DURING SORBING SOLUTE TRANSPORT THROUGH HOMOGENEOUS SOILS. *WATER RESOURCES RESEARCH* 22 NO. 12: 1693-1701.

VALOCCHI, A.J., R.L. STREET, AND P.V. ROBERTS. 1981. TRANSPORT OF ION-EXCHANGING SOLUTES IN GROUNDWATER: CHROMATOGRAPHIC THEORY AND FIELD SIMULATION. *WATER RESOURCES RESEARCH* 17 NO. 5: 1517-1527.

VAN WAGENINGEN, W.F.C, H.M. WENTINCK AND C. OTTO. 2009. REPORT AND MODELLING OF MOVECBM FIELD TESTS IN POLAND AND SLOVENIA. *ENERGY PROCEDIA* 1, NO. 1: 2071-2078.

VANDENBOHEDE, A., A. LOUWYCK, AND L. LEBBE. 2008. IDENTIFICATION AND RELIABILITY OF MICROBIAL AEROBIC RESPIRATION AND DENITRIFICATION KINETICS USING A SINGLE-WELL PUSH–PULL FIELD TEST. *JOURNAL OF CONTAMINANT HYDROLOGY* 95 NO. 1-2: 42-56.

VANDERZALM, J., P. DILLON, AND C. LE GAL LA SALLE. 2007. ARSENIC MOBILITY UNDER VARIABLE REDOX CONDITIONS INDUCED DURING ASR. IN *MANAGEMENT OF AQUIFER RECHARGE FOR SUSTAINABILITY*, ED. P. FOX, 209-219. PHOENIX, ARIZONA: ACACIA PUBLISHING.

VANDERZALM, J.L., P.J. DILLON, K.E. BARRY, K. MIOTLINSKI, J.K. KIRBY, AND C. LE GAL LA SALLE. SUBMITTED. ARSENIC MOBILITY UNDER VARIABLE REDOX CONDITIONS INDUCED DURING ASR. *APPLIED GEOCHEMISTRY*.

VELING, E.J.M., AND C. MAAS. 2009. STRATEGY FOR SOLVING SEMI-ANALYTICALLY THREE-DIMENSIONAL TRANSIENT FLOW IN A COUPLED N-LAYER AQUIFER SYSTEM. *JOURNAL OF ENGINEERING MATHEMATICS* 64: 145-161.

WALLIS, I., H. PROMMER, C.T. SIMMONS, V. POST, AND P.J. STUYFZAND. 2010. EVALUATION OF CONCEPTUAL AND NUMERICAL MODELS FOR ARSENIC MOBILIZATION AND ATTENUATION DURING MANAGED AQUIFER RECHARGE. *ENVIRONMENTAL SCIENCE & TECHNOLOGY* 44 NO. 13: 5035-5041.

WALLIS, I., H. PROMMER, T. PICHLER, V. POST, S.B. NORTON, M.D. ANNABLE, AND C.T. SIMMONS. 2011. PROCESS-BASED REACTIVE TRANSPORT MODEL TO QUANTIFY ARSENIC MOBILITY DURING AQUIFER STORAGE AND RECOVERY OF POTABLE WATER. *ENVIRONMENTAL SCIENCE & TECHNOLOGY* 45 NO. 16: 6924-6931.

WANG, H.Q., AND N. CRAMPON. 1995. METHOD FOR INTERPRETING TRACER EXPERIMENTS IN RADIAL FLOW USING MODIFIED ANALYTICAL SOLUTIONS. *JOURNAL OF HYDROLOGY* 165 NO. 1-4: 11-31.

WARD, J.D., C.T. SIMMONS, AND P.J. DILLON. 2007. A THEORETICAL ANALYSIS OF MIXED CONVECTION IN AQUIFER STORAGE AND RECOVERY: HOW IMPORTANT ARE DENSITY EFFECTS? *JOURNAL OF HYDROLOGY* 343 NO. 3-4: 169-186.

WELCH, A.H., D.B. WESTJOHN, D.R. HELSEL, AND R.B. WANTY. 2000. ARSENIC IN GROUND WATER OF THE UNITED STATES: OCCURRENCE AND GEOCHEMISTRY. *GROUND WATER* 38 NO. 4: 589-604.

WELCH, A.H., R.S. OREMLAND, J.A. DAVIS, AND S.A. WATKINS. 2006. ARSENIC IN GROUND WATER: A REVIEW OF CURRENT KNOWLEDGE AND RELATION TO THE CALFED SOLUTION AREA WITH RECOMMENDATIONS FOR NEEDED RESEARCH. *SAN FRANCISCO ESTUARY & WATERSHED SCIENCE* 4 NO. 2.

WILKIE, J.A., AND J.G. HERING. 1996. INTERACTIONS OF ARSENIC WITH HYDROUS METAL OXIDE SURFACES: THE POSSIBLE ROLE OF OXIDATION OF ARSENITE BY HYDROUS FERRIC OXIDE. *ABSTRACTS OF PAPERS OF THE AMERICAN CHEMICAL SOCIETY* 211: 71-COLL.

WILLIAMSON, M.A., AND J.D. RIMSTIDT. 1994. THE KINETICS AND ELECTROCHEMICAL RATE-DETERMINING STEP OF AQUEOUS PYRITE OXIDATION. *GEOCHIMICA ET COSMOCHIMICA ACTA* 58 NO. 24: 5443-5454.

WOLTHERS, M., L. CHARLET, C. H. VAN DER WEIJDEN, P. R. VAN DER LINDE AND D. RICKARD. 2005. ARSENIC MOBILITY IN THE AMBIENT SULFIDIC ENVIRONMENT: SORPTION OF ARSENIC(V) AND ARSENIC(III) ONTO DISORDERED MACKINAWITE. *GEOCHIMICA ET COSMOCHIMICA ACTA*, 69: NO. 14:3483–3492.

ZHENG, C., AND P.P. WANG. 1999. MT3DMS, A MODULAR THREE-DIMENSIONAL MULTI-SPECIES TRANSPORT MODEL FOR SIMULATION OF ADVECTION, DISPERSION AND CHEMICAL REACTIONS OF CONTAMINANTS IN GROUNDWATER SYSTEMS; DOCUMENTATION AND USER'S GUIDE. U.S. ARMY ENGINEER RESEARCH AND DEVELOPMENT CENTER CONTRACT REPORT 202.